Water dissociation and water-gas shift energetics on MgO, MgO/Ag and Au/MgO/Ag surfaces

Janne Nevalaita

UNIVERSITY OF JYVÄSKYLÄ
DEPARTMENT OF PHYSICS

Abstract

Water dissociation and the energetics of the WGS reaction on a bulk MgO, an Ag supported MgO thin film and Au/MgO/Ag surfaces is studied based on the density functional theory. The literature results for water splitting on MgO and MgO/Ag surfaces with a step type defect are repeated and further analysis on the origin of the energetically favored dissociative water adsorption are made. The reactivity towards water dissociation on the stepped MgO and MgO/Ag surfaces is attributed to four contributing factors:

1. The change in the interlayer distance of the surface in dissociative adsorption is diminished on the stepped surfaces compared to the flat surfaces. On the flat surfaces the dissociative adsorption of water leads to an increased interlayer distance between the first and second MgO layer while the molecular adsorption does not change the distance.

2. A surface OH group is formed in the H adsorption. On the stepped surface the adsorbed OH and surface OH form aligned dipoles. On the flat surface the adsorbed OH and the surface OH group do not align.

3. The density difference analysis shows that the charge transfer in the co-adsorption of H and OH on the stepped MgO/Ag surface is mainly between the adsorbed H and OH. This leads to an attractive Coulomb interaction between the adsorbed species.

4. The p-band center of the edge O atoms show a strong shift towards the Fermi energy compared to the average surface O atoms. On the bulk MgO surfaces the p-band center of the O atom at the H adsorption site is shown to correlate with the H adsorption energy. Similar trend is seen in the MgO/Ag surfaces.

The energetics of a WGS reaction on a surface with large Au clusters deposited on an Ag supported MgO thin film is studied. The large Au cluster is modeled with an Au stripe set with the periodic boundary conditions to produce similar distances between the Au atoms as for a large Au cluster. The Bader charges of the edge atoms of the Au stripe are similar to the charges for the edge atoms of a large Au cluster. Water dissociation at the edge of the Au stripe is not deemed probable due to the weak binding of OH to the Au/MgO/Ag surface.

Tiivistelmä

Vetyä energian tuottamiseen käyttävien PEM-polttokennojen avulla voidaan pienentää ilmastonmuutosta edistäviä haitallisia päästöjä. Tarvittava polttoaine saa kuitenkin sisältää ainoastaan pieniä määriä hiilimonoksidia, sillä se estää kennojen toiminnan. Hiilimonoksidin määrää voidaan pienentää vesikaasureaktiolla, jossa vesi ja hiilimonoksidi muodostavat vetyä ja hiilidioksia. Veden hajoaminen on tärkeä vaihe tässä reaktiossa. Teollisissa sovelluksissa vesikaasureaktiota tehostetaan rautaa tai kuparia sisältävillä katalyyteilla. Viimeaikaisten tutkimusten perusteella metallioksidipinnoilla olevat kultaklusterit voivat sopivasti valmistettuina olla huomattavasti tällä hetkellä teollisuudessa käytettyjä katalyyttejä tehokkaampia. Tässä työssä tutkittiin vesikaasureaktion lähtöaineiden, välituotteiden ja reaktiotuotteiden energioita magnesiumoksidilla sekä ultraohuella hopeatuetulla magnesiumoksidikalvolla. Erityisesti tutkittiin veden hajoamista. Tutkimusmenetelmänä käytettiin tiheysfunktionaaliteoriaan perustuvia tietokonesimulaatioita. Tiheysfunktionaaliteoriaan perustuvat laskentamenetelmät ovat yleisesti käytettyyjä niiden luotettavuuden ja laskennallisen tehokkuuden vuoksi. Työn aluksi kirjallisuustulokset veden hajoamiselle pinnalla olevan askelman reunalla toistettiin sekä oksidipinnalle, että ohutkalvolle. Dissosiatiivisen adsorption suotuisuuteen yhdistettiin neljä tekijää:

1. Tasaisen ohutkalvon atomikerrosten välinen etäisyys kasvaa kun pinalle adsorboituva vesi hajoaa. Vesimolekyylin adsorptiossa atomikerrosten välinen etäisyys pysyy likimain samana. Askelmaisella pinnalla veden hajoaminen ei muuta atomikerrosten välisiä etäisyyksiä.

2. Askelmaisella pinnalla veden hajoamisessa syntyvä hydroksyyliryhmä muodostaa adsorboituneen hydroksyyliryhmän kanssa samansuuntaiset sähköiset dipolit. Tasaisella pinnalla dipolit ovat erisuuntaiset.

3. Varaus siirtyy vetyatomilta hydroksyyliryhmälle dissosiatiivisessa adsorptiossa askelmaiselle ohutkalvolle. Adsorboituneen vetyatomin ja hydroksyyliryhmän välillä on siten positiivinen Coulombin vuorovaikutus.

4. Elektronirakenneanalyysi osoittaa, että askelman reunalla olevien happiatomien elektronirakenne poikkeaa keskimääräisestä happiatomista. Oksidipinnalla vedyn adsorptiopaikalla sijaitsevan happiatomin elektronirakenteen muutos vastaa vedyn voimakkaampaa sitoutumista pintaan. Vastaava käyttäytyminen havaittiin myös hopeatuetulla ohutkalvolla.

Lisäksi tutkittiin vesikaasureaktion energetiikkaa suuren, hopeatuetulle magnesiumoksidikalvolle adsorboituneen, kultaklusterin reunalla. Todettiin, että vesi ei hajoa kultaklusterin reunalla, koska hydroksyyliryhmä ei sitoudu pintaan riittävän voimakkaasti.

Contents

1 Introduction

1.1 Water-gas shift reaction

Reducing the usage of fossil fuels and finding sustainable alternatives for them is one of the main challenges in order to reduce global warming. The search for effective and renewable sources of energy has not turned out to be an easy task. Hydrogen based polymer electrolyte membrane (PEM) fuel cells offer one solution for portable applications [1]. Even though hydrogen is the most common element in the universe, on Earth it is usually found in compounds. Most common of these compounds is water. Extracting hydrogen from water can be done with electrolysis but this process is very energy consuming. Hydrogen can also be produced by steam reforming which has a high molar ratio of H_2/CO [2]. This is preferred since carbon monoxide poisons the electrolytes in PEM fuels cells. Recent publications indicate a possibility of manufacturing PEM fuel cells with CO-tolerant anodes [3]. An another possibility is to use a further reaction to remove the excess CO. This is possible by the water-gas shift (WGS) reaction

$$CO + H_2O \rightarrow CO_2 + H_2 \tag{1.1}$$

where CO and water form carbon dioxide and hydrogen. Ideally this reaction should be done at a relatively low temperature, below 150°C, since the WGS reaction is limited by a thermodynamical equilibrium as seen in figure 1. Low temperature makes a high conversion rate of CO possible.
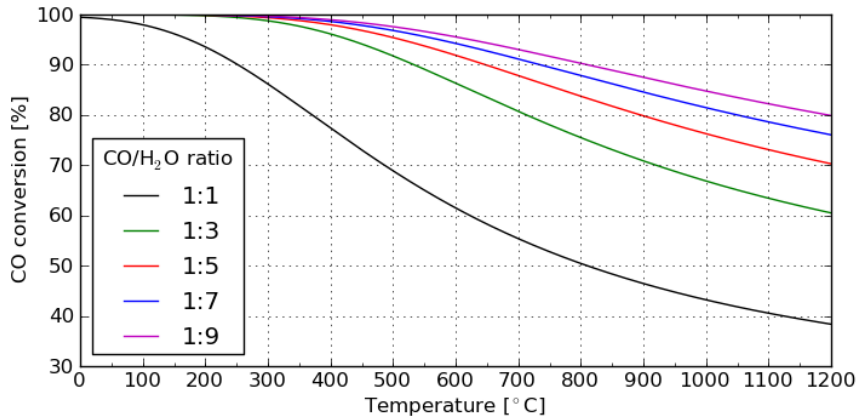
Figure 1: The thermodynamical equilibrium conversion of CO at atmospheric pressure for different molar ratios of CO/H_2O in the WGS reaction. The figure is plotted from equations given in ref [4].

1.2 Gold clusters as catalysts

Despite the relative chemical inertness of bulk gold, nanosized gold clusters have been found to be chemically active. Two observations in the early 1980s changed the view of gold as a chemically inert material. Au^{+3} was predicted and subsequently confirmed as a very good catalyst for ethyne hydrochlorination on a carbon support and supported gold nano-crystals were identified as a highly effective catalysts for the CO oxidation at very

low temperatures [5]. Since then gold clusters have been found to catalyze many reactions including the WGS reaction.

The focus of this thesis is to study the energetics of a catalytic WGS reaction at the edge of a large supported Au cluster with numerical methods based on the density functional theory. The calculations with large Au clusters containing up to several hundreds of atoms can be computationally really expensive. In order to reduce the cost the edge of a large Au cluster was modeled by a stripe of Au atoms on a MgO/Ag support with periodic boundary conditions to produce similar distances between the Au atoms as observed for large Au clusters. The model system with an Au stripe was computationally affordable since only under hundred atoms were needed to model the edge of a large Au cluster and the Au-oxide interface.

1.3   Water dissociation on MgO

Water dissociation is an important step in the WGS reaction. For catalysts consisting of Au clusters on an oxide support the water dissociation has been deemed to occur on the oxide support rather than on the Au cluster as discussed in the section 5. The support oxide is assumed to contain an oxygen vacancy where water molecule can be adsorbed. The dissociation of water then occurs near the edge of the adsorbed Au cluster. Possible support oxides include CeO_2, MoO_2, TiO_2 and ZnO which is frequently used in industry [6]. The studied oxide in this thesis is MgO in bulk and as an Ag supported thin film.

Water is known to spontaneously dissociate on both an Ag supported MgO thin film and a bulk MgO surface, when there is a step type defect in the top MgO layer [7]. The literature results for water dissociation on both an Ag supported MgO thin film and a bulk MgO surface were repeated. Comparative calculations between surfaces with and without a step defect were made. The electronic structures in four different surfaces were analyzed by considering the local density of states in each case. The band centers were calculated and compared in order to quantify the differences between the stepped and flat surfaces.

2   Density functional theory

Density functional theory (DFT) is an *ab initio* method which means that the only needed parameters to characterize a system are the coordinates and proton numbers of the elements. DFT was developed in the early 1960s by Walter Kohn in cooperation with Pierre Hohenberg [8] and Lu J. Sham [9]. Kohn was awarded the Nobel prize in chemistry 1998 for his work [10].

DFT has become a widely used method in both physics and chemistry with many different implementations and approximations [11]. One of the many reasons to the popularity of DFT formalism is the possibility to study relatively large systems. DFT also offers a good chemical accuracy with the effective computing. This is also enhanced by the increasingly faster modern computers and the development of parallelized implementations. The properties of bulk materials or surfaces can be determined by utilizing periodic boundary conditions and approximating large systems as infinite or semi-infinite.

2.1   The Schrödinger equation

In this section the presentation in ref [12] has been followed for the most part. To describe the interactions of electrons and nuclei in solids one would in principle need to solve the

Schrödinger equation

$$\hat{H}\Psi(\boldsymbol{r}_1,\ldots,\boldsymbol{r}_N,\boldsymbol{R}_1,\ldots,\boldsymbol{R}_M) = E\Psi(\boldsymbol{r}_1,\ldots,\boldsymbol{r}_N,\boldsymbol{R}_1,\ldots,\boldsymbol{R}_M) \tag{2.1}$$

where $\hat{H}$ is the many-body Hamiltonian, E is the energy of the eigenstate and Ψ is the eigenstate wave function. The value of Ψ depends on the position vectors of the electrons $\boldsymbol{r}_1,\ldots,\boldsymbol{r}_N$ and the nuclei $\boldsymbol{R}_1,\ldots,\boldsymbol{R}_M$. This equation describes a system with N electrons and M nuclei. In atomic units

$$e = m_e = \hbar = \frac{1}{4\pi\epsilon_0} = 1 \tag{2.2}$$

where e is the charge of an electron, m_e is the mass of an electron, $\hbar$ is the reduced Planck constant and ϵ_0 is the vacuum permittivity, the many-body Hamiltonian can be written as a sum of the kinetic energies of the electrons, the kinetic energies of the nuclei, the electron-electron interactions, the nuclei-nuclei interactions and the electron-nuclei interactions

$$\begin{aligned} \hat{H} = \quad & -\frac{1}{2}\sum_{i=1}^{N}\nabla_i^2 - \frac{1}{2}\sum_{I=1}^{N}\nabla_I^2 + \sum_{i}^{N}\sum_{j>i}^{N}\frac{1}{|\boldsymbol{r}_i - \boldsymbol{r}_j|} \\ + \quad & \sum_{I}^{M}\sum_{J>I}^{M}\frac{Z_I Z_J}{|\boldsymbol{R}_I - \boldsymbol{R}_J|} - \sum_{i=1}^{N}\sum_{I=1}^{M}\frac{Z_I}{|\boldsymbol{r}_i - \boldsymbol{R}_I|} \end{aligned} \tag{2.3}$$

where M_I is the mass of the nucleus I in atomic units and Z_I is the proton number for the nucleus I. Since the mass of a proton is over thousand times larger than the mass of an electron and forces acting on them are of a similar order of magnitude, the relaxation of electrons to their ground state happens much faster than relaxation of the nuclei. Thus one can use the Born-Oppenheimer approximation [13, p. 53] and assume that the electrons stay in their ground state while the nuclei move adiabatically to theirs. With this approximation the kinetic energy of the nuclei can be neglected and the nuclei-nuclei interaction is only a parameter depending on their position vectors. Thus, the original many-body problem is divided into solving the electronic part with the Hamiltonian

$$\hat{H}_{elec} = -\frac{1}{2}\sum_{i=1}^{N}\nabla_i^2 + \sum_{i}^{N}\sum_{j>i}^{N}\frac{1}{|\boldsymbol{r}_i - \boldsymbol{r}_j|} - \sum_{i=1}^{N}\sum_{I=1}^{M}\frac{Z_I e^2}{|\boldsymbol{r}_i - \boldsymbol{R}_I|} \tag{2.4}$$

and the nuclear part separately. Solving the electronic eigenvalue equation with the Hamiltonian $\hat{H}_{elec}$ gives the eigenenergy E_{elec} and assuming that position vectors are known, the nuclei-nuclei interaction energy E_{II} can be calculated as the classical interaction energy of a group of point charges

$$E_{II} = \sum_{I=1}^{M}\sum_{J>I}^{M}\frac{Z_I Z_J}{|\boldsymbol{R}_I - \boldsymbol{R}_J|}. \tag{2.5}$$

The energy of the whole system E can then be approximated as the sum of the energy of electrons on their ground state E_{elec} and the classical Coulomb interaction energy of the nuclei, i.e. $E \approx E_{elec} + E_{II}$.

2.2 The Hohenberg-Kohn theorems

The electronic Hamiltonian is an example of a Hamiltonian of the form

$$\hat{H} = \hat{T} + \hat{W} + \hat{V} \tag{2.6}$$

where

$$\hat{T} = -\frac{1}{2} \sum_{i=1}^{N} \nabla_i^2 \tag{2.7}$$

is the part describing the kinetic energy of N electrons,

$$\hat{W} = \sum_{i}^{N} \sum_{j>i}^{N} \frac{1}{|\boldsymbol{r}_i - \boldsymbol{r}_j|} \tag{2.8}$$

is the part describing the interactions between electrons and

$$\hat{V} = \sum_{i=1}^{N} V_{ext}(\boldsymbol{r}_i) \tag{2.9}$$

is the part describing the potential energy of the electrons due to an external potential. The double summation in the electron-electron interaction part $\hat{W}$ is avoided by requiring $j > i$ in the other summation. The Hohenberg-Kohn theorems [8, 13, p. 122] state that for an external potential V_{ext} there is one to one correspondence with a ground state electron density $n_0(\boldsymbol{r})$. The second Hohenberg-Kohn theorem states that there is a functional $E[n]$ of density that gives the energy of the system at the density $n(\boldsymbol{r})$ and that the ground state electron density $n_0(\boldsymbol{r})$ minimizes that functional i.e. $E[n_0(\boldsymbol{r})] = E_0$ where E_0 is the ground state energy. Proofs of the Hohenberg-Kohn theorems are considered in Appendix A. Thus instead of trying to solve the $3N$ variable eigenvalue equation one can instead examine the functional of electron density

$$E[n] = \langle \Psi[n(\boldsymbol{r})] | \hat{H} | \Psi[n(\boldsymbol{r})] \rangle. \tag{2.10}$$

Using linearity of the inner product, the functional (2.10) can be divided into two parts and for a defined external potential v the energy can be written as

$$E[n] = \langle \Psi[n(\boldsymbol{r})] | \hat{T} + \hat{W} | \Psi[n(\boldsymbol{r})] \rangle + V[n] \tag{2.11}$$

where

$$V[n] = \int \mathrm{d}\boldsymbol{r}\, n(\boldsymbol{r}) v(\boldsymbol{r}). \tag{2.12}$$

Since the ground state energy E_0 is less or equal than the energy E_i of any other state i, the ground state density minimizes the functional (2.11). Then by requiring

$$\frac{\delta E[n]}{\delta n(\boldsymbol{r})} = 0 \tag{2.13}$$

for the functional derivative one obtains the equation

$$\frac{\delta F_{HK}[n]}{\delta n(\boldsymbol{r})} + \frac{\delta V[n]}{\delta n(\boldsymbol{r})} = 0 \tag{2.14}$$

where

$$F_{HK}[n] = \langle \Psi[n(\boldsymbol{r})] | \hat{T} + \hat{W} | \Psi[n(\boldsymbol{r})] \rangle \tag{2.15}$$

is the Hohenberg-Kohn functional that does not depend on the external potential. The functional derivative for the later term can be calculated as shown in Appendix B. This leads to the equation

$$\frac{\delta F_{HK}[n]}{\delta n(\boldsymbol{r})} = -v(\boldsymbol{r}). \tag{2.16}$$

Thus, when potential of a system is defined on the right hand side the ground state density can be obtained from the left hand side.

2.3   The Kohn-Sham system

Since the Hohenberg-Kohn functional does not depend on the external potential it is useful to define a non-interacting system which has the same ground state density as the interacting one. This is done with the Hamiltonian

$$\hat{H}_s = \hat{T}_s + \hat{V}_s = \frac{1}{2} \sum_{i=1}^{N} \nabla_i^2 + \sum_{i=1}^{N} V_s(\boldsymbol{r}_i) \tag{2.17}$$

where V_s is the effective single particle potential. This is called the Kohn-Sham system [9]. The eigenvalue equation for this Hamiltonian is

$$\hat{H}_s \Phi_s[n] = E_s \Phi_s[n]. \tag{2.18}$$

Since this Hamiltonian describes a non-interacting system the eigenstates Φ_s can be separated into a product of single particle states ϕ_i. Because electrons are fermions the wave function must be antisymmetric to a permutation of particles. This wave function can be formed as a Slater determinant

$$\Phi_s[n] = \frac{1}{\sqrt{N!}} \begin{vmatrix} \phi_1(\boldsymbol{r}_1) & \cdots & \phi_N(\boldsymbol{r}_1) \\ \vdots & & \vdots \\ \phi_1(\boldsymbol{r}_N) & \cdots & \phi_N(\boldsymbol{r}_N) \end{vmatrix}. \tag{2.19}$$

Energy for the whole non-interacting system E_s can be calculated as a sum of the single particle energies ϵ_i in the single particle equation

$$\left(-\frac{1}{2} \nabla^2 + V_s[n](\vec{r}) \right) \phi_i(\vec{r}) = \epsilon_i \phi_i(\vec{r}). \tag{2.20}$$

Thus

$$E_s = \sum_{i=1}^{N} \epsilon_i. \tag{2.21}$$

Derivation of equation (2.21) is considered in Appendix C. The Hohenberg-Kohn functional can then be written as

$$F_{HK}[n] = T_s[n] + V_H[n] + E_{XC}[n] \tag{2.22}$$

where $T_s[n]$ is the kinetic energy functional defined by the non-interacting system with the same ground state density, $V_H[n]$ is the Coulomb energy of the electron cloud

$$V_H[n] = \frac{1}{2} \int \int \mathrm{d}\boldsymbol{r}\mathrm{d}\boldsymbol{r}' \frac{n(\boldsymbol{r})n(\boldsymbol{r}')}{|\boldsymbol{r} - \boldsymbol{r}'|} \tag{2.23}$$

and $E_{XC}[n]$ is the exchange and correlation energy functional. Substituting back into equation (2.16) gives

$$\frac{\delta T_s[n]}{\delta n(\boldsymbol{r})} + \frac{\delta V_H[n]}{\delta n(\boldsymbol{r})} + \frac{\delta E_{XC}[n]}{\delta n(\boldsymbol{r})} = -v(\boldsymbol{r}). \tag{2.24}$$

Calculating the functional derivatives for the known functionals

$$\frac{\delta T_s[n]}{\delta n(\boldsymbol{r})} = -V_s[n](\boldsymbol{r}) \tag{2.25}$$

and

$$\frac{\delta V_H[n]}{\delta n(\boldsymbol{r})} = \int \mathrm{d}\boldsymbol{r}' \frac{n(\boldsymbol{r}')}{|\boldsymbol{r} - \boldsymbol{r}'|} = v_H[n](\boldsymbol{r}) \tag{2.26}$$

yields an equation for the effective single particle potential which produces the ground state density of the interacting system

$$V_s[n](\boldsymbol{r}) = v[n](\boldsymbol{r}) + v_H[n](\boldsymbol{r}) + v_{XC}[n](\boldsymbol{r}). \tag{2.27}$$

In above equation (2.27) the definition

$$v_{XC}[n](\boldsymbol{r}) = \frac{\delta E_{XC}[n]}{\delta n(\boldsymbol{r})}. \tag{2.28}$$

for the exchange and correlation potential $v_{XC}[n](\boldsymbol{r})$ has been used. Substituting result (2.27) into equation (2.20) the single particle states ϕ_i can be obtained

$$\left(-\frac{1}{2}\nabla^2 + v[n](\boldsymbol{r}) + v_H[n](\boldsymbol{r}) + v_{XC}[n](\boldsymbol{r}) \right) \phi_i(\boldsymbol{r}) = \epsilon_i \phi_i(\boldsymbol{r}). \tag{2.29}$$

The ground state density can then be calculated from the equation

$$n(\boldsymbol{r}) = \sum_{\sigma} \sum_{i=1}^{N} |\phi_i(\boldsymbol{r})|^2. \tag{2.30}$$

Approximating the exchange and correlation energy or the exchange and correlation potential the effective single particle potential can be calculated from equation (2.27) with an educated guess for the initial density. The single particle states can then be determined from equation (2.29). New density can then be obtained from equation (2.30). Continuing this process iteratively until the density does not change one obtains the ground state electron density of the interacting system.

2.4 Local Density Approximation

As seen in the previous subsection in order to calculate the ground state density one needs an approximation for the exchange and correlation energy E_{XC} or the exchange and correlation potential v_{XC}. Perhaps the simplest assumption is to consider a slowly varying density. In this case the exchange and correlation energy can be approximated with the exchange and correlation energy of a homogeneous electron gas $\epsilon_{XC}(n(\boldsymbol{r}))$ with the same density $n(\boldsymbol{r})$ as the system has in point $\boldsymbol{r}$. This approximation is known as the local density approximation (LDA). In this case the exchange and correlation energy E_{XC}^{LDA} is

$$E_{XC}^{\text{LDA}} = \int \mathrm{d}\boldsymbol{r} n(\boldsymbol{r}) \epsilon_{XC}(n(\boldsymbol{r})). \tag{2.31}$$

This simple approximation is not without limits. The LDA has problems including the prediction of metallic properties to materials which are known to be insulating. Examples of such materials are CoO and FeO. LDA is also known to give too small band gaps for certain materials including many semiconductors [14]. LDA has been found to over bind adsorbates about 1.5eV [15]. Possible improvements into LDA are considered in the next subsection.

2.5 Gradient Approximations

An intuitive and simple way to attempt to correct the problems with LDA would be to include terms with gradient expansion of the density. The gradient terms should in principle account for the variations in density. Inclusion of terms of the form $|\nabla n|^2$ was proposed already by Kohn and Sham [9]. This is known as the gradient expansion approximation (GEA). Unfortunately the GEA often gives worse results than the LDA and is known to violate some of the exact conditions known for the exchange and correlation functional [16].

It is also possible to construct gradient corrected functionals that try to conserve the strengths of the LDA and fulfill known conditions for the exchange and correlation functional. These are known as the generalized gradient approximations (GGA). While atomization energies have drastically improved compared to LDA, construction of the GGA functionals has also lead to usage of many different functionals in the literature resulting in different energies for the same system depending on the used functional [17].

GGA functionals can be expressed as functionals of the spin densities $n_\uparrow$ and $n_\downarrow$ [18]

$$E_{\text{XC}}^{\text{GGA}}[n_\uparrow, n_\downarrow] = \int \mathrm{d}\boldsymbol{r} n(\boldsymbol{r}) \epsilon_{\text{X}}^{\text{unif}}(n) F_{\text{XC}}^{\text{GGA}}(r_s, \zeta, s) \tag{2.32}$$

where $F_{\text{XC}}^{\text{GGA}}(r_s, \zeta, s)$ is the enchantment factor, $\epsilon_{\text{X}}^{\text{unif}}(n)$ is the exchange energy per particle of the unpolarized uniform electron gas, r_s is a density parameter related to density as $n = 3/4\pi r_s^3$, ζ is relative spin polarization

$$\zeta = \frac{n_\uparrow - n_\downarrow}{n_\uparrow + n_\downarrow} \tag{2.33}$$

and s is the reduced density gradient defined as

$$s = \frac{|\nabla n|}{2(3\pi^2)^{1/3} n^{4/3}}. \tag{2.34}$$

Multiple GGA functionals are used in the literature. Improvements from LDA to GGA include more accurate atomization energies for molecules, more realistic binding energy curve for rare-gas dimers, correct crystal structure and magnetic properties for Fe, better lattice constants for several materials and many more. GGA has still problems including unrealistic description of the interaction between core and valence electrons [19].

3   Numerical methods

3.1   Periodic systems

Consider the Schrödinger equation with a similar Hamiltonian $\hat{H}_s$ as for the single particle equation (2.20)

$$\hat{H}_s = -\frac{1}{2}\nabla^2 + \hat{V}_s. \tag{3.1}$$

In a periodic system the potential is also periodic and for a lattice vector $\boldsymbol{R}$ the equation

$$V_s(\boldsymbol{r} + \boldsymbol{R}) = V_s(\boldsymbol{r}) \tag{3.2}$$

holds. Thus the Hamiltonian is also invariant under the same translation

$$\hat{H}_s(\boldsymbol{r} + \boldsymbol{R}) = \hat{H}_s(\boldsymbol{r}). \tag{3.3}$$

Two eigenvalue equations

$$\hat{H}_s(\boldsymbol{r})\phi_i(\boldsymbol{r}) = \epsilon_i \phi_i(\boldsymbol{r}) \tag{3.4}$$

and

$$\hat{H}_s(\boldsymbol{r} + \boldsymbol{R})\phi_i(\boldsymbol{r} + \boldsymbol{R}) = \epsilon_i \phi_i(\boldsymbol{r} + \boldsymbol{R}) \tag{3.5}$$

hold for the original and the translated wave functions. By summing equations (3.4) and (3.5) a third eigenvalue equation is obtained

$$\hat{H}_s(\boldsymbol{r})(\phi_i(\boldsymbol{r}) + \phi_i(\boldsymbol{r} + \boldsymbol{R})) = \epsilon_i(\phi_i(\boldsymbol{r}) + \phi_i(\boldsymbol{r} + \boldsymbol{R})) \tag{3.6}$$

where equation (3.3) has been used on the left hand side. Thus the state $\phi_i(\boldsymbol{r}) + \phi_i(\boldsymbol{r} + \boldsymbol{R})$ is also the eigen state of $\hat{H}_s(\boldsymbol{r})$. This occurs when

$$\phi_i(\boldsymbol{r} + \boldsymbol{R}) = c(\boldsymbol{R})\phi_i(\boldsymbol{r}) \tag{3.7}$$

where $c(\boldsymbol{R})$ is a constant depending only on the lattice vector $\boldsymbol{R}$. The translation must conserve the norm of the wave function

$$\int \mathrm{d}\boldsymbol{r}|\phi_i(\boldsymbol{r})|^2 = \int \mathrm{d}\boldsymbol{r}|\phi_i(\boldsymbol{r} + \boldsymbol{R})|^2. \tag{3.8}$$

Combining equations (3.7) and (3.8) shows that

$$|c(\boldsymbol{R})|^2 = 1. \tag{3.9}$$

This holds when

$$c(\boldsymbol{R}) = \exp(i\boldsymbol{k} \cdot \boldsymbol{R}) \tag{3.10}$$

for a reciprocal vector $\boldsymbol{k}$. Consider a function $u_{i,\boldsymbol{k}}(\boldsymbol{r})$ that depends on the reciprocal vector $\boldsymbol{k}$ and is defined as

$$u_{i,\boldsymbol{k}}(\boldsymbol{r}) = \exp(-i\boldsymbol{k} \cdot \boldsymbol{r})\phi_i(\boldsymbol{r}). \tag{3.11}$$

The function $u_{i,\boldsymbol{k}}(\boldsymbol{r})$ can be shown to have the periodicity of the lattice

$$\begin{aligned}
u_{i,\boldsymbol{k}}(\boldsymbol{r} + \boldsymbol{R}) &= \exp(-i\boldsymbol{k} \cdot (\boldsymbol{r} + \boldsymbol{R}))\phi_i(\boldsymbol{r} + \boldsymbol{R}) \\
&= \exp(-i\boldsymbol{k} \cdot (\boldsymbol{r} + \boldsymbol{R}))\exp(i\boldsymbol{k} \cdot \boldsymbol{R})\phi_i(\boldsymbol{r}) \\
&= \exp(-i\boldsymbol{k} \cdot \boldsymbol{r})\phi_i(\boldsymbol{r}) \\
&= u_{i,\boldsymbol{k}}(\boldsymbol{r})
\end{aligned} \tag{3.12}$$

where equations (3.7) and (3.10) have been used on the second line. Thus the wave function of the periodic system can be expressed as

$$\phi_{i,\boldsymbol{k}}(\boldsymbol{r}) = u_{i,\boldsymbol{k}}(\boldsymbol{r})\exp(i\boldsymbol{k} \cdot \boldsymbol{r}) \tag{3.13}$$

where the wave function has been split into a plane wave part and a modulating function with the periodicity of the lattice. This result is known as the Bloch's theorem. For wave functions of this form and potential with periodicity $\boldsymbol{R}$ the Bloch's boundary conditions

$$\phi_{i,\boldsymbol{k}}(\boldsymbol{r} + \boldsymbol{R}) = \exp(i\boldsymbol{k} \cdot \boldsymbol{R})\phi_{i,\boldsymbol{k}}(\boldsymbol{r}) \tag{3.14}$$

hold. In order to model periodic systems in the DFT formalism Bloch's boundary conditions can be applied to the Kohn-Sham single particle equations. The density can then be calculated as the average over the first Brillouin zone in the reciprocal space

$$n(\boldsymbol{r}) = \sum_i^N \frac{1}{\Omega_{BZ}} \int_{\Omega_{BZ}} \mathrm{d}\boldsymbol{k} |\phi_{i,\boldsymbol{k}}(\boldsymbol{r})|^2 \tag{3.15}$$

where Ω_{BZ} is the volume of the first Brillouin zone in the reciprocal space. The energy of the non-interacting Kohn-Sham system can be calculated similarly

$$E_{\mathrm{KS}} = \sum_i^N \frac{1}{\Omega_{BZ}} \mathrm{d}\boldsymbol{k} f_{i,\boldsymbol{k}} \epsilon_i(\boldsymbol{k}) \tag{3.16}$$

where $f_{i,\boldsymbol{k}}$ is the occupation number for state i at point $\boldsymbol{k}$ in the $\boldsymbol{k}$-space. Numerically only finite amount of $\boldsymbol{k}$-point depended values can be solved. Thus integrations in $\boldsymbol{k}$-space need to be converted into summations over finite amount of $\boldsymbol{k}$-points

$$\frac{1}{\Omega_{BZ}} \int_{\Omega_{BZ}} \mathrm{d}\boldsymbol{k} \rightarrow \frac{1}{N_k} \sum_{\boldsymbol{k}} \tag{3.17}$$

where N_k is the number of used $\boldsymbol{k}$-points. In this thesis the Monkhorst-Pack scheme for the $\boldsymbol{k}$-point distribution was used in all performed calculations [20].

3.2 Real space grids

The usage of real space grids is useful since it is possible to parallelize computations by dividing the grid points between different processors. Also more asymmetric systems are not as problematic as in implementations relying on base functions. The external potential in real space grid formalism can be approximated as

$$\int \mathrm{d}\boldsymbol{r} V(\boldsymbol{r}) n(\boldsymbol{r}) \sim \Omega_G \sum_{\boldsymbol{G}} V(\boldsymbol{G}) n(\boldsymbol{G}) \tag{3.18}$$

where the continuous functions are at the left hand side and discrete functions defined in points $\boldsymbol{G} = (G_x, G_y, G_z)$ are on the right hand side. Ω_G is the volume corresponding to point $\boldsymbol{G}$. There are many numerical methods for the evaluation of partial derivatives. In a fixed point $\boldsymbol{G}_0$ partial derivative with respect to x-coordinate can be approximated as

$$\left. \frac{\partial^2 \psi_i(\boldsymbol{r})}{\partial x^2} \right|_{\boldsymbol{G}_0} \sim \Omega_G \sum_{-m}^{m} c_m \psi_i(G_x + mh, G_y, G_z) \tag{3.19}$$

where h is the real space grid spacing, m is an integer defining the number of points used in the approximation of the derivative and c_m is a constant depending on the real space grid. Since the Laplace operator in the Cartesian coordinates can be written as

$$\nabla^2 = \frac{\partial^2}{\partial x^2} + \frac{\partial^2}{\partial y^2} + \frac{\partial^2}{\partial z^2} \tag{3.20}$$

it can be expressed in discrete form $L_{\boldsymbol{G}\boldsymbol{G}'}$ and the total energy of the system is

$$E = \sum_n f_n \Omega_G \sum_{\boldsymbol{G}} \psi_n^*(\boldsymbol{G}) \sum_{\boldsymbol{G}'} (-\frac{1}{2} L_{\boldsymbol{G}\boldsymbol{G}'}) \psi_n(\boldsymbol{G}') + \frac{1}{2} \Omega_G \sum_{\boldsymbol{G}} V_H(\boldsymbol{G}) n(\boldsymbol{G}) + E_{XC}[n(\boldsymbol{G})] + E_{II} \tag{3.21}$$

where f_n is occupation number, $E_{XC}[n(\boldsymbol{G}), \Omega_G]$ is approximation for exchange and correlation energy and E_{II} is the interaction energy between nuclei.

3.3 Projector-augmented wave method

The wave function oscillates rapidly near the atomic nuclei due to the large momentum of the core electrons and the orthogonality requirement for the quantum states. Chemical properties though are more depended on the smaller energy valence electrons. Because of this, it is useful to describe the nuclei and strongly bound core electrons as so called pseudo potentials with which the valence electrons interact. The projector-augmented wave (PAW) method [13, p. 225] utilizes a similar idea while still conserving the true wave function ψ. Since further away from the nuclei the true wave function is smooth, it is enough to operate only near the nuclei. Within a certain cut-off radius r_c^a from the nuclei the true wave function is transformed to a smoother wave function $\tilde{\psi}$ with a linear transformation $\hat{\mathcal{T}}$

$$|\psi\rangle = \hat{\mathcal{T}}|\tilde{\psi}\rangle. \tag{3.22}$$

Since further than the cut-off radius from the nuclei the true wave function is also smooth, continuity at that point can be required

$$|\psi\rangle = |\tilde{\psi}\rangle, \text{ when } |\boldsymbol{r} - \boldsymbol{R}^a| \geq r_c^a \text{ for all } a \qquad (3.23)$$

where $\boldsymbol{R}^a$ is the position vector of the nucleus a. The transformation $\hat{\mathcal{T}}$ can thusly be represented as a linear combination with the unity operator

$$\hat{\mathcal{T}} = \hat{1} + \sum_a \hat{\mathcal{T}}^a \qquad (3.24)$$

where the operators $\hat{\mathcal{T}}^a$ transform the wave functions only at a distance smaller than r_c^a from the nucleus a. The wave function $\tilde{\psi}$ can be expanded in partial waves $\tilde{\psi}_i^a$ around the nucleus a

$$|\tilde{\psi}\rangle = \sum_i P_i^a |\tilde{\psi}_i^a\rangle \qquad (3.25)$$

where the coefficients P_i^a are determined with the projection functions $|\tilde{p}_i^a\rangle$

$$P_i^a = \langle \tilde{p}_i^a | \tilde{\psi} \rangle. \qquad (3.26)$$

By combining equations (3.25) and (3.26) one obtains

$$|\tilde{\psi}\rangle = \sum_i |\tilde{\psi}_i^a\rangle \langle \tilde{p}_i^a | \tilde{\psi} \rangle \qquad (3.27)$$

which shows that

$$\sum_i |\tilde{\psi}_i^a\rangle \langle \tilde{p}_i^a| = \hat{1}. \qquad (3.28)$$

By demanding that partial waves behave similarly in the transformation $\hat{\mathcal{T}}$, eg. demand $|\psi_i^a\rangle = \hat{\mathcal{T}}|\tilde{\psi}_i^a\rangle$, it can be seen from equation (3.24) that

$$\hat{\mathcal{T}}^a|\tilde{\psi}_i^a\rangle = |\psi_i^a\rangle - |\tilde{\psi}_i^a\rangle \text{ for all } i, a \qquad (3.29)$$

By combining equations (3.28) and (3.29) the linear transformation operator $\hat{\mathcal{T}}^a$ can be written as

$$\hat{\mathcal{T}}^a = \sum_i \hat{\mathcal{T}}^a |\tilde{\psi}_i^a\rangle \langle \tilde{p}_i^a| = \sum_i (|\psi_i^a\rangle - |\tilde{\psi}_i^a\rangle) \langle \tilde{p}_i^a|, \text{ for all } a \qquad (3.30)$$

and the complete transformation $\hat{\mathcal{T}}$ is

$$\hat{\mathcal{T}} = \hat{1} + \sum_a \sum_i (|\psi_i^a\rangle - |\tilde{\psi}_i^a\rangle) \langle \tilde{p}_i^a|. \qquad (3.31)$$

The partial waves and the projection operators do not depend on the studied system, so it is enough to calculate them once for each element. For each operator of the true wave function $\hat{A}$ there can be defined an operator $\tilde{A}$ that acts on the smooth wave functions

$$\tilde{A} = \hat{\mathcal{T}}^\dagger \hat{A} \hat{\mathcal{T}}. \qquad (3.32)$$

For the single particle equations one obtains equation

$$\hat{\mathcal{T}}^\dagger \hat{H} \hat{\mathcal{T}} |\tilde{\psi}_n\rangle = \epsilon_n \hat{\mathcal{T}}^\dagger \hat{\mathcal{T}} |\tilde{\psi}_n\rangle \qquad (3.33)$$

where $\hat{H}$ is the single particle Hamiltonian.

11

3.4 Computational details

The density functional theory was used in a real space grid formalism together with the projector augmented wave (PAW) method as implemented in the GPAW code [21, 22] with the Atomic Simulation Environment (ASE) [23]. Visual Molecular Dynamics (VMD) [24] was used in visualization of density difference and figures of the relaxation geometries were generated with Jmol [25]. The grid spacing was set to 0.2Å in all calculations and it was adjusted in all directions in order to get an even spacing of the grid points. All systems were treated as spin compensated except for the single atoms and molecules with uneven number of electrons in the gas phase. The relativistic corrections were used for the projection operators of Au and Ag. The Perdew-Burke-Ernzerhof (PBE) [26] approximation was used for the exchange and correlation energy functional. The lattice constant for Ag was 4.17Å and the lattice constant for MgO was adjusted 0.10Å to match silver introducing a minor compressive stress to the MgO film. The lattice constant for the bulk MgO was 4.27Å [7]. The oxygen anions in the thin oxide film were aligned with the support metal atoms since this is known to be the preferred structure [27]. The geometries were considered fully relaxed when the forces acting to atoms were below 0.05eV/Å. The surfaces were modeled with periodic boundary conditions for the Kohn-Sham equations

$$|\psi(x,y,z)|^2 = |\psi(x+nU_x, y+mU_y, z)|^2 \text{ for all integers } n, m \qquad (3.34)$$

where U_x is the width of the unit cell in x-direction, U_y is the width of the unit cell in y-direction and n and m are integers. In all calculations (3×2) unit cell was used. The unit cell is shown in figure 2 in the case of the studied Au/MgO/Ag system.
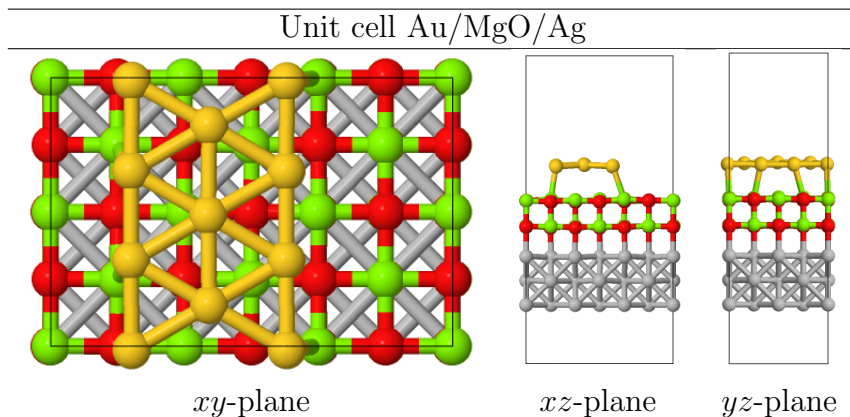
Figure 2: The black line shows the (3×2) unit cell. The thickness of the MgO film is two atomic layers and the support metal is modeled with three atomic layers. The atomic color codes in order Ag, Au, Mg and O are light gray, yellow, green and red respectively.

In all calculations there was 5Å of vacuum under the support metal atoms and at least 5Å of vacuum above the adsorbates to ensure the vanishing of the wave function before the unit cell edge. The band structure of the support metal was modeled with the Monkhorst-Pack scheme for the $\boldsymbol{k}$-point sampling.

The energy of a two layers thick MgO thin film supported by three atomic layers of Ag was calculated with different $\boldsymbol{k}$-point samplings. The results are given in figure 3. The difference in energy between 12 and 15 $\boldsymbol{k}$-points is relatively small but due to the number of $\boldsymbol{k}$-points in the irreducible part of the Brillouin zone the calculation done with 15 k-points converges faster. For 12 $\boldsymbol{k}$-points there are 6 $\boldsymbol{k}$-points in the irreducible part

of the Brillouin zone and for 15 $\boldsymbol{k}$-points there are 8 $\boldsymbol{k}$-points in the irreducible part of the Brillouin zone. Because $8 = 2^3$ it is better for parallelization over $\boldsymbol{k}$-points leading to a shorter calculation time. In this thesis the 3×5 $\boldsymbol{k}$-point sampling was used in all calculations.
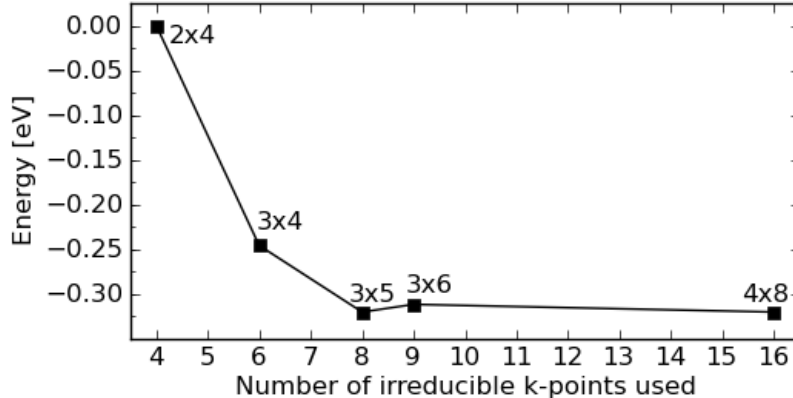
Figure 3: The energy as a function of the number of $\boldsymbol{k}$-points used in the calculation. The distribution for $\boldsymbol{k}$-points in x- and y-direction has been given above each point.

4 Methods for analysis

4.1 Adsorption and interaction energy

In order to deduce which adsorption geometry is the most stable, the energy difference between the initial state before adsorption and the final state after adsorption were compared. This energy difference is called the adsorption energy E_{ads} and it can be defined as

$$\mathrm{E_{ads}(X) = E(X/surface) - (E(surface) + E(X))} \tag{4.1}$$

where E(X/surface) is the total energy of the fully relaxed final state with the adsorbate X on the surface, E(surface) is the energy of the fully relaxed surface without the adsorbate and E(X) is the gas phase energy of the adsorbate. The energy of the initial state is thus defined as the summed energy of the surface and adsorbate without any interaction between them. With this sign convention negative values of the adsorption energy correspond to an exothermic and thus energetically favorable adsorption since the final state has a lower energy than the initial state. For multiple similar adsorbates it is useful to define the average adsorption energy

$$\frac{\Delta \mathrm{E}}{n(\mathrm{X})} = \frac{\mathrm{E}(n(\mathrm{X}) \cdot \mathrm{X/surface}) - \mathrm{E(surface)} - n(\mathrm{X}) \cdot \mathrm{E(X)}}{n(\mathrm{X})} \tag{4.2}$$

where $n(\mathrm{X})$ is the number of adsorbates X, $\mathrm{E}(n(\mathrm{X}) \cdot \mathrm{X/surface})$ is the energy of a fully relaxed final state with all $n(\mathrm{X})$ adsorbates on the surface and E(X) is the energy of a single adsorbate X in the gas phase. In order to study the interactions between adsorbates, the interaction energy E_{int} can be defined as the energy difference between the adsorption energy for a high coverage of adsorbates E_{ads} and the sum of adsorption energies for the low coverage of adsorbates [28]

$$E_{\text{int}} = E_{\text{ads}} - \sum E_{\text{ads}}^{\text{LC}} \tag{4.3}$$

where $\sum E_{\text{ads}}^{\text{LC}}$ is the sum of adsorption energies for the individual species constituting the high coverage scheme.

4.2   Bader analysis

The charges of individual atoms, molecules and surfaces were determined by using the Bader analysis [29, 30, 31] where the electron density of the whole system is divided and assigned to individual atoms. The algorithm examines the electron density and finds its maximum values which are usually at the nuclei of atoms. Then around these maxima the zero-flux surfaces are formed in a way that the inner product of the gradient of density n with a normal vector of the surface $\boldsymbol{u}$ is zero at every point of the surface

$$\nabla n(\boldsymbol{r}) \cdot \boldsymbol{u}(\boldsymbol{r}) = 0. \tag{4.4}$$

The charge of an individual atom can then be considered as the charge enclosed by these surfaces. This algorithm scales linearly with the size of the studied system making it easily applicable to larger systems. In this thesis the Bader charge analysis was mostly used to study the charges of adsorbate atoms on the surface but also the Bader charges of different parts of the system were considered. The Bader charges of the support metal, the MgO thin film and the Au stripe were defined as the summed Bader charge of the individual atoms inside the unit cell. For the Au/MgO/Ag system the charges of different parts were normalized so that the Bader charges of all parts before adsorption were zero. After adsorption the Bader charges $q(\text{X})$ were defined as the difference between the charge state of initial state $q_{\text{initial}}(\text{X})$ and final state $q_{\text{final}}(\text{X})$

$$q(\text{X}) = q_{\text{initial}}(\text{X}) - q_{\text{final}}(\text{X}). \tag{4.5}$$

A negative sign in the Bader charge indicates an increase in the electron density and thus a larger negative charge.

4.3   Density difference analysis

The density difference analysis provides a way to visualize the charge transfer in adsorption. The density difference n_{diff} can be defined as

$$n_{\text{diff}} = n(\text{adsorbates/surface}) - (n(\text{adsorbates}) + n(\text{surface})) \tag{4.6}$$

where $n(\text{adsorbates/surface})$ is the density of the fully relaxed final system with adsorbates on the surface, $n(\text{adsorbates})$ is the density of the adsorbates at same atomic positions as on the final system and $n(\text{surface})$ is the density of the surface at the same atomic positions as in the final system with adsorbates on the surface. The density difference shows the accumulation or depletion of charge due to adsorption. The integrated density difference can be defined as

$$n_{\text{diff}}(z) = \int \int n_{\text{diff}}(x, y, z) \mathrm{d}x \mathrm{d}y \tag{4.7}$$

where the density difference defined in equation (4.6) is integrated over the xy-plane. With this definition the integrated density difference shows the charge transfer in z-direction. Since the surfaces studied within this thesis are set along the xy-plane the

14

integrated density difference plots can be used to visualize charge transfer between different parts of the system.

4.4 Local density of states

The density of states $\rho(\epsilon)$ describes how many states have energy ϵ in the energy interval $[\epsilon, \epsilon + \mathrm{d}\epsilon]$. It can be defined with the systems eigenstates ψ_n as

$$\rho(\epsilon) = \sum_n \langle \psi_n | \psi_n \rangle \delta(\epsilon - \epsilon_n) \tag{4.8}$$

where ϵ_n is the eigenvalue of state ψ_n. Using the unity operator

$$\hat{1} = \int \mathrm{d}\boldsymbol{r} |\boldsymbol{r}\rangle\langle\boldsymbol{r}| \tag{4.9}$$

this can be expressed in the spatial basis

$$\rho(\epsilon) = \int \mathrm{d}\boldsymbol{r} \sum_n \langle \psi_n | \boldsymbol{r} \rangle \langle \boldsymbol{r} | \psi_n \rangle \delta(\epsilon - \epsilon_n) \tag{4.10}$$

where

$$\rho(\boldsymbol{r}, \epsilon) = \sum_n \langle \psi_n | \boldsymbol{r} \rangle \langle \boldsymbol{r} | \psi_n \rangle \delta(\epsilon - \epsilon_n) \tag{4.11}$$

is the local density of states (LDOS). Solving the ground state electron density gives the single particle states ϕ_i in the equation (2.29) which can be used as the eigenstates ψ_i. In order to quantify differences in the LDOS it is useful to define the d-band center [32]

$$\epsilon_d = \frac{\int_{E_f - E_c}^{E_f} E \rho_d(E) \mathrm{d}E}{\int_{E_f - E_c}^{E_f} \rho_d(E) \mathrm{d}E} \tag{4.12}$$

where ρ_d is the LDOS for the d electrons, E_f is the Fermi energy and E_c is the cut-in energy. In principle $E_c \to \infty$ but for numerical reasons the value $E_c = 7.0\mathrm{eV}$ has been used in the d-band calculations. Similarly the s- and p-band centers can be defined.

5 Water-gas shift reaction mechanisms

5.1 The redox mechanism

In this chapter three different mechanisms for a gold catalyzed WGS reaction analyzed in ref. [33] are considered. The aim is to motivate the selection of adsorption sites so that the possible intermediate species in the WGS reaction can be formed and to emphasize the key steps in the reaction. The gold clusters are assumed to be on an oxide support. Only mechanisms where CO is adsorbed on an Au site and water is adsorbed to an oxide site are considered. The adsorbates on Au sites indicate an intermediate species in the WGS reaction rather than stable compounds. An example of the redox mechanism in the case of ceria can be written as

$$\begin{aligned}
CO &\rightarrow CO_{ads}^{Au} & (5.1)\\
CO_{ads}^{Au} + 2CeO_2 &\rightarrow CO_2 + Ce_2O_3 \\
H_2O + Ce_2O_3 &\rightarrow H_2 + 2CeO_2
\end{aligned}$$
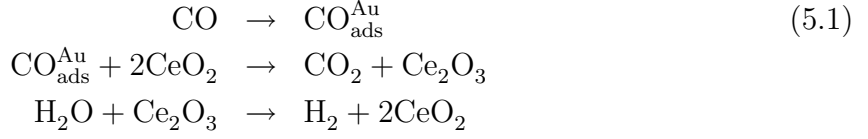
where CO first adsorbs on an Au site, then CO_{ads}^{Au} is oxidized to form CO_2. The Ce_2O_3 is formed to the oxide surface which in turn re-oxidizes by water dissociation into O and H_2. For a general oxide one assumes the existence of an anionic surface defect $\square_{ads}$ where the water molecule can adsorb. Then the reaction can be written as

$$\begin{aligned}
CO &\rightarrow CO_{ads}^{Au} & (5.2)\\
H_2O + \square_{ads} &\rightarrow H_2O_{ads} \\
H_2O_{ads} &\rightarrow OH_{ads} + H_{ads}^{Au} \\
OH_{ads} + H_{ads}^{Au} &\rightarrow O_{ads} + H_2 \\
O_{ads} + CO_{ads}^{Au} &\rightarrow CO_2 + \square_{ads}
\end{aligned}$$
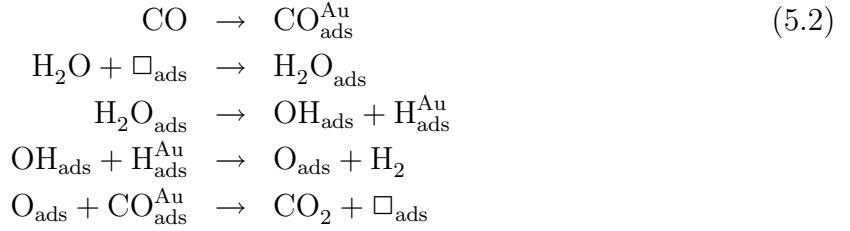
where CO is adsorbed to an Au site and water is adsorbed onto the oxide surface. Then the adsorbed water is dissociated leaving OH to the oxide surface and H on the Au site. The H_2 is formed directly in an interaction between the adsorbed OH and H_{ads}^{Au}. The O stays adsorbed on the oxide surface and the surface vacancy is reformed in the CO oxidation.

5.2 The formate mechanism

In the redox mechanism no intermediate states of the form CH_xO_y are possible. Experiments on the other hand indicate the formation of such compounds. Set of reactions for the formate mechanism can be written as

$$\begin{aligned}
CO &\rightarrow CO_{ads}^{Au} & (5.3)\\
H_2O + \square_{ads} &\rightarrow OH_{ads} + H_{ads}^{Au} \\
CO_{ads}^{Au} + OH_{ads} &\rightarrow HCO_{2ads}^{Au} + \square_{ads} \\
H_2O + \square_{ads} &\rightarrow OH_{ads} + H_{ads}^{Au} \\
HCO_{2ads}^{Au} + OH_{ads} &\rightarrow CO_2 + H_2O + \square_{ads} \\
2H_{ads}^{Au} &\rightarrow H_2
\end{aligned}$$
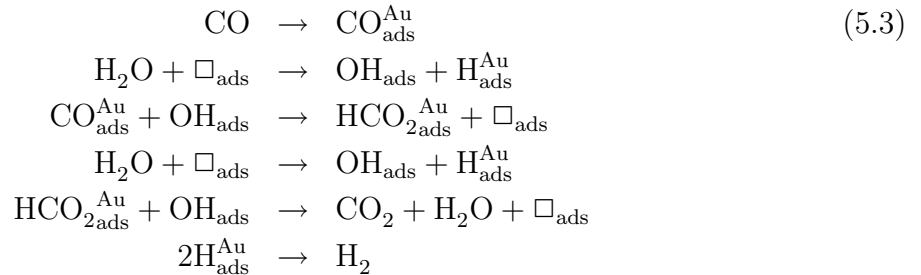
where CO first adsorbs on an Au site and water dissociatively adsorbs on the surface. The OH group is adsorbed on the defect site of the oxide surface and H on an Au site. The adsorbed OH then interacts with CO_{ads}^{Au} leaving a vacant surface defect and a HCO_{2ads}^{Au} intermediate is formed. A schematic of the HCO_2 intermediate is shown in figure 4. Water dissociation is repeated, since two adsorbed OH groups are needed. The intermediate state HCO_{2ads}^{Au} interacts with the second adsorbed OH group and dissociates into CO_2 and water leaving an empty surface defect. The hydrogen molecule is produced in the last step.

HCO$_2$	HOCO
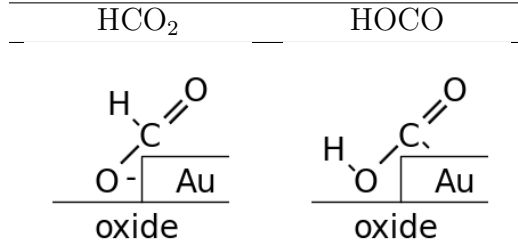
Figure 4: The schematic representations of the intermediate reaction products HCO$_2$ and HOCO in the WGS reaction.

5.3 The carboxyl mechanism

In ref [33] the carboxyl mechanism was suggested as the most probable of the presented mechanisms because it is simpler in a way that less bonds need to be formed or broken. The needed energy input is smaller for the simpler mechanism. It can be written as

$$
\begin{aligned}
\text{CO} &\rightarrow \text{CO}_{\text{ads}}^{\text{Au}} && (5.4)\\
\text{H}_2\text{O} + \square_{\text{ads}} &\rightarrow \text{OH}_{\text{ads}} + \text{H}_{\text{ads}}^{\text{Au}}\\
\text{CO}_{\text{ads}}^{\text{Au}} + \text{OH}_{\text{ads}} &\rightarrow \text{HOCO}_{\text{ads}}^{\text{Au}} + \square_{\text{ads}}\\
\text{HOCO}_{\text{ads}}^{\text{Au}} &\rightarrow \text{CO}_2 + \text{H}_{\text{ads}}^{\text{Au}}\\
2\text{H}_{\text{ads}}^{\text{Au}} &\rightarrow \text{H}_2
\end{aligned}
$$
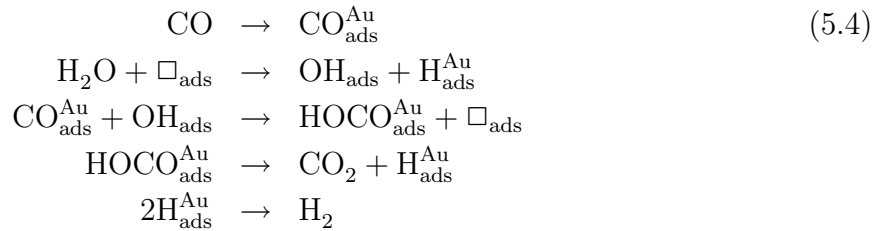
where CO adsorbs on an Au site followed by dissociative water adsorption forming adsorbed OH species and $\text{H}_{\text{ads}}^{\text{Au}}$. An intermediate $\text{HOCO}_{\text{ads}}^{\text{Au}}$ species is formed in the interaction of the adsorbed OH and CO. The CO$_2$ is produced when $\text{HOCO}_{\text{ads}}^{\text{Au}}$ dissociates producing the another $\text{H}_{\text{ads}}^{\text{Au}}$ needed in the production of hydrogen. A schematic of the HOCO intermediate is shown in figure 4. In both the formate and carboxyl mechanisms the water dissociation needs to occur before the formation of the formate or carboxyl intermediate. Water dissociation has been deemed as the rate limiting step for the WGS reaction [34].

6 Water dissociation on bulk MgO

6.1 Adsorption of H, OH and water on bulk MgO

The bulk MgO surface was modeled with five atomic layers. The four topmost layers of the clean MgO surface were allowed to fully relax while the bottom layer was frozen to the bulk positions. Two bottom layers were kept frozen to the previously determined geometry after adding the adsorbates. The preferred adsorption sites for water and its dissociation products were taken from ref [7]. The reference molecules used in the calculation of adsorption energies were H$_2$ and H$_2$O in a vacuum. The reference energy $E(\text{X})$ for H adsorption was $^1\!/_2 E(\text{H}_2)$ and $E(\text{H}_2\text{O}) - ^1\!/_2 E(\text{H}_2)$ for OH.

Water adsorption to the bulk MgO surface is exothermic with the adsorption energy of -0.47eV. The adsorption of H and OH to individual computational cells is clearly endothermic. The co-adsorption energy is more negative compared to the adsorption far
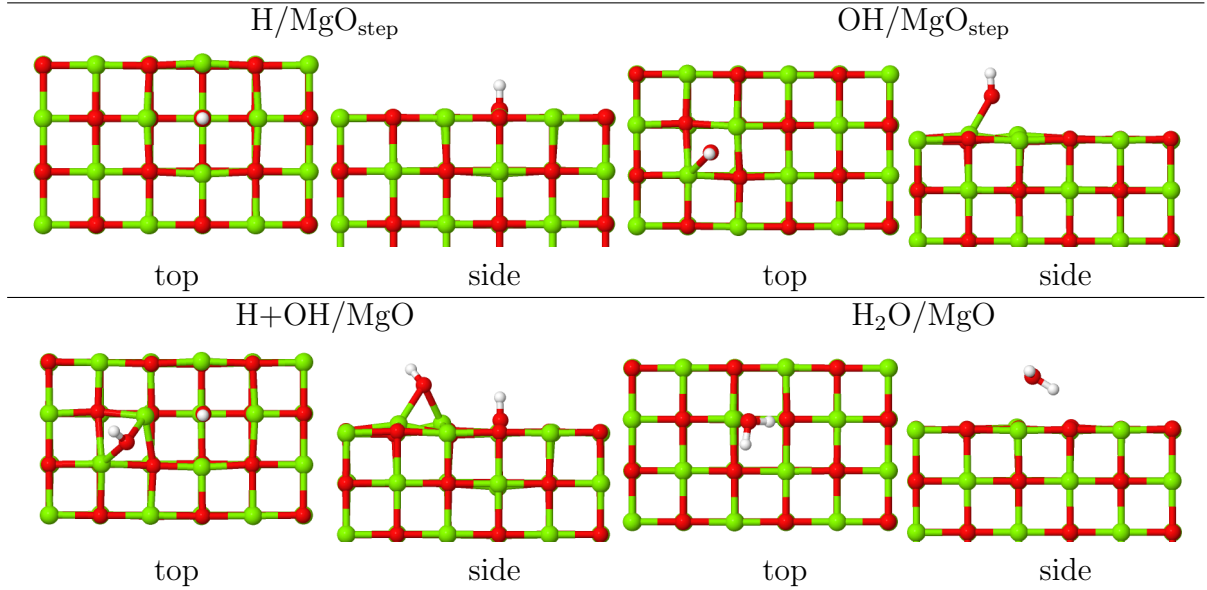
Figure 5: The relaxation geometries for the adsorption of water and its dissociation products H and OH on a bulk MgO surface. Top and side views are denoted with top and side. The atomic color codes in order H, Mg and O are white, green and red respectively.

apart, indicating binding between the adsorbates. The adsorption energies together with the atomic distances are given in table 1.

Water adsorbs close to Mg-top site with one hydrogen atom facing towards the adjacent surface oxygen as shown in figure 5. The OH group adsorbs on a bridge site between two Mg atoms. A surface OH group is formed in the H adsorption with an increase in the distance between the O atom in the top layer and the Mg atom in the second layer. When H and OH co-adsorb the average distance between the first and second MgO layer increases to 2.18Å compared to the average distance of 2.13Å for a clean MgO surface. In the adsorption of water molecule the average distance between the first and second MgO layer is 2.14Å showing a smaller change in the interlayer distance compared to the dissociative adsorption.

Table 1: The adsorption energies and atomic distances for the adsorption of water and its dissociation products H and OH on a bulk MgO surface. The distance between the first and second atomic layer $d_{1st,2nd}$ is calculated as the difference between the average z-coordinates of atoms in the top layer and the atoms in the second layer. The distance $d_{O,Mg}$ is the minimum distance between a surface Mg atom and the O atom in the OH group or water molecule. The distance $d_{H,O}$ is the minimum distance between a surface O and the adsorbed H.

	E_{ads}	$d_{1st,2nd}$	$d_{O,Mg}$	$d_{H,O}$
MgO		2.13		
H/MgO	1.56	2.15		1.00
OH/MgO	2.05	2.15	2.18	
H+OH/MgO	0.61	2.18	2.11	0.98
H$_2$O/MgO	-0.47	2.14	2.24	

The Bader charges for water and its dissociation products H and OH are given in table 2. The adsorbed H is charged positively and the adsorbed OH is charged negatively. When H and OH are co-adsorbed an additional charge transfer occurs. In this case the

negative charge obtained by OH corresponds to the additional positive charge gained by H, indicating charge transfer between the adsorbates. The increased charge transfer correlates with the decreased adsorption energy and can be viewed as binding between the adsorbates.

Table 2: The Bader charges in electrons for water and its dissociation products adsorbed on a bulk MgO surface. The given Bader charge $q(H)$ is the charge of the adsorbed H. A negative sign indicates the receiving of charge.

	q(H)	q(OH)	q(H_2O)
H/MgO	0.39		
OH/MgO		-0.66	
H+OH/MgO	0.54	-0.88	
H_2O/MgO			-0.08

6.2   Adsorption of H and OH on a stepped MgO surface
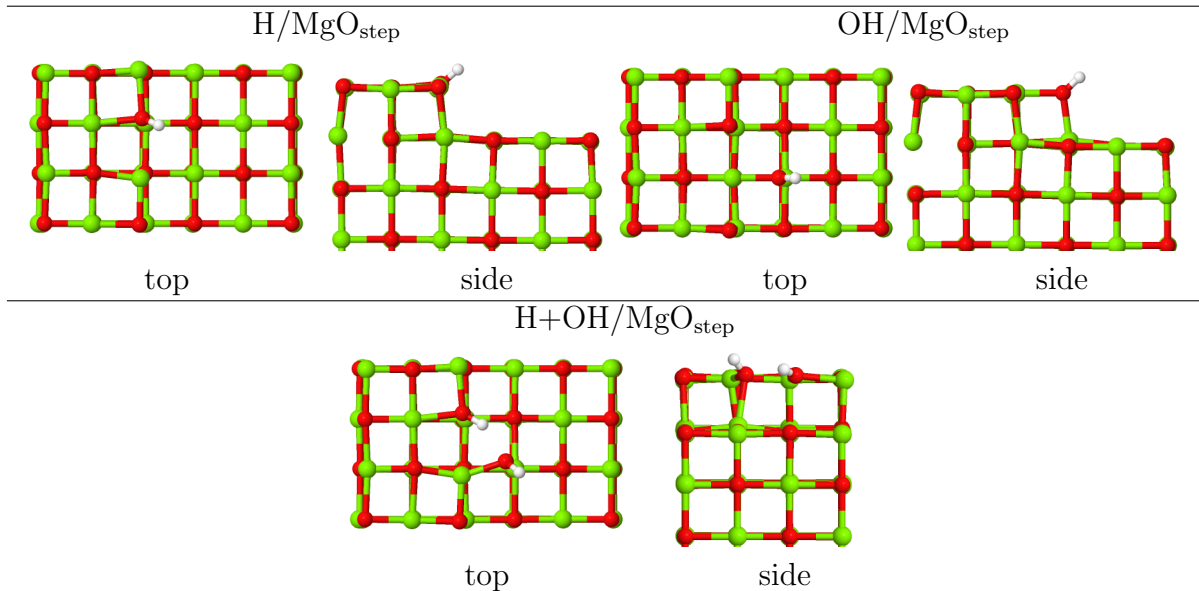
Figure 6: The relaxation geometries for the adsorption of water dissociation products H and OH on a bulk MgO surface with a step defect. Top and side views are denoted with top and side. The atomic color codes are the same as in figure 5.

Molecular and dissociative adsorption of water on a stepped bulk MgO surface was studied by using the energetically favorable adsorption sites determined in ref [7]. The step defect was modeled with a step layer that had a half monolayer coverage. Dissociative water adsorption is clearly exothermic. When dissociation products H and OH adsorb far apart, their adsorption energies are endothermic. These energies show a clear attractive interaction between the adsorbed H and OH. The adsorption energies for both H and OH adsorbed far apart are decreased compared to the adsorption energies of H and OH on the flat MgO surface, indicating stronger binding to the stepped surface. The calculated adsorption energies for different adsorbates are given in table 3. Water spontaneously dissociates on the step edge and thus no adsorption energy for a water molecule is given.

Table 3: The adsorption energies and atomic distances for the adsorption of water dissociation products H and OH on a stepped MgO surface. The distance between the step and top layer of the bulk MgO $d_{step,1st}$ is calculated as the difference between the average z-coordinates of atoms in the step layer and the top layer. The distances $d_{1st,2nd}$, $d_{O,Mg}$ and $d_{H,O}$ are defined as in table 1.

	E_{ads}	$d_{step,1st}$	$d_{1st,2nd}$	$d_{O,Mg}$	$d_{H,O}$
MgO_{step}		2.16	2.14		
H/MgO_{step}	0.68	2.19	2.14		0.99
OH/MgO_{step}	0.81	2.16	2.15	1.97	
$H+OH/MgO_{step}$	-1.79	2.17	2.15	1.97	0.99

H adsorbs on top of an edge O atom and OH adsorbs on an adjacent Mg site. When H and OH are co-adsorbed the alignment of the H atom in the adsorbed OH group is changed. H in the surface OH group faces towards the O atom in the adsorbed OH while the H in the adsorbed OH group faces away from the adsorbed H. The distance between the adsorbed H atom and the O in the adsorbed OH group is 1.88Å indicating hydrogen bonding between the adsorbed species. The adsorption geometries corresponding to given adsorption energies are shown in figure 6.

The Bader charges for water dissociation products H and OH are given in table 4. H is positively charged and OH is charged negatively. The charge transfer from surface to H and OH is increased compared to the adsorption on a flat MgO surface. The additional charge transfer could be viewed as increased binding to the surface since it correlates with the decreased adsorption energy. The charging of the adsorbates is increased when they are co-adsorbed similarly as on the flat MgO surface.

Table 4: The Bader charges in electrons for H and OH adsorbed on a stepped MgO surface. The Bader charge $q(H)$ is the charge of the adsorbed H. A negative sign indicates the receiving of charge.

	q(H)	q(OH)
H/MgO_{step}	0.46	
OH/MgO_{step}		-0.78
$H+OH/MgO_{step}$	0.59	-0.85

6.3 LDOS comparison between flat and step MgO surface

In order to compare the differences in the electronic structures of flat and stepped MgO surfaces, the LDOS plots for the systems with different adsorbates are presented in this section. The band centers for different atoms were calculated and are given in the figures. The band centers for specific atoms were determined from the LDOS summed over each atom of that type. The LDOS and the band centers were also calculated for geometrically interesting individual atoms shown in the figure 7. For a flat surface the LDOS and the band centers were given for a single Mg atom near the site of OH adsorption and for the O atom at the site of H adsorption. For the stepped surface the LDOS and the band centers were given for a single Mg atom at the edge of the step layer, adjacent to the site of OH adsorption and for a single O atom at the site of H adsorption.
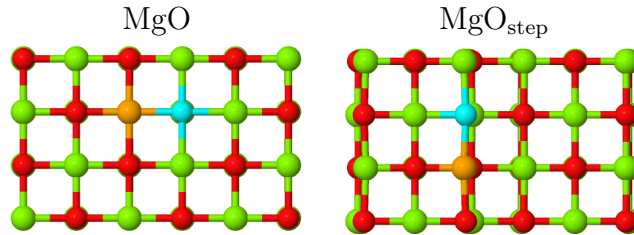
Figure 7: The considered individual atoms for flat and stepped MgO. The LDOS is given to the single light blue O atom and to the single orange Mg atom. Rest of the atomic color codes are as in figure 5.

The LDOS plots for a flat MgO surface and a stepped MgO surface are given in figure 8. There is a clear difference between the LDOS and the p-band centers for the single O atoms. In the flat surface the top O atom has a similar LDOS to the LDOS of all oxygen atoms indicating that there are only small differences between the different oxygen atoms. The LDOS for the oxygen atom at the step edge on the other hand differs more from the LDOS of all O atoms. The step O atom has a LDOS with a clear peak near the edge of the MgO band gap. This difference is also seen in the calculated O p-band centers. For both surfaces the p-band center for all O atoms is close to -3.4eV. The top O atom has a p-band center near -3.1eV while the edge O atom has a p-band center at -2.6eV. Values of the p-band centers are in agreement with the observed relation between the band center and the coordination number of an atom. The band center for a surface atom is closer to the Fermi energy when the atom has a low coordination number [35]. Comparison of the individual Mg atoms shows only small differences between the terrace and step sites and in both systems the s- and p-band centers for all Mg atoms are almost equal.

H adsorption on a flat MgO surface or on a stepped MgO surface shifts the edge of the band gap to a lower energy as seen in figure 9. The edge of the band gap is close to -3.4eV for a flat and -3.0eV for a stepped surface. In both cases the p-band center for the studied O atom shifts away from the Fermi energy and is clearly at a lower energy than the p-band center of all O atoms. The LDOS of the top O atom at the H adsorption site has a peak close to -7.4eV. The LDOS for the edge O atom has no clear peaks.

The LDOS plots for OH adsorption on flat and stepped MgO surfaces are given in the same figure. The edge of the MgO band gap is close to the Fermi energy in both cases. The top O atom has a similar LDOS compared to the LDOS of all O atoms with a slight shift towards the Fermi energy. The edge O atom has a LDOS with a stronger shift

MgO   MgO$_{step}$
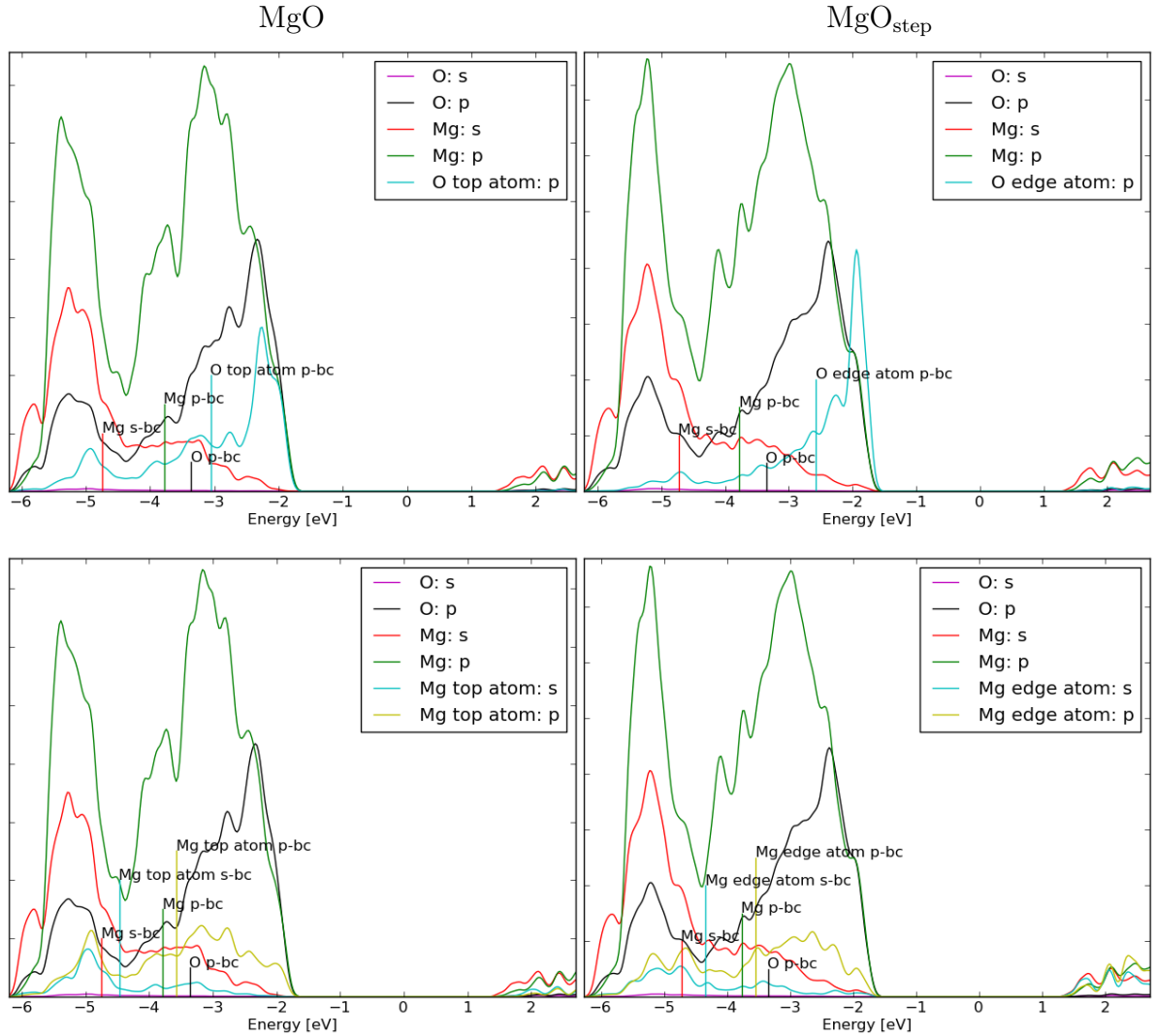
Figure 8: The local density of states given in arbitrary units on the y-axis for a bulk MgO surface with and without a step type defect. The left (right) figures are for a flat (stepped) MgO surface. The top (bottom) figures show the LDOS plots for the individual O (Mg) atoms. The LDOS has been multiplied by 25 for the individual O atoms and by 50 for the individual Mg atoms for easier visibility.

towards the Fermi energy. The p-band centers calculated for all the surface O atoms are close to each other. The band centers obtained for all Mg atoms are also close to equal in both cases.

Figure 10 shows the LDOS plots for dissociative water adsorption on flat and a stepped MgO surfaces. The p-band center for the top O atom at is close to -5.1eV while the p-band center for the edge O atom is near -4.4eV. The LDOS for the adsorbed OH on the flat surface shows three distinct peaks while the LDOS of OH adsorbed on a stepped surface has no clear peaks. The edge of the MgO band gap is about 0.2eV closer to the Fermi energy for the stepped surface.

Water spontaneously dissociated on a stepped MgO surface thus no comparative plot for molecular adsorption is given. The adsorbed water molecule causes the p-band center of the top O atom to shift to a lower energy. The p-band center for all oxygen atoms is almost the same as for the bare surface. The LDOS of the water molecule shows a similar
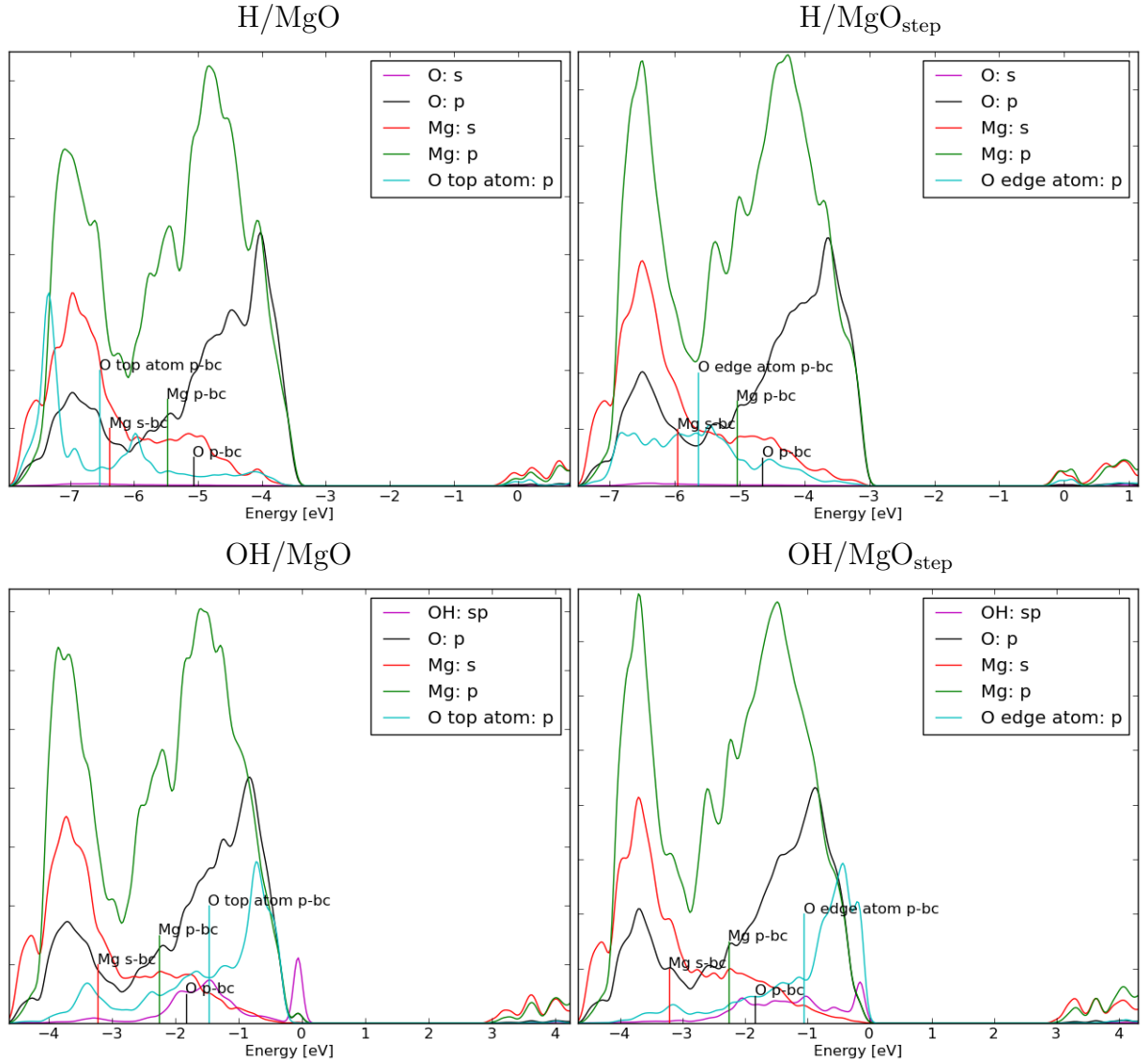
Figure 9: The local density of states given in arbitrary units on the *y*-axis for H and OH adsorbed on a bulk MgO surface with and without a step type defect. Top (bottom) figures show the LDOS plots for the surfaces with H (OH) adsorbed. The LDOS has been multiplied by 25 for the individual O atom for easier visibility.

peak below -6.0eV as the LDOS of the OH in the dissociative adsorption. The largest differences between the surfaces are in the p-band centers for the single O atoms. These band centers are summarized in figure 11.

The increased reactivity towards water dissociation on the stepped surface can be associated with the shift in the p-band center of the step O atom. Figure 12 shows that the H adsorption energy to the different surfaces depends almost linearly on the p-band center of the O atom at the H adsorption site. This can be seen as analogous to the d-band model for metal surfaces [36]. In the d-band model the differences in reactivity between different metal surfaces are attributed to the different coupling to the d-band. The coupling of the adsorbate to the narrow d-band leads to a formation of bonding and anti-bonding states. The higher the d-band center is the more anti-bonding states are above the Fermi level and unoccupied. Thus a higher d-band center correlates with a tighter binding of adsorbate on the surface. In this case the sharp peaks formed by the

23
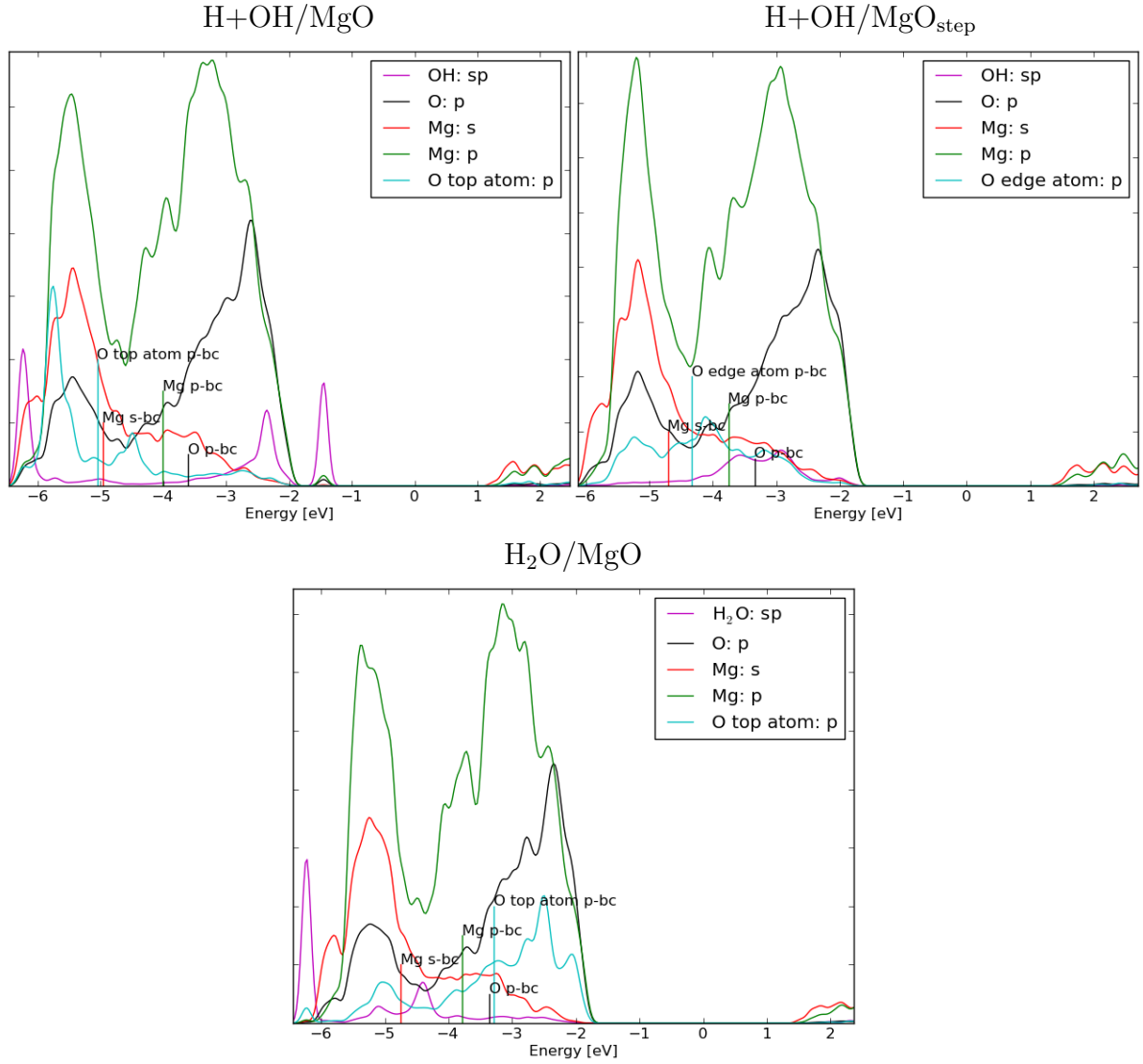
Figure 10: The local density of states given in arbitrary units on the y-axis for H and OH adsorbed on a bulk MgO surface with and without a step type defect. The top figures show the LDOS plots for the surfaces with H and OH adsorbed. The bottom figure shows the LDOS plot for a flat surface with water adsorbed. The LDOS has been multiplied by 10 for the adsorbed OH and H_2O, and by 25 for the individual surface O atom for easier visibility.

LDOS of the single O atoms at the H adsorption site can be seen as an analogy for the narrow d-band. The coupling of H to the rest of the surface states can be approximated as similar in all considered surfaces and the difference in the adsorption energy arises from the location of the p-band of the O atom at the H adsorption site. Thus the higher the p-band center of the O atom at the H adsorption site the more anti-bonding states remain unoccupied and the lower the adsorption energy.
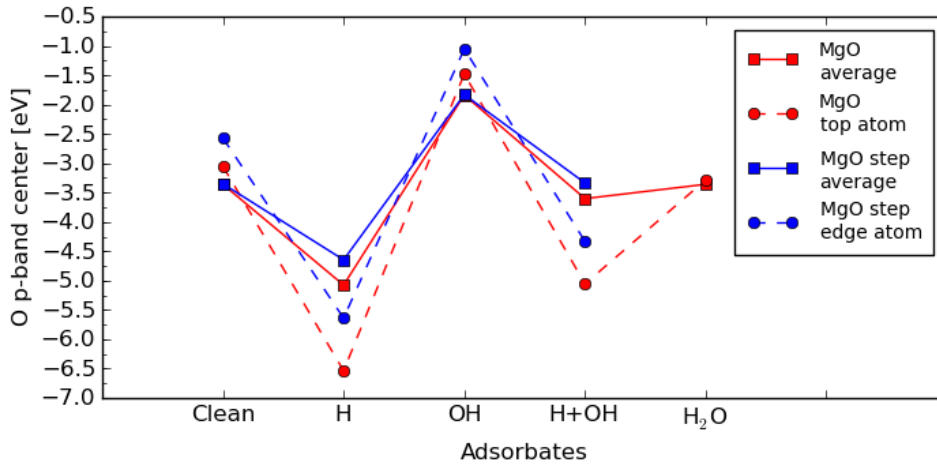
Figure 11: Values of the oxygen p-band centers for a flat and a stepped bulk MgO surfaces. The p-band centers for a flat (stepped) surface are given in red (blue). The circles connected with a dashed line show the p-band centers calculated to an O atom at the H adsorption site and the squares connected with a solid line show the p-band centers calculated from the LDOS of all surface oxygen atoms. All the p-band centers are given as the energy difference from the Fermi energy.
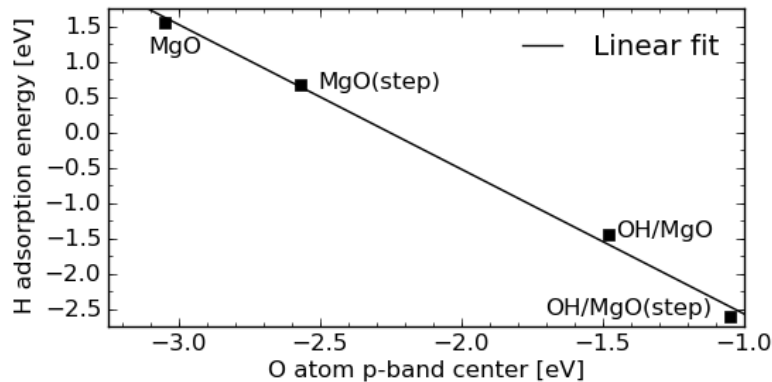
Figure 12: The H adsorption energies as a function of the oxygen atom p-band centers at the H adsorption site. The adsorption surfaces are given beside each point. The stepped surfaces are noted with (step) and OH indicates the H adsorption to the same computational cell with a hydroxyl group. The solid line is a linear fit to the data.

7 Water dissociation on an Ag supported MgO film

7.1 Setting up an Ag supported MgO film

The support metal was modeled with three atomic layers and the thickness of the MgO thin film was two atomic layers. The surface structure was allowed to fully relax while the bottom Ag layer was frozen to the bulk geometry. The step layer had a 0.5ML coverage and the relaxed structures are shown in figure 13. The stepped MgO thin film is stretched compared to the flat MgO film. This is seen in the increased MgO-Ag distance underneath the step layer. Distortion of the film has a local nature because the average distance between MgO and Ag is 2.65Å for the stepped and flat MgO film. The step layer

is also compressed from the step edges. Atoms at the opposite side of the step are closer to each other compared to the atoms in the flat MgO film. The support metal gains a negative Bader charge of 0.58 electrons and the flat MgO film is charged positively by 0.59 electrons. The charge transfer between MgO and Ag is similar with the stepped MgO film. The support metal gains a negative Bader charge of 0.65 electrons and the stepped MgO film is charged positively by 0.65 electrons.
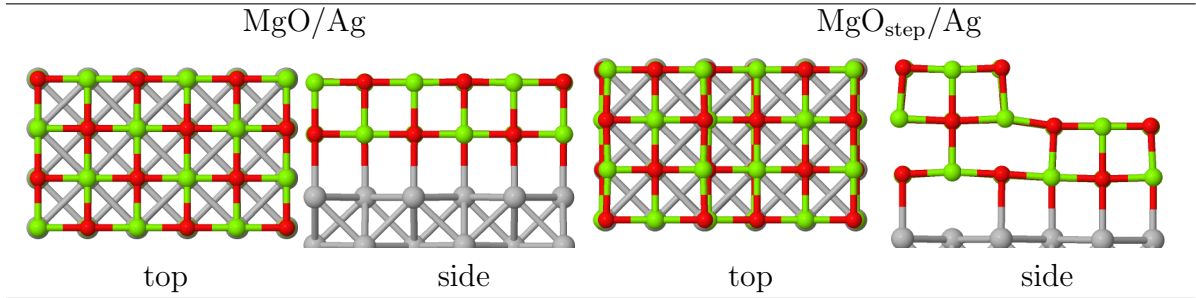
Figure 13: The relaxation geometry for an Ag supported 2ML MgO thin film with and without a step defect. Top and side views are denoted with top and side. The atomic color code for Ag is light gray and the rest are as in figure 5.

7.2 Adsorption of H, OH and water on a flat MgO/Ag surface
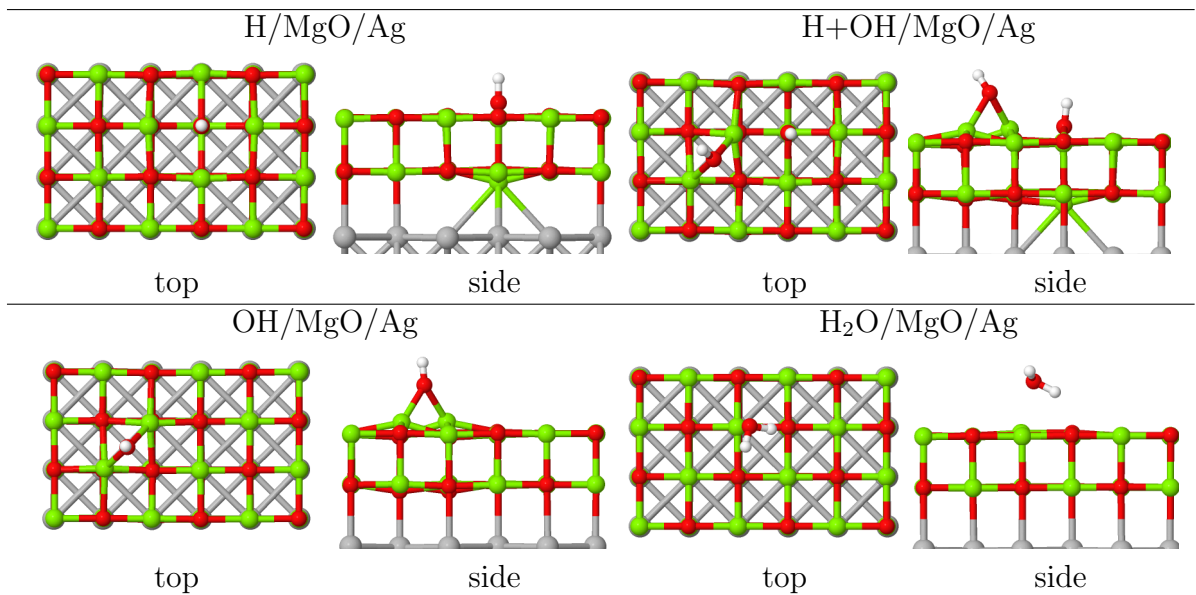
Figure 14: The relaxation geometries for a water molecule and its dissociation products H and OH adsorbed on a flat MgO/Ag surface. Top and side views are denoted with top and side. The atomic color codes are the same as in figure 13.

Water dissociation on an Ag supported flat MgO film was studied by considering the adsorption of water and its dissociation products H and OH. The preferred adsorption sites were taken from ref [7]. The adsorption of water on a flat MgO/Ag surface is exothermic. The adsorption of H and OH is slightly endothermic both far apart and close to each

Table 5: The adsorption energies and atomic distances for the adsorption of water and its dissociation products H and OH on a flat MgO/Ag surface. The distance $d_{MgO,Ag}$ is the difference between the average z-coordinate for the Ag top layer and the MgO bottom layer. The distance between the top and bottom layer of MgO film $d_{1st,2nd}$ is calculated similarly. The distance $d_{H,O}$ is the minimum distance between the adsorbed H and a surface O. The distance $d_{O,Mg}$ is the minimum distance between a surface Mg atom and the O in the water molecule or the hydroxyl group.

	E_{ads}	$d_{H,O}$	$d_{O,Mg}$	$d_{1st,2nd}$	$d_{MgO,Ag}$
MgO/Ag				2.18	2.65
H/MgO/Ag	0.29	0.98		2.22	2.68
OH/MgO/Ag	0.21		2.07	2.22	2.61
H+OH/MgO/Ag	0.23	0.98	2.06	2.27	2.67
H_2O/MgO/Ag	-0.42		2.25	2.18	2.67

other. The adsorption energies for H and OH are decreased compared to adsorption on a bulk MgO surface indicating stronger binding on the MgO/Ag surface.

The relaxation geometries for different adsorbates are given in figure 14. H adsorbs on an O-top site and the interlayer distance between the two MgO layers is increased to 2.22Å mostly due to the increased distance between the formed surface OH group and the bottom layer Mg atom. The OH group is adsorbed to a bridge site between two surface Mg atoms. The adsorption of OH also increases the interlayer distance between the two MgO layers to 2.22Å. When H and OH are co-adsorbed the interlayer distance is 2.27Å which is clearly larger than the distance 2.18Å for the bare MgO/Ag surface. In the molecular water adsorption the interlayer distance is the same as for the clean surface. The decreased interlayer distance in the molecular adsorption correlates with the decreased adsorption energy. The atomic distances together with the adsorption energies are given in table 5.

Table 6: The Bader charges for adsorbates in the adsorption of water and its dissociation products H and OH on a flat MgO/Ag surface. The charges for H and OH are for the dissociated water molecule. The charge of the intact molecule is not given. The Bader charges for MgO and Ag are the total charges.

	q(H)	q(OH)	q(MgO)	q(Ag)
MgO/Ag			0.59	-0.58
H/MgO/Ag	0.53		0.66	-1.18
OH/MgO/Ag		-0.88	0.99	-0.10
H+OH/MgO/Ag	0.54	-0.88	0.99	-0.64
H_2O/MgO/Ag			0.65	-0.58

The Bader charges of the adsorbates are given in table 6. H is charged positively and the charge transfer is larger compared to the H adsorption on the bulk MgO surfaces. This additional charge transfer correlates with a more negative adsorption energy and could be viewed as increased binding on the surface. The adsorbed OH is negatively charged and the charge transfer to the adsorbed OH is larger compared to the OH adsorption on

a bulk MgO surface. The additional charge transfer again correlates with a more negative adsorption energy. The charge from the adsorbed H is transfered to the support metal while the charge is transfered from the support metal in the OH adsorption. When H and OH are co-adsorbed the charge transfer towards adsorbed OH is mainly from the adsorbed H. The charge of the support metal in this case is close to the charge of Ag for a bare MgO/Ag surface.

7.3 Adsorption of H, OH and water on a stepped MgO/Ag surface
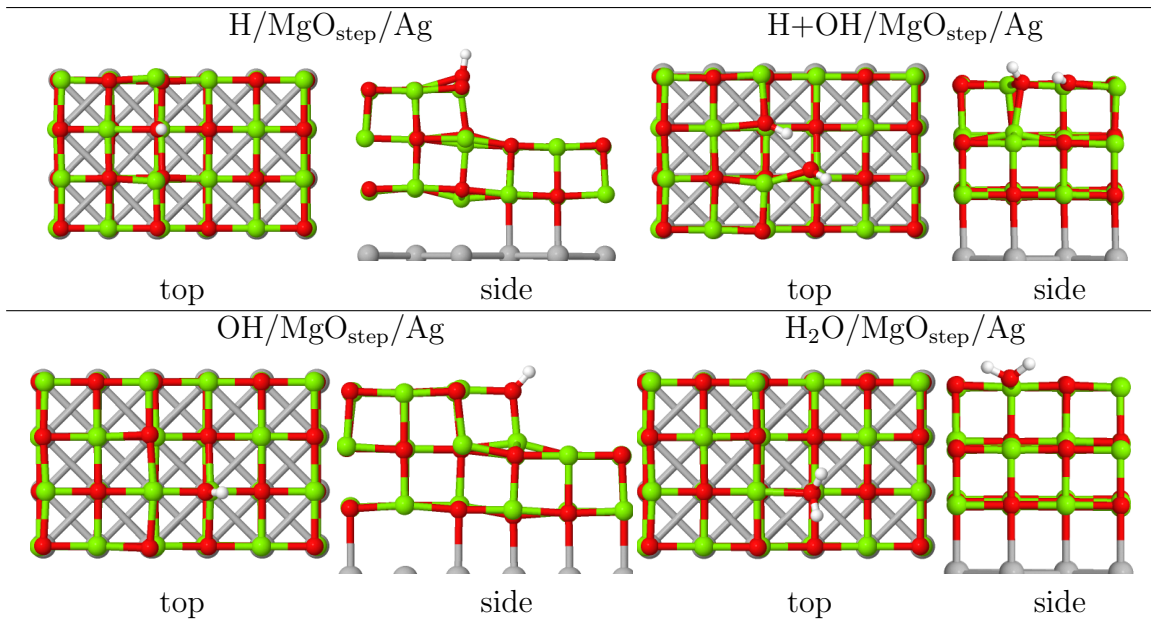
Figure 15: The relaxation geometries for a water molecule and its dissociation products H and OH adsorbed on a stepped MgO thin film supported by Ag. Top and side views are denoted with top and side. The atomic color codes are the same as in figure 13.

The water dissociation on an Ag supported stepped MgO film was studied by considering the adsorption of water and its dissociation products H and OH. The preferred adsorption sites for H and OH were taken from ref [7]. The molecular adsorption of water is exothermic but the dissociative adsorption is clearly energetically favorable. The adsorption energies for H and OH in individual unit cells are less negative than in the co-adsorption, indicating a similar attractive interaction between the adsorbed H and OH as seen on the stepped bulk MgO surface. The adsorption energies are given together with the atomic distances in table 7.

Water spontaneously dissociates on the stepped MgO thin film depending on the initial geometry of the water molecule. In molecular adsorption it is adsorbed on a Mg-top site with the H atoms turned away from the step edge. H adsorbs on a edge O atom as shown in figure 15. The interlayer spacing is increased in the H adsorption. The O atom at the H adsorption site moves upward and the Mg atom underneath moves down. The OH group adsorbs on a Mg-top site next to a edge Mg atom. The H atom in the OH group faces away from the step along the MgO film similarly as in the surface OH group formed in H adsorption. When H and OH are co-adsorbed the alignment of the H atoms is different.

Table 7: The adsorption energies and atomic distances for the adsorption of water and its dissociation products H and OH on a stepped MgO/Ag surface. The distance $d_{step,1st}$ is the difference between the average z-coordinate for the MgO step layer and the first complete MgO layer. The distances $d_{1st,2nd}$, $d_{MgO,Ag}$ and $d_{O,Mg}$ are as in table 5.

	E_{ads}	$d_{O,Mg}$	$d_{step,1st}$	$d_{1st,2nd}$	$d_{MgO,Ag}$
MgO_{step}/Ag			2.25	2.19	2.65
$H/MgO_{step}/Ag$	0.01		2.36	2.23	2.67
$OH/MgO_{step}/Ag$	-0.75	1.98	2.26	2.22	2.64
$H+OH/MgO_{step}/Ag$	-1.68	1.99	2.25	2.21	2.69
$H_2O/MgO_{step}/Ag$	-0.77	2.13	2.26	2.19	2.67

Table 8: The Bader charges for adsorbates in the adsorption of water and its dissociation products H and OH on a stepped MgO film. The charges for H and OH are for dissociated water molecule. The charge of the intact water molecule is not given. The Bader charges for MgO and Ag are the total charges.

	q(H)	q(OH)	q(MgO)	q(Ag)
MgO_{step}/Ag			0.65	-0.65
$H/MgO_{step}/Ag$	0.54		0.62	-1.16
$OH/MgO_{step}/Ag$		-0.87	0.96	-0.08
$H+OH/MgO_{step}/Ag$	0.62	-0.85	0.85	-0.61
$H_2O/MgO_{step}/Ag$			0.66	-0.62

The adsorbed H is turned towards the O atom in the adsorbed OH and H in the adsorbed OH group is turned away from the adsorbed H similarly as on the stepped bulk MgO surface. The distance between adsorbed H and the O in the adsorbed OH group is 1.79Å.

The Bader charges for adsorbates on a stepped MgO/Ag surface are given in table 8. The adsorbed H is charged positively and Ag obtains most of the charge. The total charge of the MgO film remains almost constant in the H adsorption. In the OH adsorption the charge is transfered from the support metal and the MgO film to OH. When H and OH are co-adsorbed the charge transfer occurs mainly between H and OH as seen in the integrated density difference plots given in figure 16. The integrated density difference plots show a polarization of the MgO film when H and OH adsorb far apart. When H and OH are co-adsorbed there is almost no charge transfer before the MgO top layer shown by the rightmost green vertical line. The charge transfer directly from the adsorbed H to the adsorbed OH correlates with the more negative adsorption energy indicating attractive electrostatic interaction between the adsorbates.
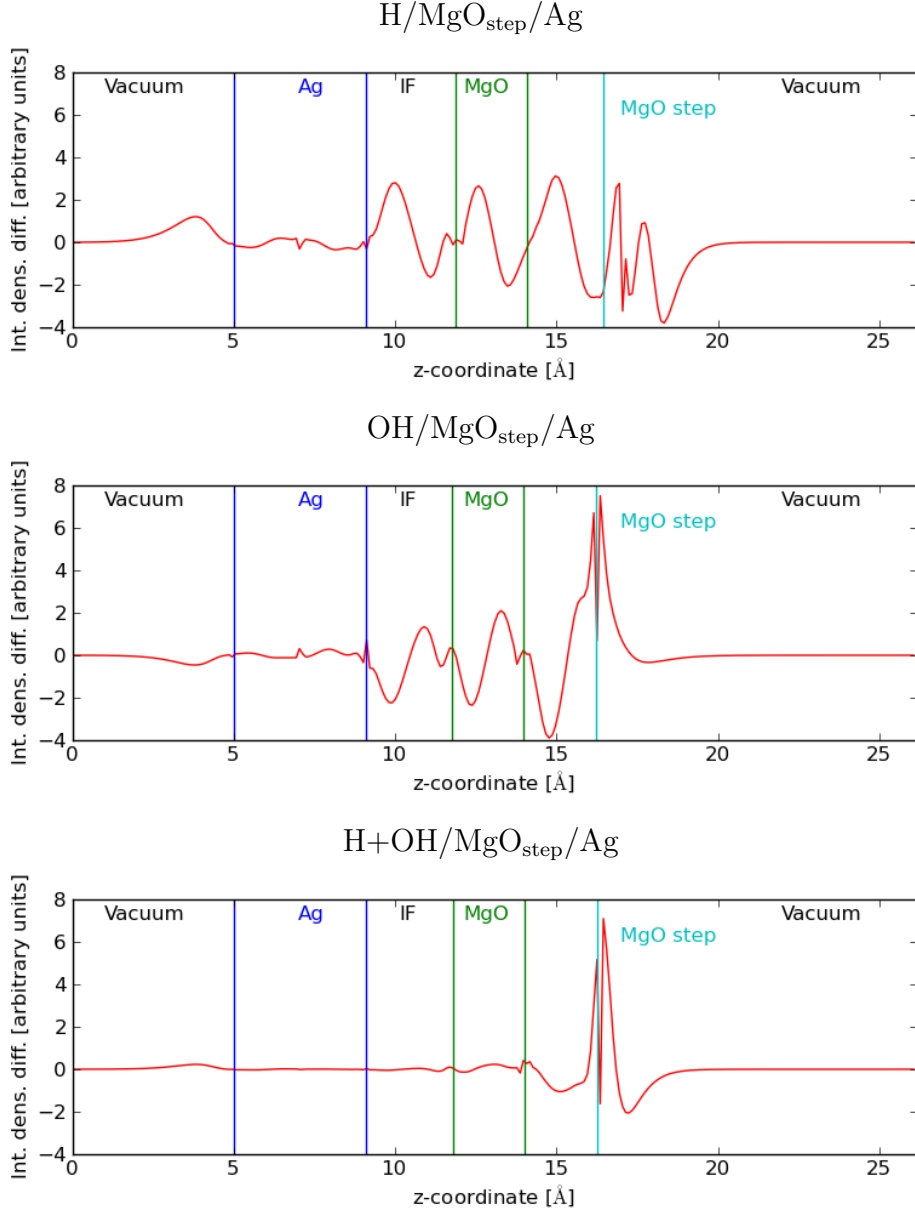
Figure 16: The integrated density difference plots for the adsorption of H and OH on a stepped MgO/Ag surface. The average z-coordinate of the top and bottom Ag layers are given in blue, the top and bottom MgO layers are given in green and the average z-coordinate for the step layer is given as a light blue vertical line. The interface between Ag and MgO is noted with IF.

7.4 LDOS comparison between flat and stepped MgO/Ag surface

Clear differences in the electronic structures between flat and stepped bulk MgO surfaces were seen in the previous section. The main difference was in the p-band center of the single O atom at the H adsorption site. In this section a similar electronic structure comparison is made for the MgO thin film surfaces. Again the LDOS of a single O atom at the H adsorption site is considered individually for both surfaces. The LDOS plots for the single Mg atoms at the top and step layer are not shown for other cases than the clean MgO/Ag surfaces, since no significant differences in the electronic structures were

found between surfaces.
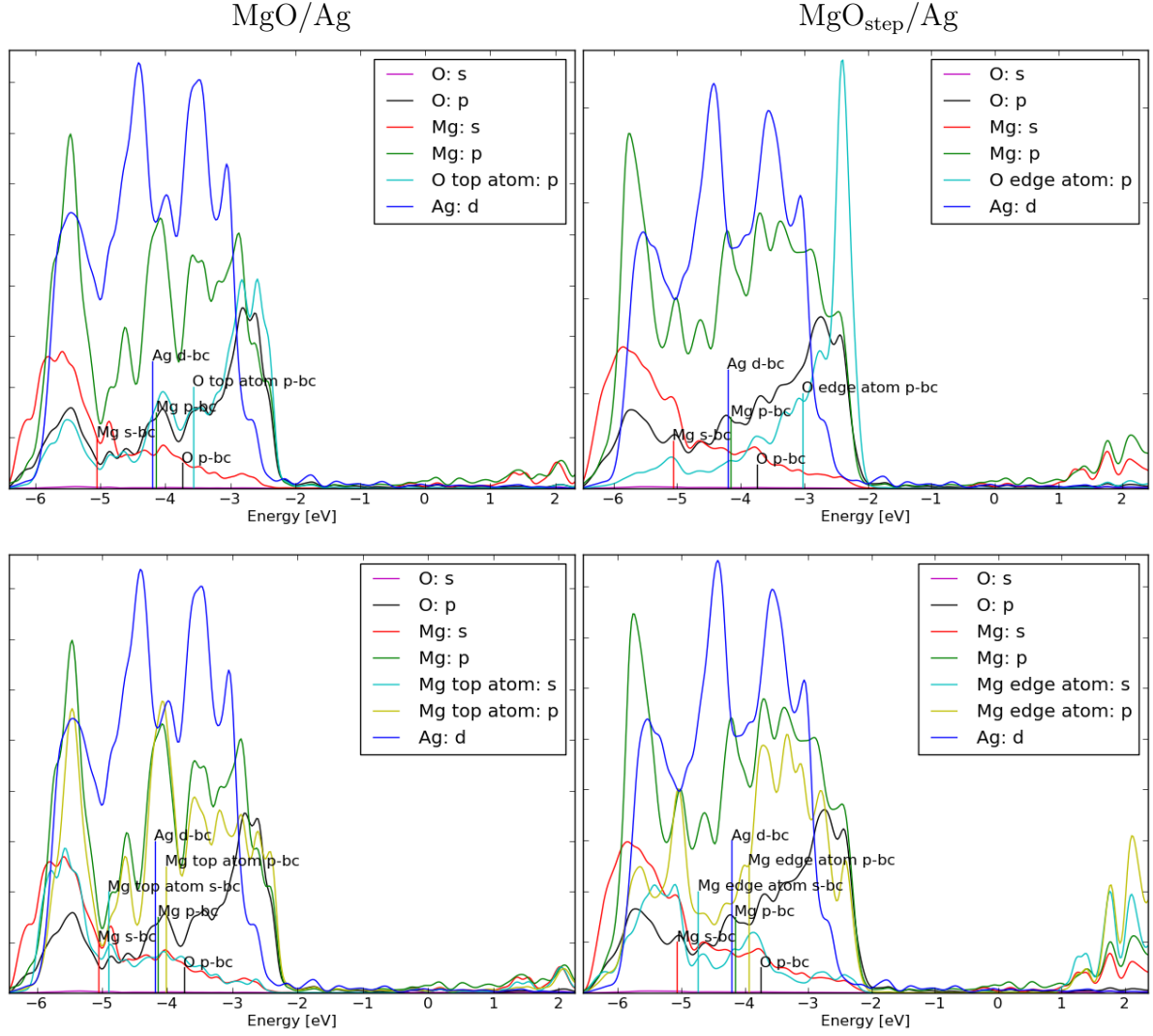
Figure 17: The local density of states given in arbitrary units on the *y*-axis for an Ag supported MgO film with and without a step type defect. The left (right) figures are for a flat (stepped) MgO film. The upper (lower) figures show the LDOS for the individual O (Mg) atoms. The LDOS has been multiplied by 25 for the individual O atoms and by 50 for the individual Mg atoms for easier visibility.

The LDOS plots for bare surfaces are given in figure 17. There is again a clear difference between the LDOS and the p-band centers of the single O atoms. The top O atom has a similar LDOS as the LDOS of all O atoms, indicating that there are only small differences between the different surface O atoms. The LDOS for the edge O atom differs from the all-O LDOS. The edge O atom has a LDOS with a large peak near the edge of the MgO band gap. The difference is also seen in the calculated p-band centers. For both surfaces the p-band center for all O atoms is close to -3.7eV. The top O atom at has a p-band center near -3.6eV whereas for the edge O atom the p-band center is $\sim -3.0\text{eV}$. Comparison between the individual Mg atoms shows only small differences in the occupied states below the Fermi energy.

Figure 18 shows the LDOS plots for H adsorption on flat and step surfaces. In both cases the edge of the MgO band gap shifts to a lower energy together with the p-band
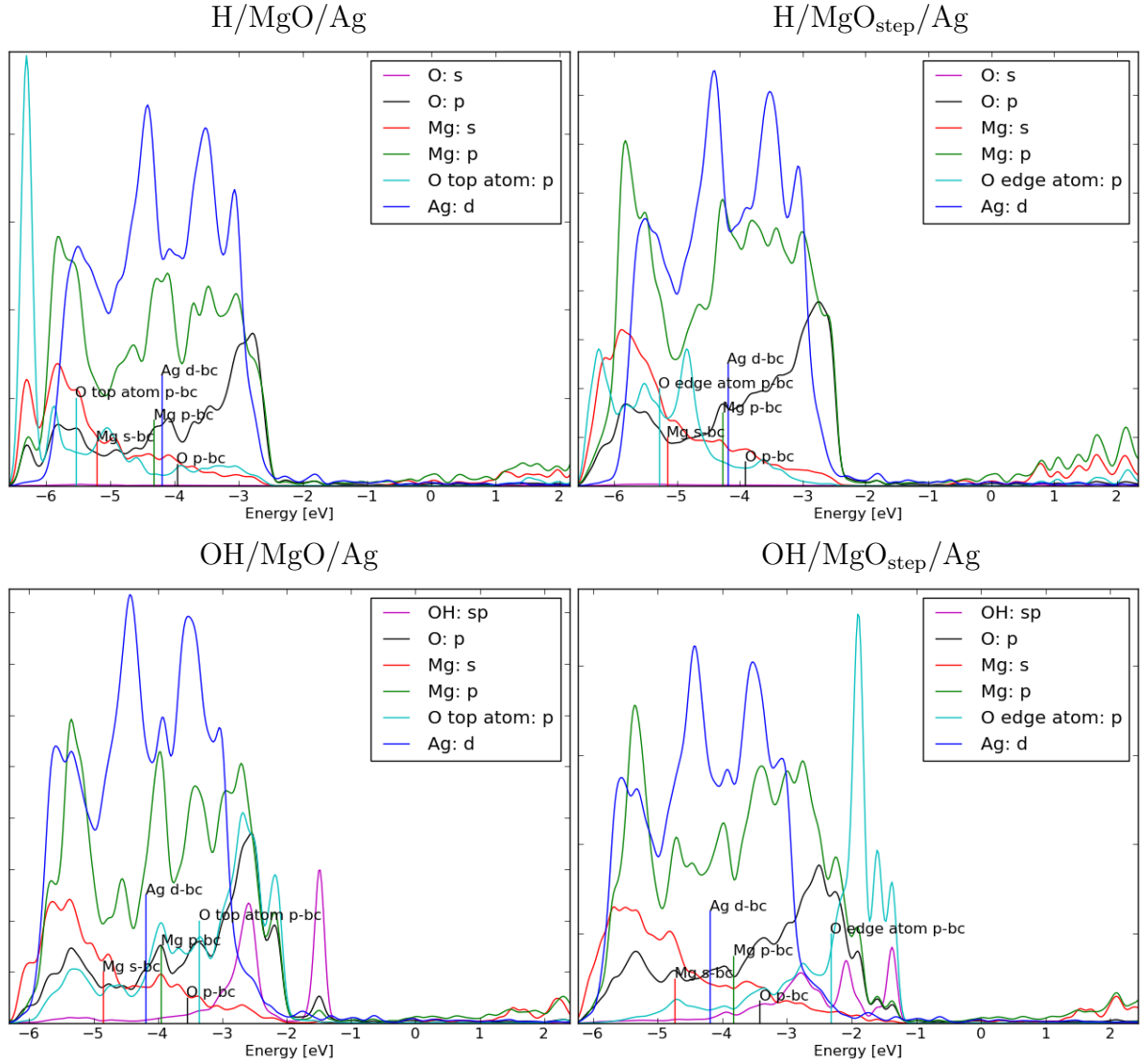
Figure 18: The local density of states given in arbitrary units on the *y*-axis for H and OH adsorbed on a MgO/Ag surface with and without a step type defect. The left (right) figures are for a flat (stepped) MgO film. The LDOS has been multiplied by 25 for the individual O atoms for easier visibility.

center of all O atoms compared to the bare surfaces. The top O atom at the H adsorption site has a sharp peak close to -6.3eV and the p-band center of that atom is clearly at a lower energy than the p-band center of all O atoms. The LDOS of the edge O atom has no clear peaks. The p-band center for the edge O atom is also at a significantly lower energy than the p-band center calculated for all O atoms.

The LDOS plots for a flat and a stepped surfaces with OH adsorbed on the respective adsorption sites are shown in the same figure. Again the LDOS for the top O atom has a similar LDOS to the LDOS of all O atoms. The edge O atom has a LDOS with three distinct peaks close to the edge of MgO band gap. The difference between the p-band centers is also clear. The p-band center for the edge O atom is close to -2.3eV while the p-band center of all O atoms is near -3.4eV. A change towards the Fermi energy is also seen for the flat MgO film. In that case the p-band center for all O atoms is about -3.6eV and the p-band center is -3.4eV for the top O atom.
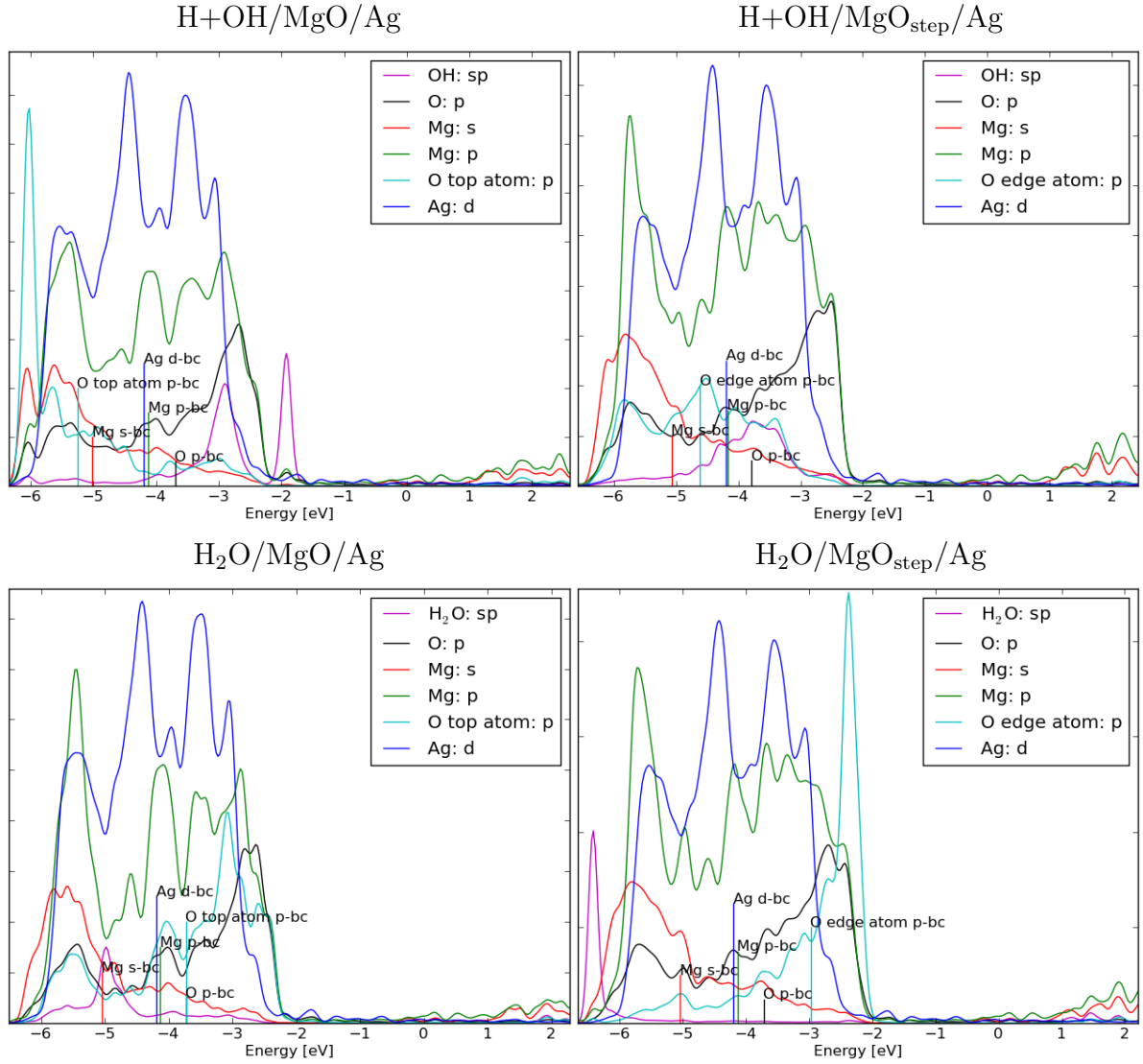
Figure 19: The local density of states given in arbitrary units on the y-axis for water adsorbed on an Ag supported MgO film with and without a step type defect. The left (right) figures are for a flat (stepped) MgO film. The upper (lower) figures are for dissociative (molecular) adsorption. LDOS has been multiplied by 10 for the adsorbed OH and by 25 for the individual O atoms for easier visibility.

Figure 19 shows the LDOS in molecular and dissociative water adsorption. For dissociative adsorption on the flat surface the LDOS of the adsorbed OH shows two peaks around the edge of the MgO band gap similarly as for the OH/MgO/Ag. In the step surface the peaks for OH have vanished when H is co-adsorbed. The individual O atoms at the site of H adsorption show a similar LDOS as in the H adsorption far apart from OH.

In molecular adsorption the p-band center for the top O atom is at a slightly lower energy compared to the p-band center of all O atoms. For the step surface the LDOS and the p-band center for the edge O atom resemble the LDOS and the p-band center of a clean step surface. The edge O atom has a large peak near the beginning of the MgO band gap. The LDOS for the adsorbed water molecule has a sharp peak close to $-6.5\,\mathrm{eV}$ on the step surface and a wider peak close to $-5.0\,\mathrm{eV}$ on the flat surface.

The largest differences between the stepped and the flat surfaces are again in the O p-band centers. The values of the O p-band centers for the different surfaces and different adsorbates are shown in figure 20.
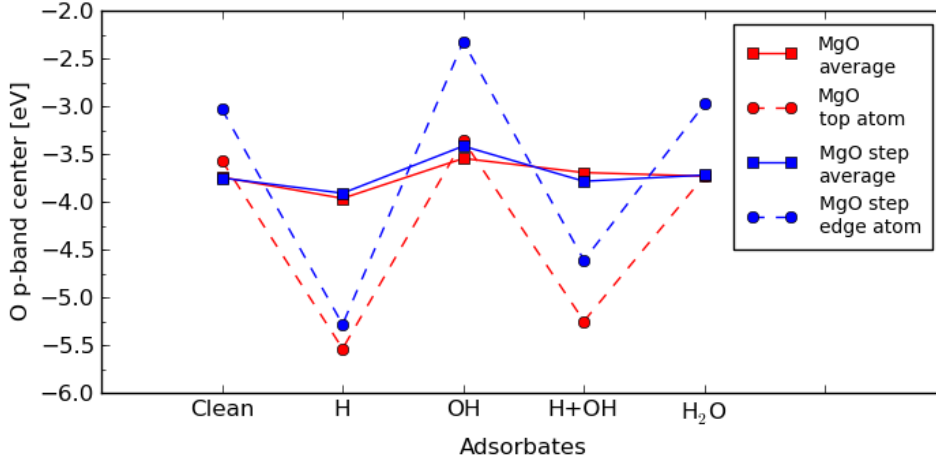
Figure 20: The O p-band centers for a flat and stepped MgO/Ag surface. The values for a flat (stepped) surface are given in red (blue). The circles connected with a dashed line show the values of the p-band centers calculated to the O atom at the H adsorption site and the squares connected with a solid line show the values of the p-band centers calculated from the LDOS of all the surface oxygen atoms. All p-band centers are given as the energy difference from the Fermi energy.

The correlation between H adsorption energy and the p-band center of the O atom at the H adsorption site is no longer linear for the Ag supported thin film. There is still a similar trend for the H adsorption energy as seen on the bulk surface. The p-band center is higher for the edge O atom and it corresponds to a more negative H adsorption energy. The H adsorption energy as a function of the p-band center of O atom at the H adsorption site is shown in figure 21. The non-linearity is due to the increased MgO film thickness of the stepped surface. The binding of adsorbed H is weaker on the three layers thick stepped surface compared to the two layers thick flat surface. This causes the H adsorption energies to be higher for the stepped surface.

The p-band center of all O atoms in a flat MgO/Ag surface correlates linearly with the charge difference between the summed charge of adsorbates on the surface and the charge of the support metal. The values together with a linear fit are shown in the figure 22. The charge difference between adsorbates and Ag is defined as $q(\mathrm{Ag}) - \sum q(\mathrm{X}_i)$, where $q(\mathrm{Ag})$ is the Bader charge of all Ag atoms and the sum is over all adsorbates i with a Bader charge $q(\mathrm{X}_i)$. The Bader charges are given as deviations from the neutral atoms. The correlation is no longer linear for the stepped MgO/Ag surface since the H and OH co-adsorption is anomalous but a similar trend can be seen as shown in figure 23.
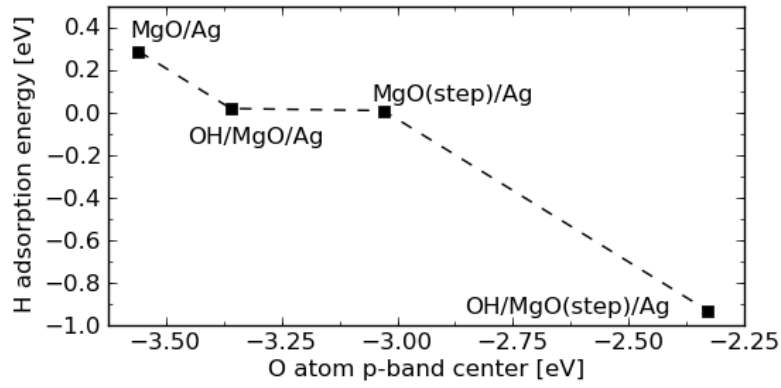
Figure 21: The H adsorption energies as a function of the individual oxygen atom p-band centers at the H adsorption site. The adsorption surfaces are given beside each point. The stepped surfaces are noted with (step) and OH indicates H adsorption to the same computational cell with a hydroxyl group.
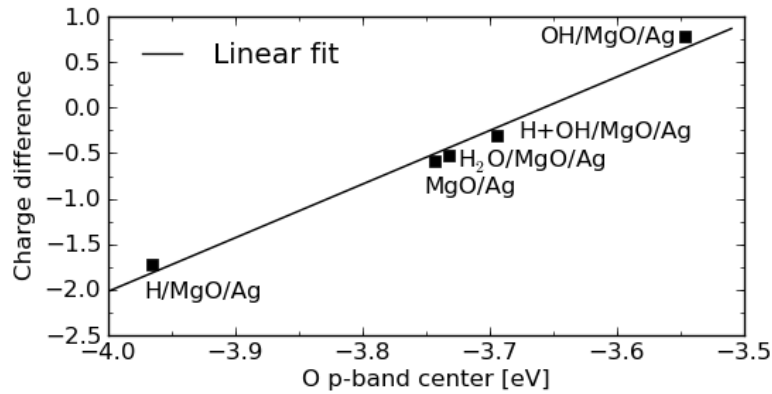
Figure 22: The charge difference between surface adsorbates and the support metal for a flat MgO/Ag surface as a function of the p-band center calculated from the LDOS of all surface O atoms. The corresponding system is given beside each point. The solid line is a linear fit to the data.
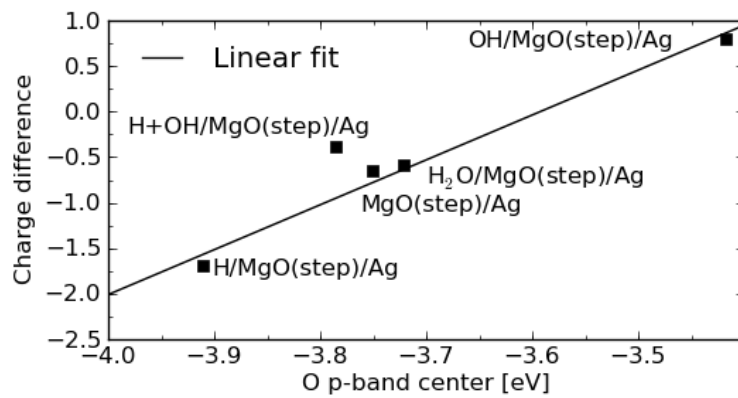
Figure 23: The charge difference between surface adsorbates and the support metal for a stepped MgO/Ag surface as a function of the p-band center calculated from the LDOS of all surface O atoms. The corresponding system is given beside each point. The solid line is a linear fit to the data with H+OH point excluded.

7.5   Interaction energies between OH-OH and O-H₂O
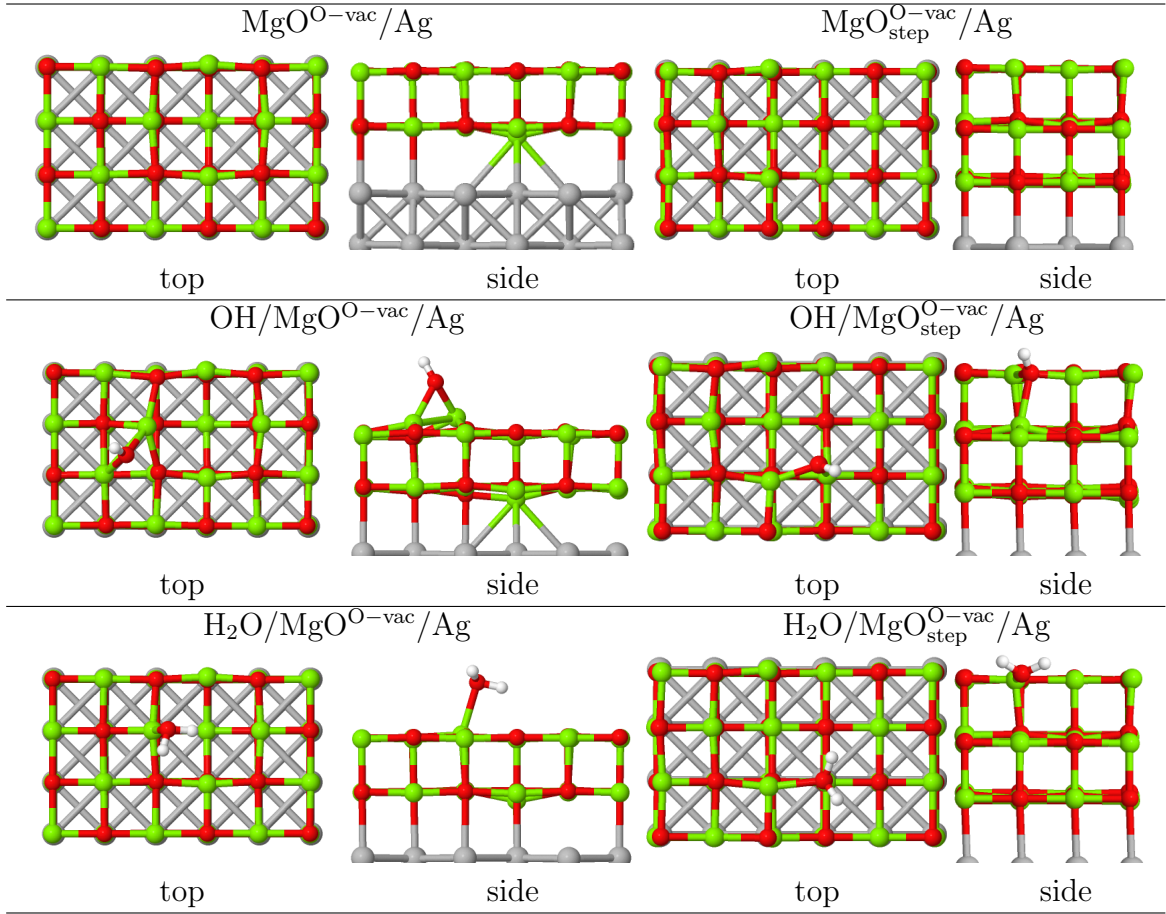
Figure 24: The relaxation geometries for the reference systems needed in the calculations of presented interaction energies. Top and side views are denoted with top and side. The atomic color codes are the same as in figure 13.

The interaction energies between $OH - OH$ and $O - H_2O$ on a flat and a stepped MgO/Ag surfaces were calculated in order to characterize the role of direct interactions between the adsorbates. For $OH - OH$ the studied interactions are between the adsorbed OH and the surface OH. In this case there are two low coverage adsorbate configurations. The first configuration has only the surface OH adsorbed. This is the same system as H adsorbed on a MgO/Ag surface. The second configuration has the OH adsorbed adjacent to a surface O-vacancy. For adsorbates $O - H_2O$ the studied interactions are between the adsorbed H_2O and an edge or top oxygen. Again there are two low coverage configurations. The first configuration has an oxygen adsorbed on the O-vacancy leaving just the plain surface. The second configuration has the H_2O adsorbed adjacent to a surface O-vacancy. The relaxation geometries for the needed reference systems are given in figure 24. The needed reference systems include the second low coverage cases where OH and H_2O are adsorbed next to a surface O-vacancy and the energies of flat and step surfaces with an O-vacancy.

The surface OH group and the adsorbed OH group on the step surface had an interaction energy of -0.20eV where the negative sign indicates binding between the adsorbates. On the flat surface the interaction energy between the surface OH and the adsorbed OH

was 0.10eV where the positive sign shows repulsion between the adsorbates. The interaction energy between an adsorbed water molecule and a step oxygen was 0.09eV and the interaction energy between an adsorbed water molecule and a top layer surface oxygen was −0.03eV.

7.6   Adsorption of CO and CO$_2$ on a stepped MgO/Ag surface

Since water dissociation can occur spontaneously on a stepped MgO/Ag surface the possibility of the rest of the WGS reaction occurring on the step was considered in terms of the adsorption energies of the intermediate species. The studied reaction mechanism was the carboxyl mechanism, deemed the most probable in the section 5. The adsorption of CO on the step layer and CO$_2$ on a Mg-top site at the step edge was studied. The possible formation of an intermediate species was also considered. The CO adsorbed on the Mg-top site of the step layer and when dissociated water was present a HCO$_2$ species was formed at the step edge. The energetically favored intermediate species was the formate HCO$_2$ and not the carboxyl HOCO. The relaxation geometries are given in figure 25. The CO was adsorbed with the C atom facing a Mg atom at the step edge. The adsorption energy for CO in this adsorption geometry was −0.25eV. The adsorption energy for CO$_2$ was −0.15eV indicating that CO$_2$ would probably desorb from the MgO film allowing the WGS reaction to occur. The intermediate HCO$_2$ species with H atom co-adsorbed had a combined adsorption energy of −3.02eV. The low adsorption energy could result into formation of a stable formate species and end the WGS reaction as suggested in ref [37] for an unsupported Ti$_2$O$_4$ nanoparticle. Figure 26 shows the adsorption energies for the intermediate species in the formate mechanism.

CO/MgO$_{step}$/Ag   HCO$_2$+H/MgO^{step}/Ag

top   side   top   side

CO$_2$/MgO$_{step}$/Ag

top   side
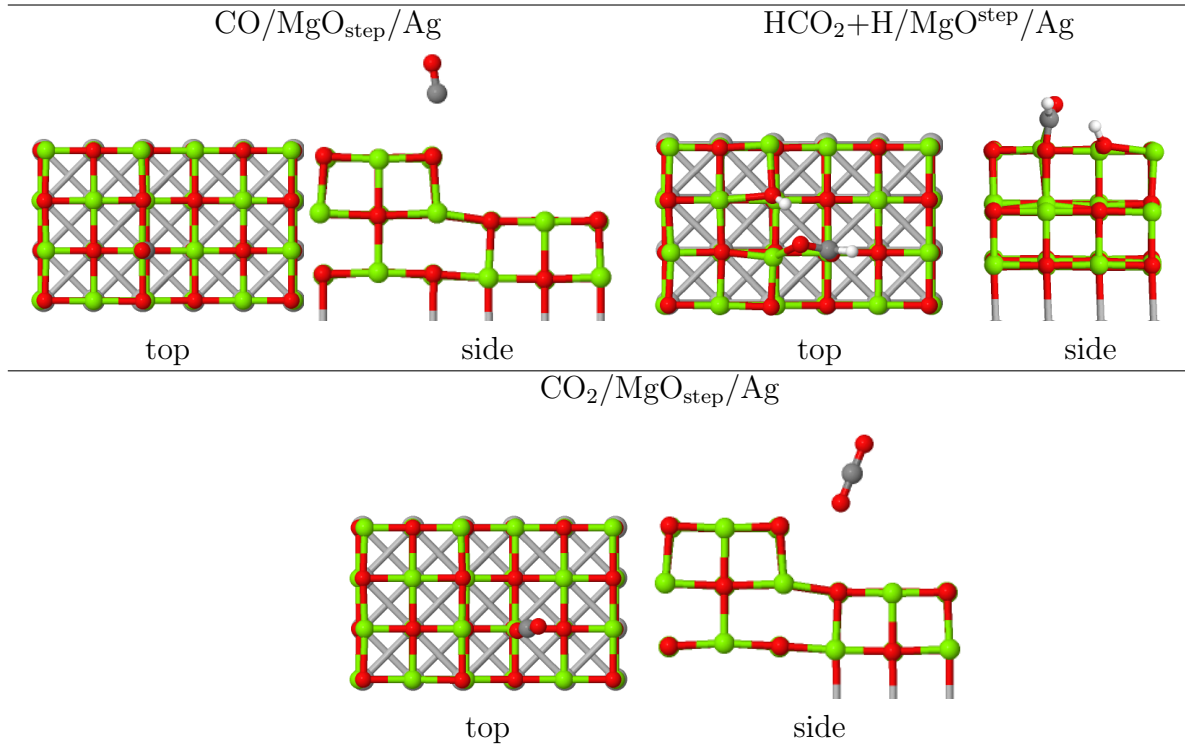
Figure 25: The relaxation geometries for CO, CO$_2$ and CO with H and OH adsorbed on a MgO/Ag step surface. Top and side views are denoted with top and side. The atomic color code for C is dark gray and rest are the same as in figure 13.
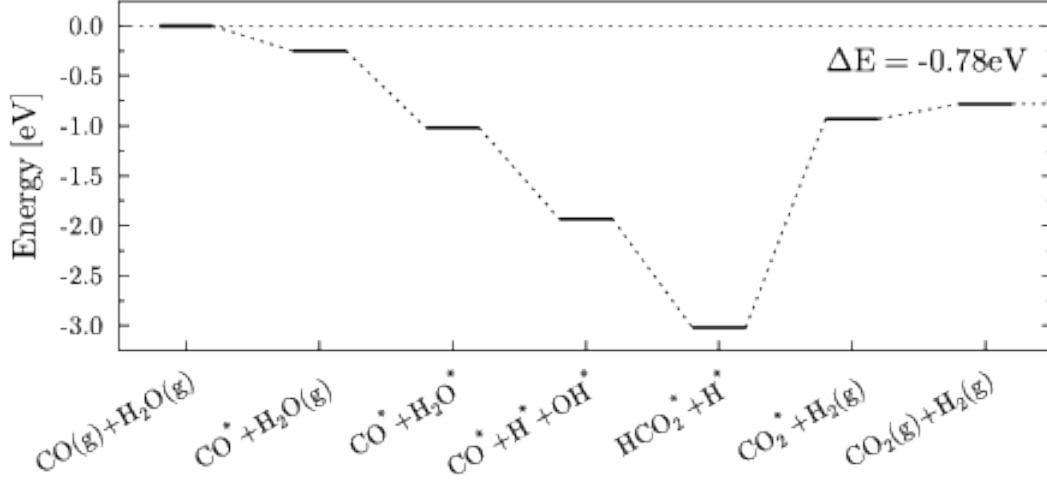
Figure 26: The adsorption energies for the intermediate species of the formate mechanism on stepped MgO/Ag surface. Gas-phase species are noted with g and adsorbed species with asterisk. Adsorbates H and OH are co-adsorbed in the fourth step as are HCO_2 and H on the fifth. Rest are far apart.

The Bader charge analysis for these adsorbates showed only negligible small charge transfer in the adsorption of CO and CO_2 as seen in table 9. The charge transfer was stronger in the case of HCO_2 and H adsorption. These charge transfers together with the adsorption energies indicate that CO and CO_2 do not interact strongly with the MgO/Ag surface. This is in agreement with the reported role of the Au cluster as the site of the CO adsorption [38].

Table 9: The Bader charges for CO, CO_2 and CO with H and OH adsorbed on a stepped MgO/Ag surface. The charge for H is for the individual atom. The Bader charges for MgO and Ag are the total charges.

	q(H)	q(CO)	q(MgO)	q(Ag)
$CO/MgO_{step}/Ag$		-0.06	0.73	-0.66
$CO_2/MgO_{step}/Ag$			0.61	-0.65
$HCO_2+H/MgO_{step}/Ag$	0.59		0.92	-0.61

8   Water adsorption and dissociation on Au/MgO/Ag

8.1   Setting up an Au stripe on an Ag supported MgO film

Au$_{\text{stripe}}$/ MgO/Ag

top   side
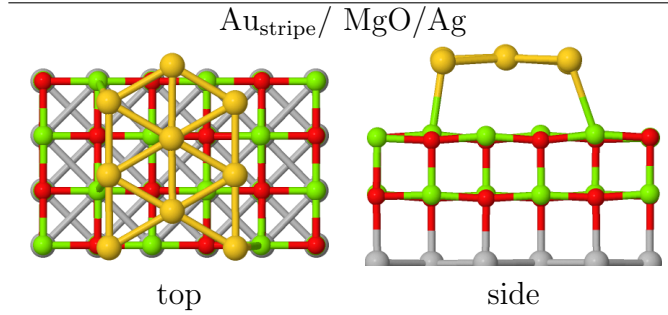
Figure 27: The relaxed structure of an Au stripe on a MgO/Ag surface. Top and side views are denoted with top and side. The atomic color code for Au is yellow and the rest are as in figure 25.

The Au stripe consisting of nine Au atoms in the unit cell was deposited on the relaxed MgO/Ag surface and the structure was allowed to fully relax with two bottom Ag layers frozen to the previously determined geometry. The relaxation geometry for the Au stripe on MgO/Ag is given in figure 27. The Au stripe models the edge of a large Au cluster on a MgO/Ag surface with less atoms and a smaller unit cell than a system including an entire large Au cluster, thus reducing the computational cost. The size of the unit cell was chosen in a way that the periodicity of a large gold cluster could be achieved together with the periodicity of the support material. On the edge of a large Au$_{14}$ gold cluster the distance between adjacent Au atoms is close to 2.7Å [39]. For the Au stripe the distance between adjacent Au atoms is 2.78Å due to the periodic boundary conditions.
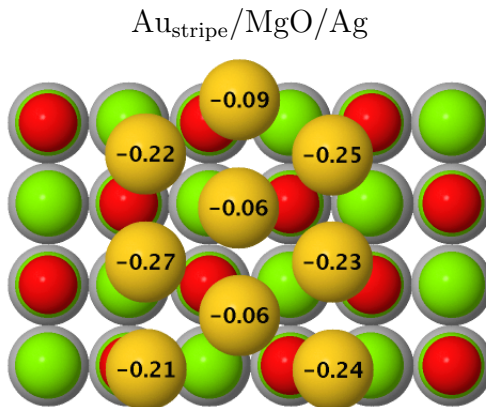
Au$_{\text{stripe}}$/MgO/Ag

Figure 28: The Bader charges of the individual Au atoms in the Au stripe adsorbed on MgO/Ag. The atomic color codes are the same as in figure 27.

For a large Au$_{14}$ gold cluster the edge atoms are negatively charged between 0.2 and 0.3 electrons [40]. The Bader charge analysis for the Au/MgO/Ag system shows a similar charge accumulation to the edge of the Au stripe. The results for the Bader charge

analysis for the individual Au atoms are shown in figure 28. The Bader charge of all Au atoms is -1.64 electrons. The MgO thin film is charged positively by 1.36 electrons and the support metal is charged positively by 0.29 electrons in the Au adsorption. The density difference plots in figure 29 show a charge accumulation to the edge of the gold stripe together with a charge depletion from the MgO-Ag interface. The top view of the density difference shows a charge accumulation to the oxygen atoms in the top layer of the MgO film. The side view of the density difference shows the formation of a polarization pattern to the MgO film.

$$Au_{stripe}/MgO/Ag$$
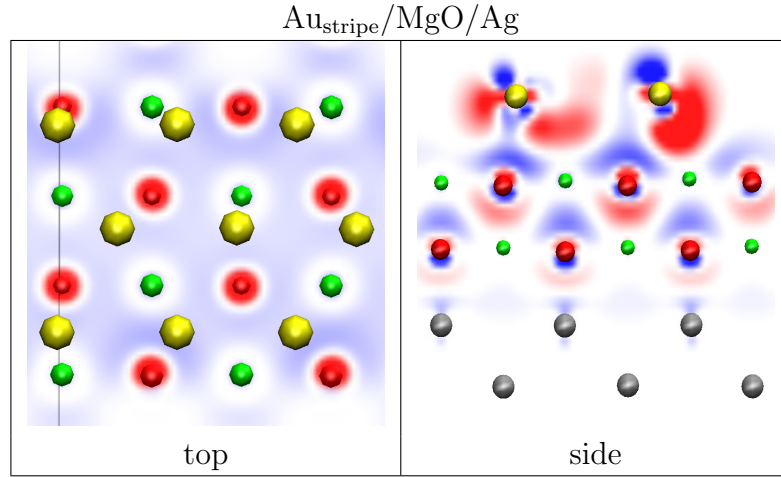
Figure 29: The density difference plots calculated for the adsorption of the whole Au stripe on an Ag supported MgO film. Top view and side view are labeled top and side. The horizontal line in the top plot indicates the cut plane along z-axis for the side plot. Red (blue) denotes the accumulation (depletion) of negative charge. The atomic color codes are the same as in figure 27.
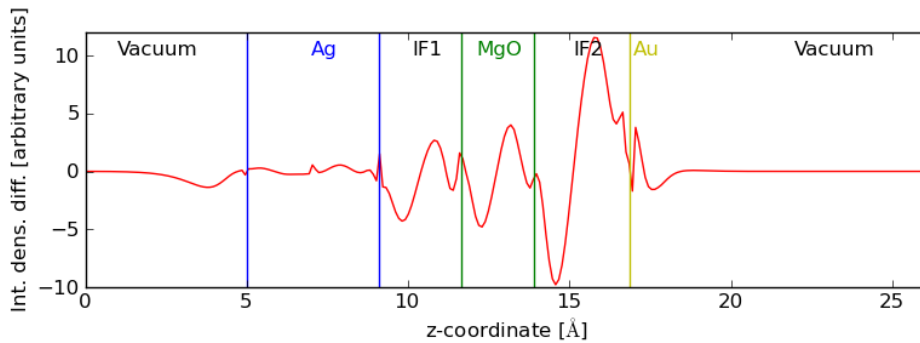
Figure 30: The integrated density difference plot obtained from the density difference in the adsorption of the whole Au stripe on the MgO/Ag surface. The average z-coordinate for the top and bottom Ag (MgO) layers are given as blue (green) vertical lines. The average z-coordinate for the Au stripe is given as a yellow vertical line. The interface between MgO and Ag is noted with IF1 and interface between Au and MgO is noted with IF2.

In order to further visualize the charge transfer between the different parts of the Au/MgO/Ag system, the integrated density difference plot is given in figure 30. The integrated density difference plot shows the charge transfer from the MgO − Ag interface to the Au − MgO interface together with the polarization of the MgO film. This charging pattern is in good agreement with the properties of a large gold cluster on similar support [12].

8.2 Water adsorption on Au/MgO/Ag

$H_2O_{Mg-top}/Au_{stripe}/MgO/Ag$ $H_2O_{Au-top}/Au_{stripe}/MgO/Ag$

top side top side

$H_2O_{Au-edge}/Au_{stripe}/MgO/Ag$ $H_2O_{r.s.}/Au_{stripe}/MgO/Ag$

top side top side

$2H_2O_{Mg-top}/Au_{stripe}/MgO/Ag$

top side
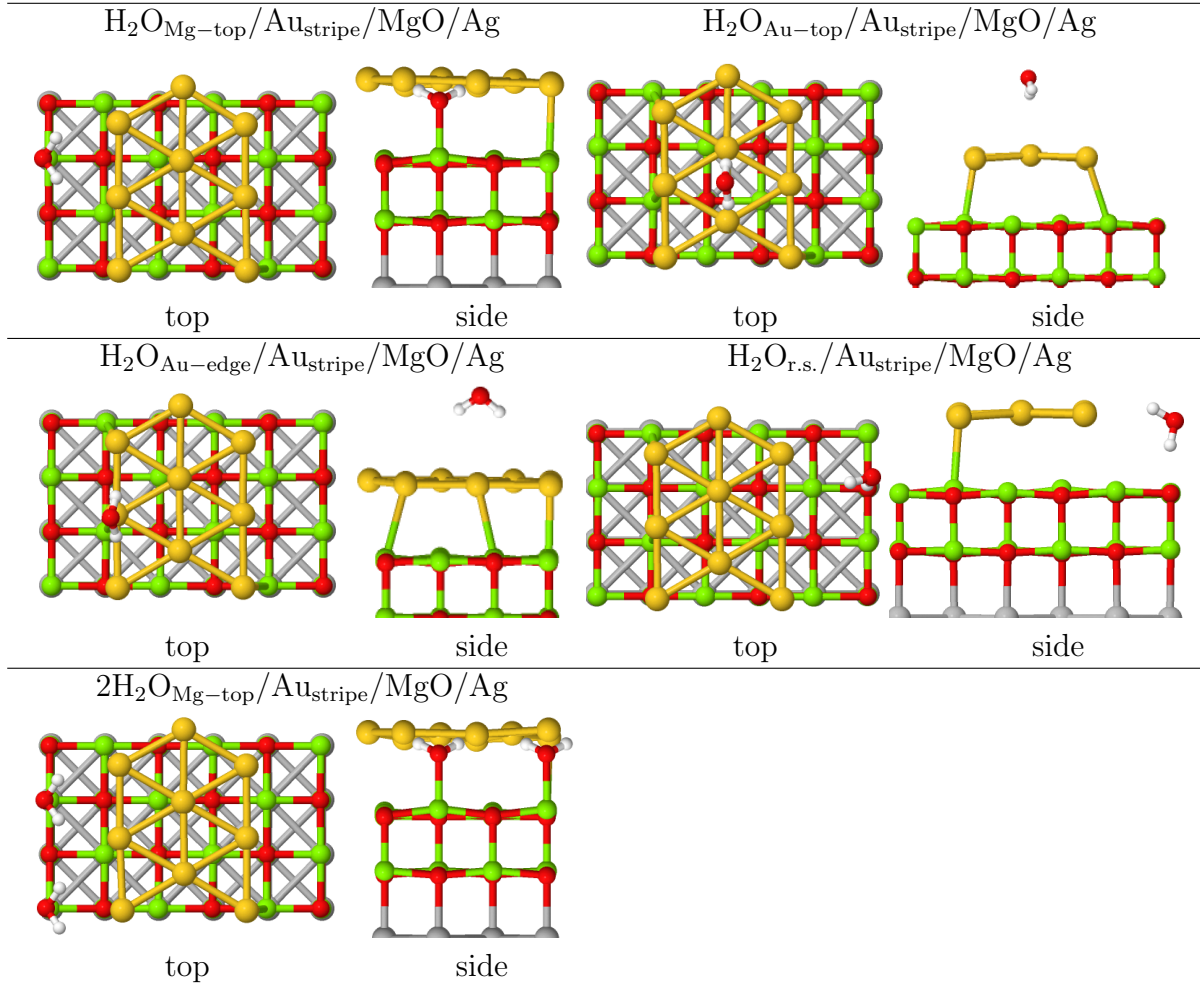
Figure 31: The relaxation geometries for the adsorption of water on different adsorption sites of the Au/MgO/Ag surface. Top and side views are denoted with top and side. The atomic color codes are the same as in figure 27. The bottom figures show the relaxation geometry for a higher coverage in the preferred adsorption site.

Water adsorption on four different adsorption sites of the Au/MgO/Ag surface was considered. Studied sites were a Mg-top, Au-edge and Au-top sites, and on the MgO film at the right side of the Au stripe (r.s.). Due to the different periodicity of the surface and the Au stripe the adsorption sites are different on the different sides of the Au stripe. The adsorption energies and atomic distances in these cases are given in table 10 and the adsorption geometries are shown in figure 31.

The adsorption on a Mg-top site was energetically most favorable with a more negative

adsorption energy than on a similar site at the MgO/Ag surface without the Au stripe. This indicates that the binding of water to the surface is enhanced by the presence of Au. Water adsorption on the top or edge site of the Au stripe was energetically unfavorable. Also adsorption on the right side of the Au stripe was energetically unfavorable.

Since the coverage of water can influence the dissociation of water, the relaxation geometry and adsorption energy for a higher water coverage at the energetically favored adsorption site was determined. The relaxed structure for two water molecules on the Mg-top sites is shown in the same figure. Neither of the molecules dissociated during the relaxation of the system and they both have a similar adsorption geometry as in the case of one adsorbed water molecule. The adsorption energy for two water molecules was -1.32 eV which is close to two times the adsorption energy of a single molecule. Based on these energies and adsorption geometries there seems to be only small coverage effects at the edge of the Au stripe.

Table 10: The adsorption energies and atomic distances for water adsorption on different sites of the Au/MgO/Ag surface. The distance $d_{MgO,Ag}$ is the difference between the average z-coordinate for the Ag top layer and the MgO bottom layer. Similarly the distance $d_{Au,MgO}$ is the difference between the average z-coordinate for the MgO top layer and the average z-coordinate of the gold atoms in the Au stripe. The minimum distances between O in the adsorbed water molecule and the surface Au and Mg atoms are given as $d_{O,Au}$ and $d_{O,Mg}$.

	E_{ads}	$d_{O,Au}$	$d_{O,Mg}$	$d_{Au,MgO}$	$d_{MgO,Ag}$
$H_2O_{Mg-top}/Au_{stripe}/MgO/Ag$	-0.71	3.29	2.13	2.96	2.55
$H_2O_{Au-top}/Au_{stripe}/MgO/Ag$	-0.08	3.58		2.74	2.55
$H_2O_{Au-edge}/Au_{stripe}/MgO/Ag$	-0.08	3.42		2.73	2.55
$H_2O_{r.s.}/Au_{stripe}/MgO/Ag$	-0.26	3.59	3.23	2.94	2.58
$2H_2O_{Mg-top}/Au_{stripe}/MgO/Ag$	-1.32	3.07	2.13	2.90	2.54

The Bader charges for the studied sites of water adsorption on the Au/MgO/Ag are given in table 11. The Bader charges of individual Au atoms are given in figure 32. The water molecule has a small negative charge in all adsorption sites. When water is adsorbed on the Au-edge site the charge is transferred to the support metal and when water is adsorbed on the Mg-top site the charge is transferred from the support metal. When molecular water adsorbs on the right side of the gold stripe the charge is transfered from the gold atoms and when water adsorbs on the left side of the gold stripe the charge

Table 11: The Bader charges in the adsorption of water on different adsorption sites of the model Au/MgO/Ag system. The Bader charges for Au, MgO and Ag are the differences in the total Bader charges due to adsorption.

	q(Au)	q(MgO)	q(Ag)
$H_2O_{Mg-top}/Au_{stripe}/MgO/Ag$	-0.04	0.06	0.07
$H_2O_{Au-top}/Au_{stripe}/MgO/Ag$	-0.01	0.07	-0.04
$H_2O_{Au-edge}/Au_{stripe}/MgO/Ag$	-0.01	0.11	-0.08
$H_2O_{r.h.}/Au_{stripe}/MgO/Ag$	0.13	0.00	-0.05
$2H_2O_{Mg-top}/Au_{stripe}/MgO/Ag$	-0.08	0.17	0.12

is transfered to the gold atoms. The changes in the Bader charges are very small in all cases.

H$_2$O/Au$_{\text{stripe}}$/MgO/Ag   2H$_2$O/Au$_{\text{stripe}}$/MgO/Ag
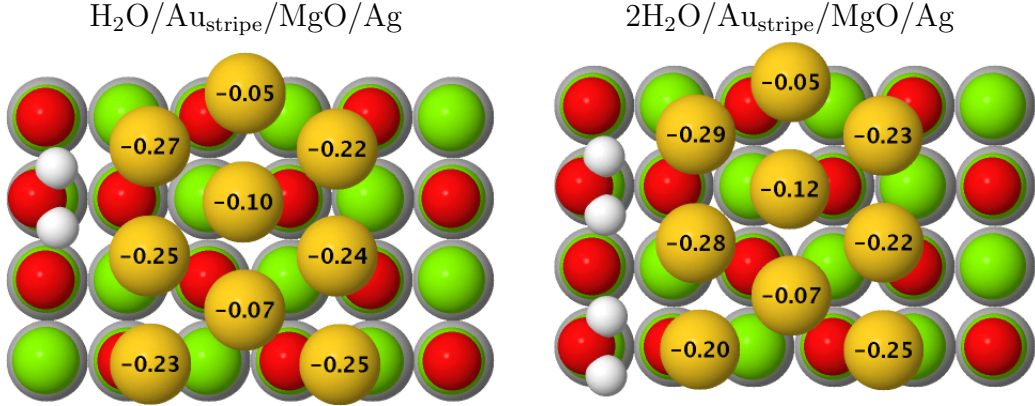
Figure 32: The Bader charges of the individual Au atoms with one and two water molecules adsorbed on the Mg-top site. The atomic color codes are the same as in figure 27.

Since the Mg-top site is the energetically most favorable site for water adsorption, it was studied in more detail. The LDOS is shown in figure 33 together with the LDOS for bare Au/MgO/Ag system. There are only minor differences between the two LDOS plots. The LDOS for water molecule has a peak close to -4.5eV. The d-band centers for Ag and Au are almost equal in both cases. The p-band centers for O atoms are also close to each other. Comparing the O p-band center of Au/MgO/Ag to a flat MgO/Ag surface shows that the adsorption of the Au stripe shifts the O p-band center 0.3eV towards the Fermi level while the Ag d-band center remains nearly constant.

Au$_{\text{stripe}}$/MgO/Ag   H$_2$O$_{\text{Mg-top}}$/Au$_{\text{stripe}}$/MgO/Ag
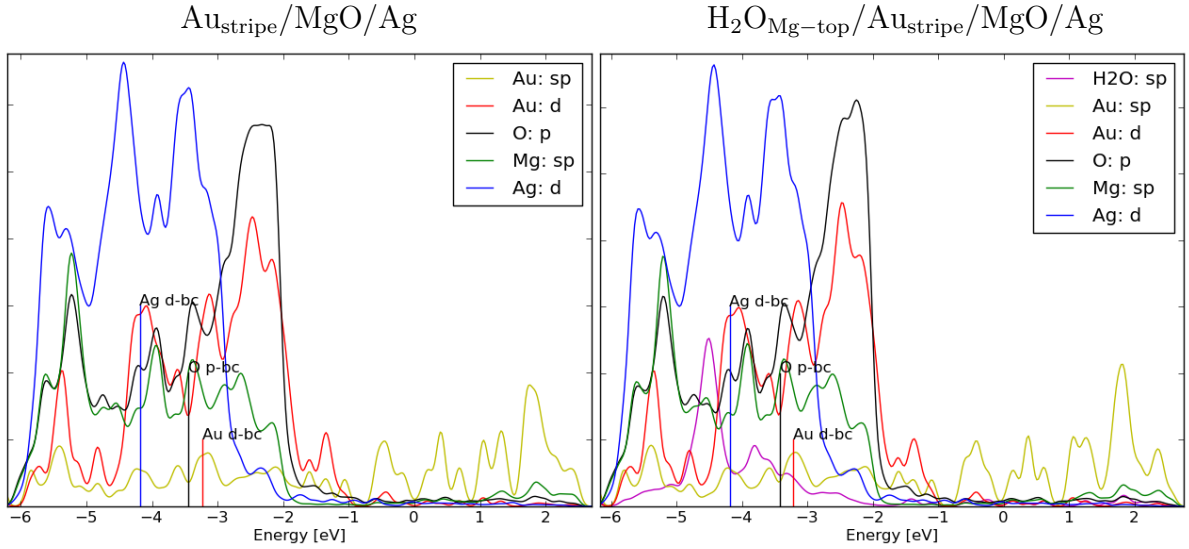
Figure 33: The local density of states given in arbitrary units on the y-axis for the bare Au/MgO/Ag and for Au/MgO/Ag with the water molecule adsorbed on a Mg-top site. The blue (red) vertical line indicates the d-band center for Ag (Au). The black vertical line indicates the p-band center for O. The Fermi energy is set to zero.

The density difference plots for water on the Mg-top site are shown in figure 34. The

43

top view shows a charge depletion from the close vicinity of the Mg atom underneath the water molecule and some polarization of the neighboring O atoms. The side view shows similar polarization of the O atoms. The integrated density difference plot for the adsorption of water on the Mg-top site is in figure 35 showing that the most intense charge transfer occurs at the $Au - MgO$ interface as seen in the side view of the density difference plot.

$$H_2O_{Mg-top}/Au_{stripe}/MgO/Ag$$
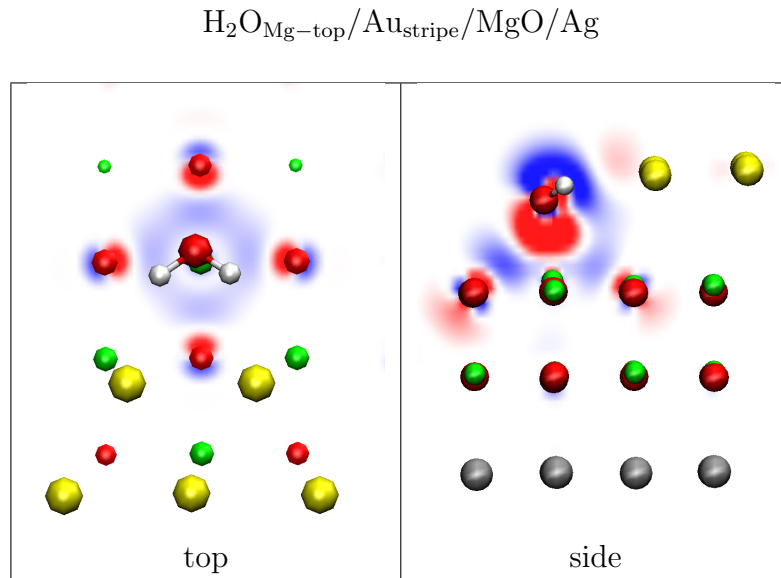
Figure 34: The density difference plots for the adsorption of water on a Mg-top site on the MgO film. Red (blue) shows the accumulation (depletion) of charge. The atomic color codes are the same as in figure 27.

$$H_2O/Au_{stripe}/MgO/Ag$$
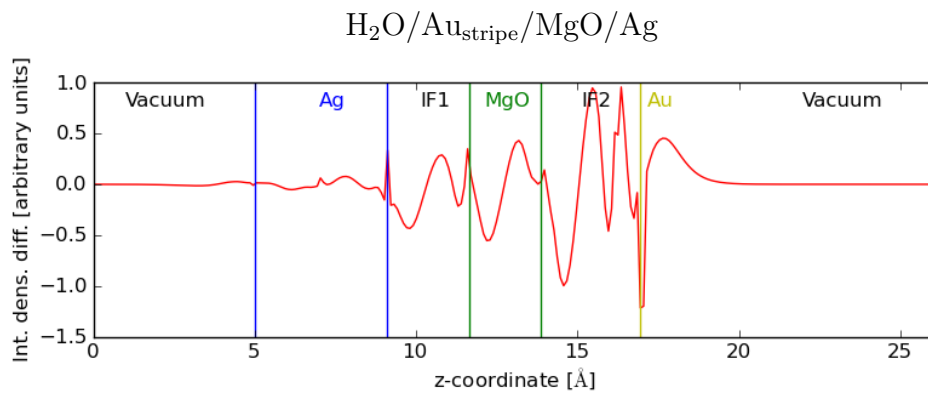
Figure 35: The integrated density difference plot for the adsorption of water on a Mg-top site of the Au/MgO/Ag surface. The colored vertical lines are as in figure 30.

8.3 Adsorption of H and OH on Au/MgO/Ag

H$_{O-top}$/Au$_{stripe}$/MgO/Ag

top   side

H$_{Au-edge}$/Au$_{stripe}$/MgO/Ag

top   side

OH$_{Mg-top}$/Au$_{stripe}$/MgO/Ag

top   side

H$_{Au-top}$/Au$_{stripe}$/MgO/Ag

top   side

OH$_{r.s.}$/Au$_{stripe}$/MgO/Ag

top   side

OH$_{Au-top}$/Au$_{stripe}$/MgO/Ag

top   side
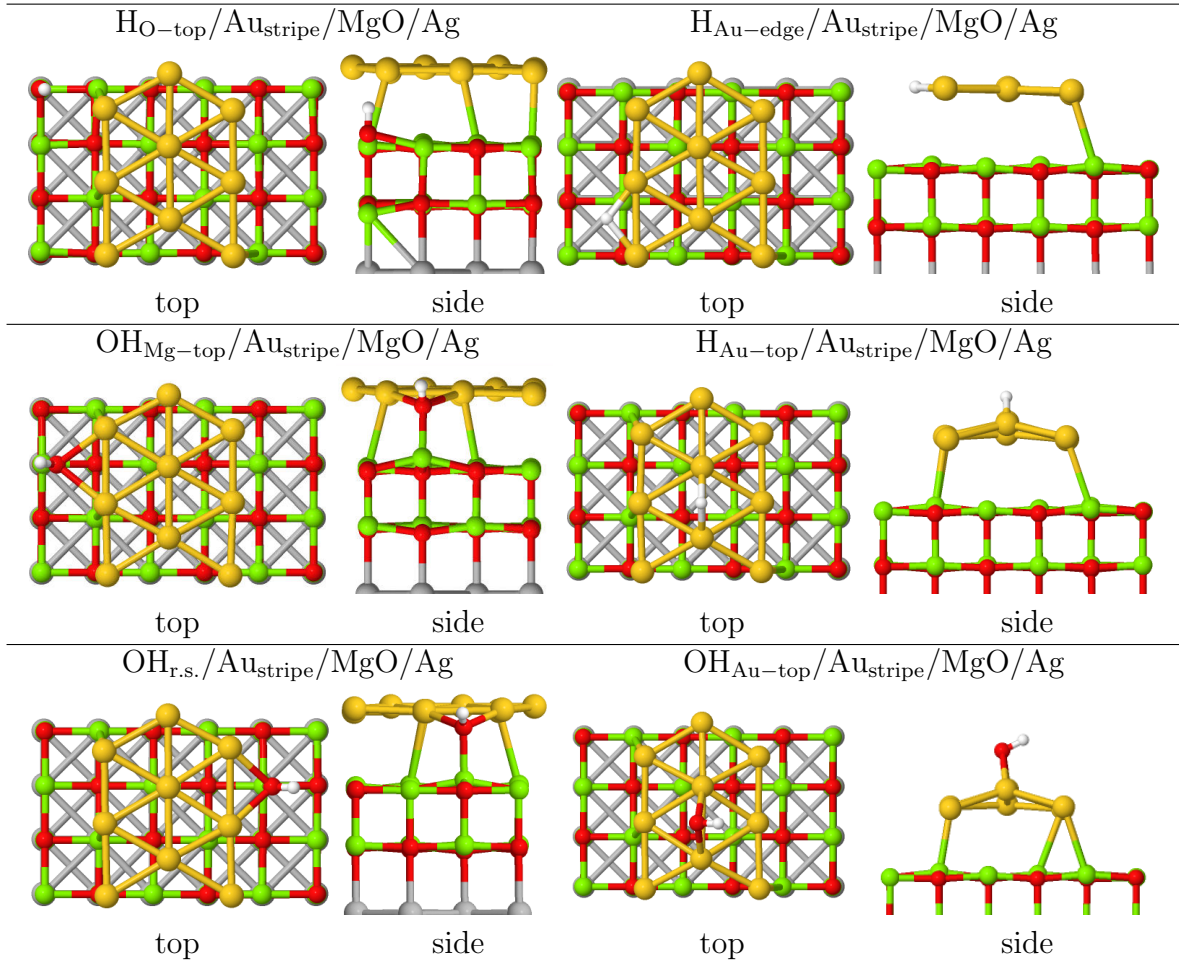
Figure 36: The relaxation geometries for H and OH on different adsorption sites on the Au/MgO/Ag surface. Top and side views are denoted with top and side. The atomic color codes are the same as in figure 27.

The adsorption of water dissociation products H and OH on different sites of the Au/MgO/Ag system were studied in order to determine the energetically favored adsorption sites. The considered sites for H adsorption were an O-top, Au-top and Au-edge sites. The considered sites for the OH adsorption were a Mg-top, Au-top and the right side of the Au stripe (r.s.). The OH adsorption on the edge of the Au stripe was also studied but during the relaxation of the system the OH group moved to the Mg-top site. Thus the adsorption of OH on the edge of the Au stripe was not deemed probable. The found relaxation geometries for different adsorption sites are shown in figure 36 and the corresponding adsorption energies are in table 12. The Mg-top site is the lowest energy adsorption site for OH and the Au-edge site had the lowest adsorption energy for H. For both adsorbates the adsorption on top of the Au stripe was not energetically favorable.

The most exothermic water adsorption occurs also on Mg-top site but adsorption geometries for water and OH are different. The H atoms in the adsorbed water are facing towards the edge of the Au stripe while the H atom in the adsorbed OH faces away from the Au stripe edge. The different orientation of the H atoms in water and OH could indicate a different charge state for the Au stripe edge in these two cases. The distance

Table 12: The adsorption energies and atomic distances for the adsorption of water dissociation products H and OH on different sites of the Au/MgO/Ag. The distances $d_{Au,MgO}$ and $d_{MgO,Ag}$ are as in table 10. The minimum distances between O in the adsorbed OH group and the surface Au and Mg atoms are given as $d_{O,Au}$ and $d_{O,Mg}$.

	E_{ads}	$d_{O,Au}$	$d_{O,Mg}$	$d_{Au,MgO}$	$d_{MgO,Ag}$
$H_{O-top}/Au_{stripe}/MgO/Ag$	-0.07			2.94	2.58
$H_{Au-top}/Au_{stripe}/MgO/Ag$	0.38			3.08	2.56
$H_{Au-edge}/Au_{stripe}/MgO/Ag$	-0.34			3.05	2.59
$OH_{Mg-top}/Au_{stripe}/MgO/Ag$	-0.06	2.37	2.07	2.88	2.55
$OH_{Au-top}/Au_{stripe}/MgO/Ag$	1.56	2.25		2.89	2.56
$OH_{r.s.}/Au_{stripe}/MgO/Ag$	0.04	2.29	2.07	2.96	2.56

Table 13: The Bader charges for the adsorbates H and OH in different adsorption sites. The Bader charges for Au, MgO and Ag are the differences in the total Bader charge due to adsorption.

	q(H)	q(OH)	q(Au)	q(MgO)	q(Ag)
$H_{O-top}/Au_{stripe}/MgO/Ag$	0.56		-0.14	0.03	-0.45
$H_{Au-top}/Au_{stripe}/MgO/Ag$	-0.04		0.11	0.00	-0.07
$H_{Au-edge}/Au_{stripe}/MgO/Ag$	-0.10		0.16	0.01	-0.07
$OH_{Mg-top}/Au_{stripe}/MgO/Ag$		-0.61	0.43	0.10	0.08
$OH_{Au-top}/Au_{stripe}/MgO/Ag$		-0.42	0.44	0.01	-0.04
$OH_{r.s.}/Au_{stripe}/MgO/Ag$		-0.60	0.50	0.10	-0.01

between O and Au was smaller for the adsorption of OH and the Au stripe edge bends towards the MgO film in the OH adsorption. This leads to a smaller average distance between the Au stripe and MgO film compared to the surface with the adsorbed water molecule.

A Bader charge analysis for the adsorbates and surfaces in case of each studied adsorption site was performed and the results are given in table 13. The charge transfer differs for the H adsorption on the Au-edge site and on the O-top site. H has a positive charge on the O-top site and a small negative charge on the Au-edge. The charge transfered from the support metal differs accordingly. When H adsorbs on the O-top site, Ag gains negative charge which corresponds to the positive charge gained by the adsorbed H. When H adsorbs on the Au-edge site the charge gained by Ag is small indicating no charge transfer between Ag and H. The Bader charges of individual Au atoms with H adsorbed on an O-top and an Au-edge sites are shown in figure 37. The Au atoms adjacent to the H adsorption site on the edge of the Au stripe have lost some negative charge.

The adsorbed OH group was negatively charged in all adsorption sites. The charge gained by OH originates mostly from the Au stripe in all cases. The charge transfer to OH is smallest when OH adsorbs on top of the Au stripe. The adsorption is clearly endothermic and the decreased charge transfer could be viewed as decreased binding between OH and the surface. Figure 38 shows the Bader charges of the individual Au atoms when OH is adsorbed on a Mg-top site. The Au atoms adjacent to the adsorbed OH are almost neutral showing a charge transfer from the Au atoms to the adsorbed OH.
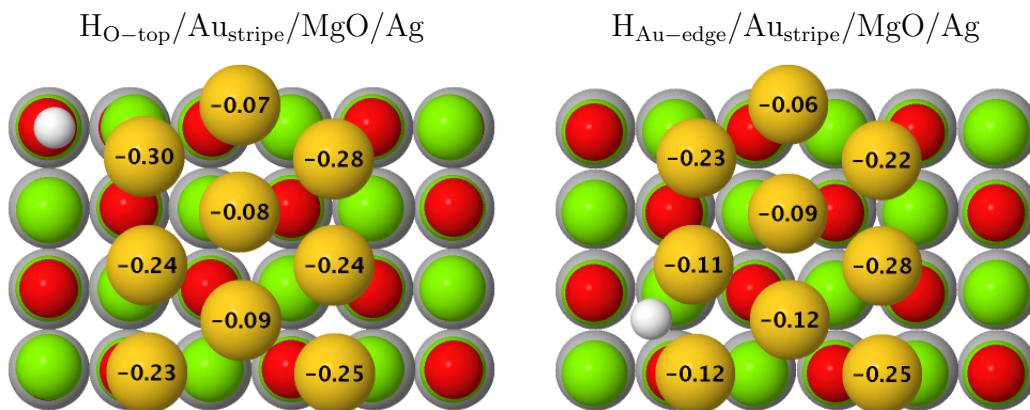
Figure 37: The Bader charges of the individual Au atoms with H adsorbed on an O-top and a Au-edge site. The atomic color codes are the same as in figure 27.
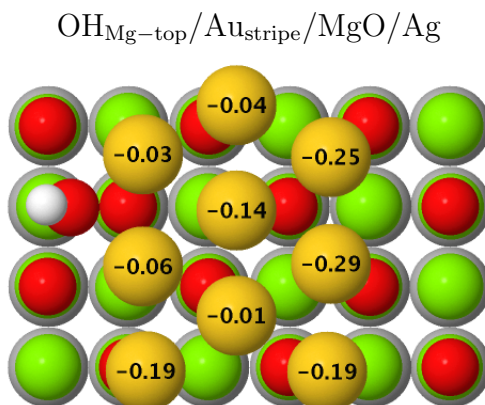
Figure 38: The Bader charges of the individual Au atoms with OH adsorbed on Mg-top site. The atomic color codes are the same as in figure 27

In figure 39 are the density difference plots for the H adsorption on an O-top and a Au-edge site in order to further visualize the different charge transfers in the H adsorption. The density difference plots for the H adsorption on the O-top site show that the charge is transferred from a formed surface OH group to the MgO-Ag interface and the edge of the Au stripe. When H adsorbs on the edge of the Au stripe a small charge transfer from the Au atoms to the adsorbed hydrogen is observed. This charge transfer pattern can also be seen in the integrated density difference plots in figure 40. The integrated density difference plots show that in case of H adsorption on the O-top site the charge is transferred trough a larger part of the system than in the case of H adsorption on the Au-edge site. When H is adsorbed on the O-top site the charge is transfered to the MgO-Ag interface and the Au atoms as seen in the density difference plots. Charge transfer is different in the case of H adsorption on the Au-edge site where charge transfer is primarily from the Au stripe.

Figure 41 shows the density difference plots for visualizing the charge transfer in OH adsorption on a Mg-top site. The side view of the density difference plot shows that charge is mainly transferred from the edge of the Au stripe to the adsorbed OH. The top view shows a polarization of the O atoms adjacent to the OH adsorption site. The integrated

$$H_{O-top}/Au_{stripe}/MgO/Ag$$

top   side

$$H_{Au-edge}/Au_{stripe}/MgO/Ag$$

top   side
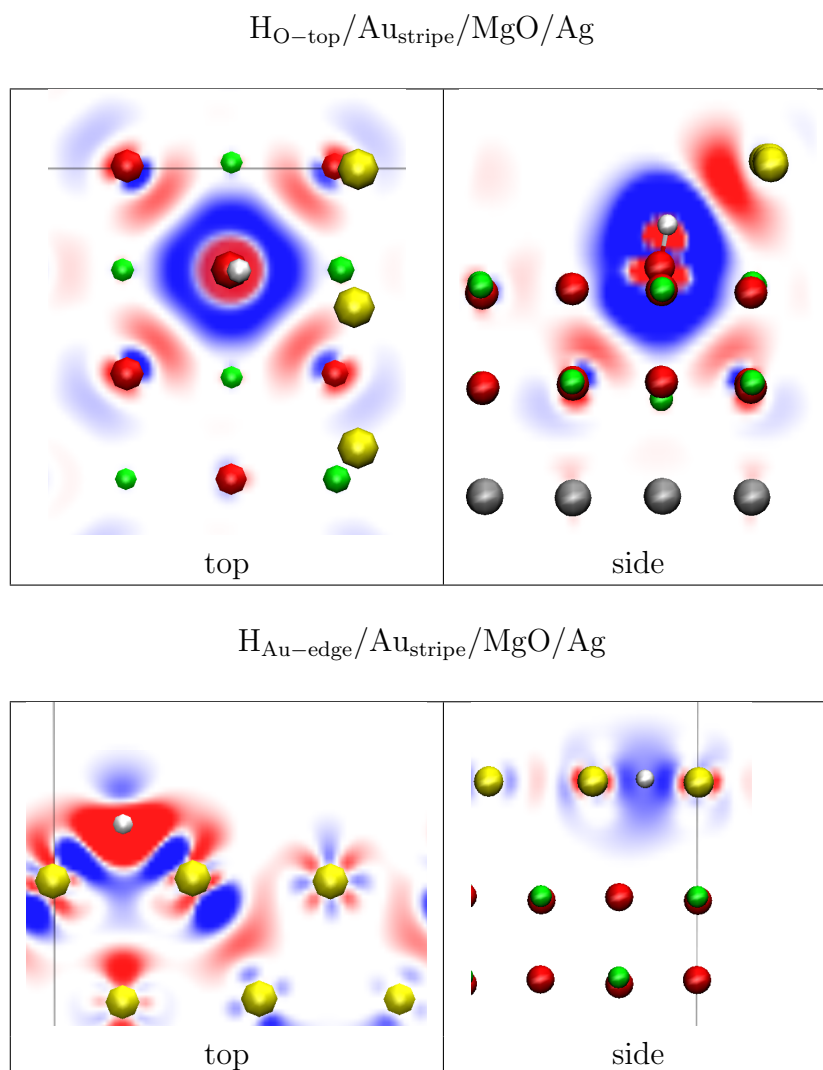
Figure 39: The density difference plots for the adsorption of hydrogen on an O-top site and a Au-edge site. Red (blue) shows accumulation (depletion) of charge. Gray lines indicate the unit cell edges. The atomic color codes are the same as in figure 27.

density difference plot in figure 42 also shows that the charge is transferred mainly from the Au stripe with a slight polarization of the MgO film.

The LDOS plots for the Au/MgO/Ag with a H adsorbed on an O-top and Au-edge sites are given in figure 43. The d-band centers for Ag and Au are nearly at the same energies in both cases but the p-band center for oxygen is closer to the Fermi energy when H is adsorbed to the Au-edge site. The shift in the O p-band center is similar to the case of H adsorption on a MgO/Ag surface without the Au stripe and correlates with the charge transfer between H and Ag. The LDOS for OH adsorbed on a Mg-top site is shown in figure 44. The O p-band center is closer to the Fermi energy than for the bare Au/MgO/Ag but the shift in the p-band center is smaller compared to the case of OH adsorption on a MgO/Ag surface without adsorbates. This could be associated with the decreased charge transfer between the adsorbed OH and the support metal. When OH adsorbs on Au/MgO/Ag most of the charge gained by OH is transfered from the Au stripe while on bare MgO/Ag surface more of the charge originates from the support metal.

$$H_{O-top}/Au_{stripe}/MgO/Ag$$

$$H_{Au-edge}/Au_{stripe}/MgO/Ag$$
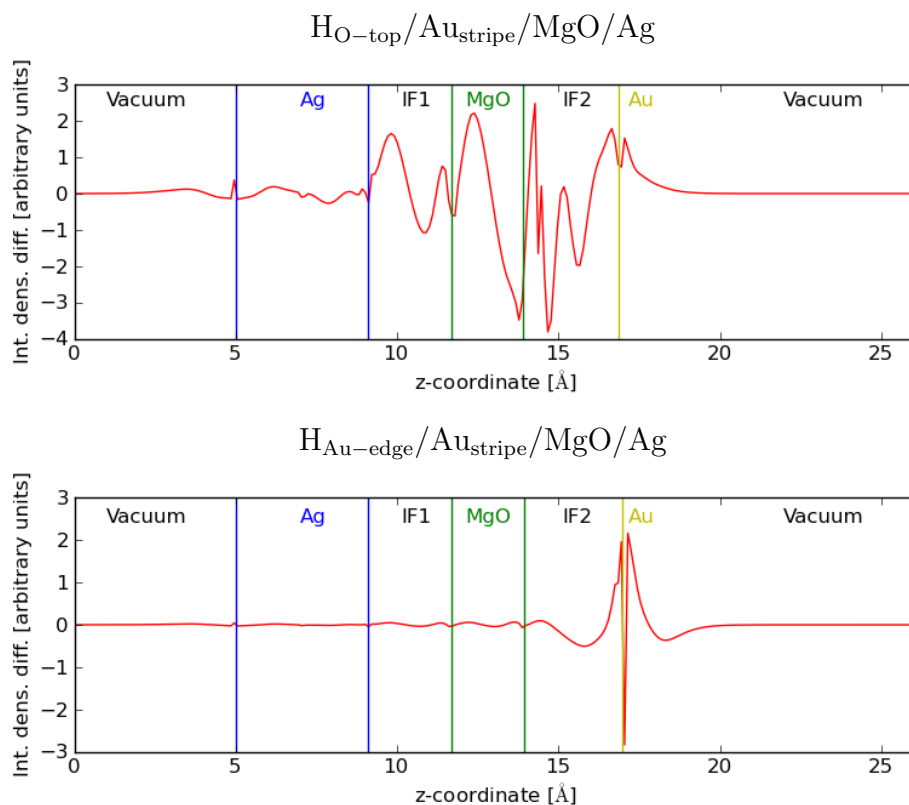
Figure 40: The integrated density difference plots for the adsorption of H on two sites on the Au/MgO/Ag surface. The side figure for H on the Au-edge site shows the charge transfer along the Au stripe edge. The colored vertical lines are as in figure 30.

$$OH_{Mg-top}/Au_{stripe}/MgO/Ag$$
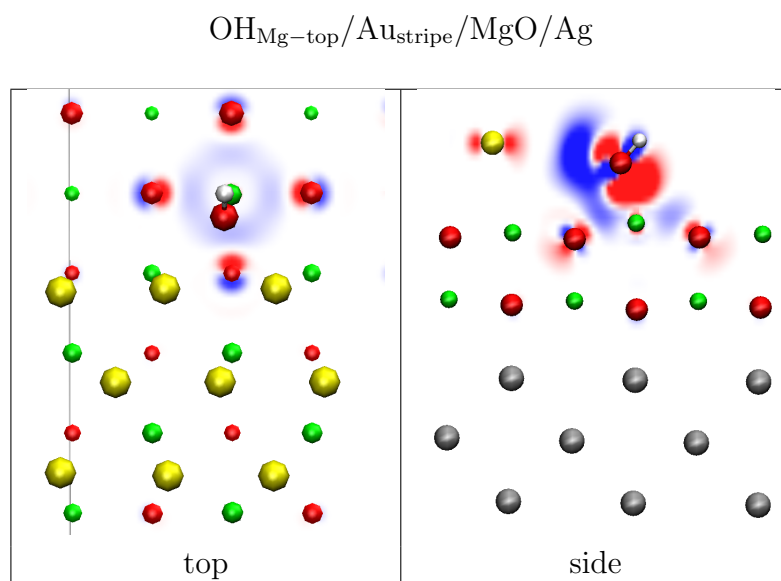
Figure 41: The density difference plots for the adsorption of OH on a Mg-top site on the Au/MgO/Ag surface. Red (blue) shows the accumulation (depletion) of charge. The atomic color codes are the same as in figure 27.

49
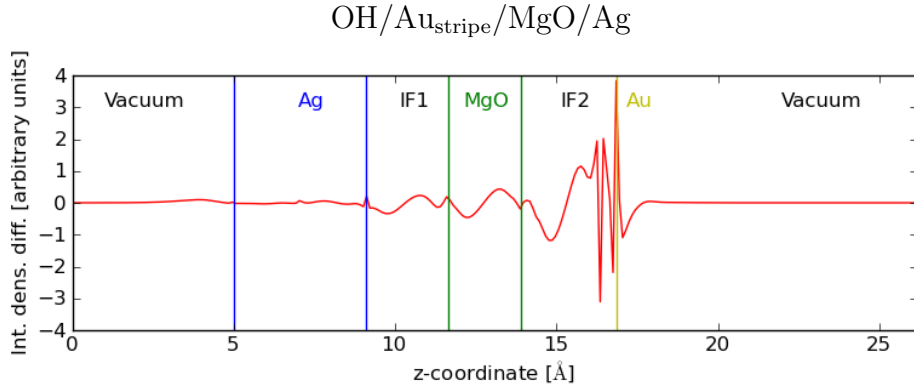
Figure 42: The integrated density difference plot for the adsorption of OH on a Mg-top site of the Au/MgO/Ag surface. The colored vertical lines are as in figure 30.
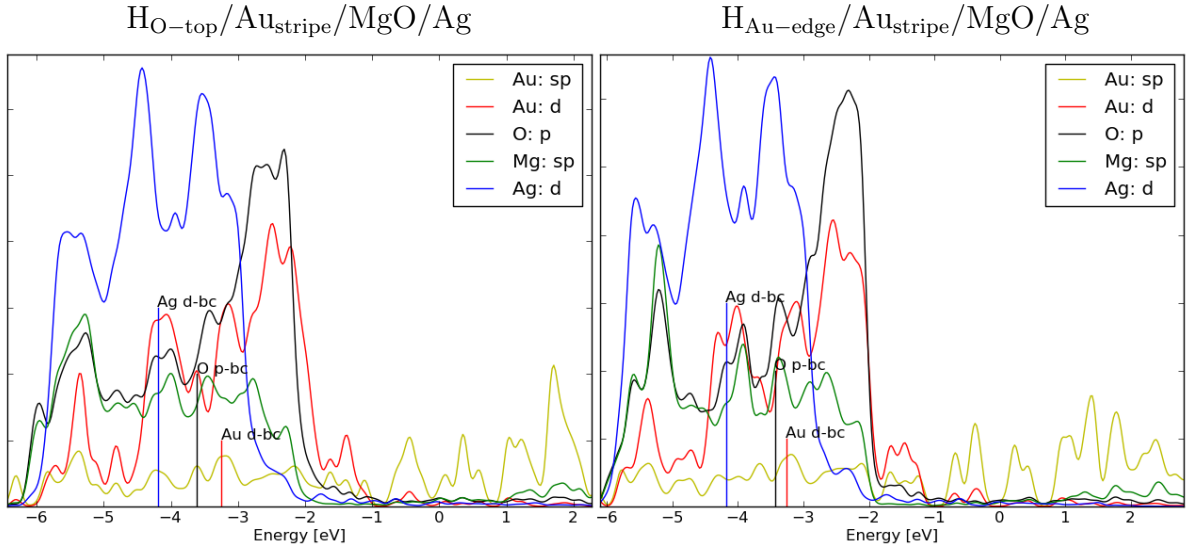
Figure 43: The local density of states given in arbitrary units on the y-axis for H adsorbed on two different sites of the Au/MgO/Ag surface. The left figure shows the LDOS plot for H adsorbed on an O-top site of the MgO film and the right figure is the LDOS plot for H adsorbed on the edge of the Au stripe. The blue (red) vertical line indicates the d-band center for Ag (Au). The black vertical line indicates the p-band center for O. The Fermi energy is set to zero in both cases.

$OH_{Mg-top}/Au_{stripe}/MgO/Ag$
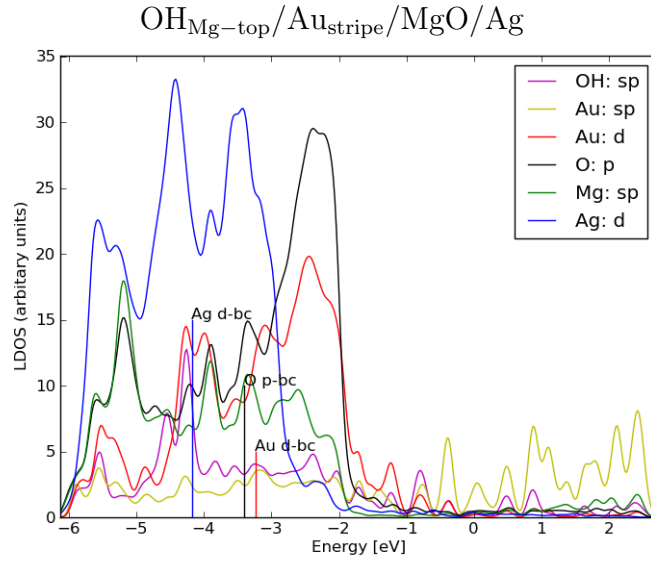
Figure 44: The local density of states for OH adsorbed on a Mg-top site of the Au/MgO/Ag surface. The blue (red) vertical line indicates the d-band center for Ag (Au) and the black vertical line indicates the p-band center for O. The Fermi energy is set to zero.

8.4 Water dissociation on Au/MgO/Ag
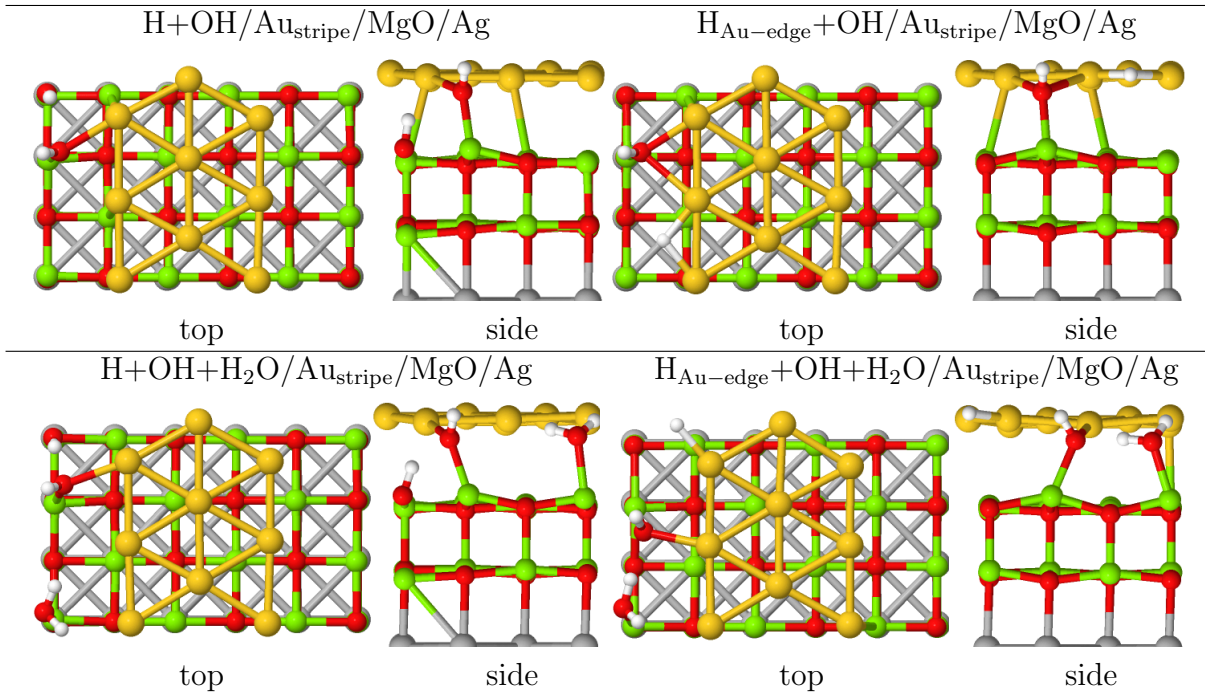
Figure 45: The relaxation geometries for the adsorption of H and OH on different adsorption sites of the same computational cell. The lower figures show the relaxation geometries with a higher water coverage. Top and side views are denoted with top and side. The atomic color codes are the same as in figure 27.

Different configurations of H and OH co-adsorption are studied to determine whether the Au/MgO/Ag surface is able to dissociate water. The preferred adsorption site for OH is the Mg-top site at the left side of the Au stripe and only adsorbate configurations with OH adsorbed on that site are considered. The adsorption of H had a difference of 0.27eV in adsorption energy between the adsorption on an O-top site and the adsorption on an Au-edge site. There was also binding between the co-adsorbed H and OH on a bulk MgO and MgO/Ag surfaces. Thus the H and OH combinations to be considered are H and OH adsorbed on the MgO film and H adsorbed on the Au-edge site with OH adsorbed on a Mg-top site. Since the coverage can influence the water dissociation, the same combinations are also considered in the case of a higher water coverage. The higher coverage adsorbate configurations have an intact water molecule on a Mg-top site adjacent to the adsorbed OH. The relaxation geometries in these cases are shown in figure 45. The corresponding adsorption energies and atomic distances are given in table 14.

The adsorption energy for H adsorbed on an O-top site and OH adsorbed on a Mg-top site is -0.20eV. When H adsorbs on an Au-edge site the combined adsorption energy is -0.26eV. The adsorption energy for an intact water molecule is -0.71eV so based on these energies the dissociative adsorption of water is not energetically favorable. When water coverage is increased by adding a water molecule on a Mg-top site the difference in adsorption energies between the two H adsorption sites is increased. The combined adsorption energy when H adsorbs on an O-top site together with OH and H_2O adsorbed on Mg-top sites was -0.82eV and when H was in an Au-edge site the adsorption energy was -1.11eV. Thus increasing the coverage does not result in an energetically favorable

Table 14: The adsorption energies and atomic distances for the adsorption of H and OH together on different sites of the same computational cell. The adsorption energies and distances for a higher water coverage are also given. The distances $d_{Au,MgO}$ and $d_{MgO,Ag}$ are as in table 10. The minimum distances between the O atom in the adsorbed OH group and the surface Au and Mg atoms are given as $d_{O,Au}$ and $d_{O,Mg}$.

	E_{ads}	$d_{O,Au}$	$d_{O,Mg}$	$d_{Au,MgO}$	$d_{MgO,Ag}$
H+OH/Au$_{stripe}$/MgO/Ag	-0.20	2.39	2.03	2.85	2.58
H$_{Au-edge}$+OH/Au$_{stripe}$/MgO/Ag	-0.26	2.31	2.05	2.89	2.55
H+OH+H$_2$O/Au$_{stripe}$/MgO/Ag	-0.82	2.44	2.06	2.82	2.58
H$_{Au-edge}$+OH+H$_2$O/Au$_{stripe}$/MgO/Ag	-1.11	2.35	2.11	2.84	2.55

Table 15: The Bader charges for adsorbates H and OH together in different adsorption sites of the same computational cell. The Bader charges for a higher water coverages are also given. The charges for H and OH are for the dissociated water molecule. The charge of the intact water molecule is not given. The Bader charges for Au, MgO and Ag are the differences in the total Bader charges due to adsorption.

	q(H)	q(OH)	q(Au)	q(MgO)	q(Ag)
H+OH/Au$_{stripe}$/MgO/Ag	0.56	-0.65	0.31	0.14	-0.36
H$_{Au-edge}$+OH/Au$_{stripe}$/MgO/Ag	-0.10	-0.62	0.49	0.10	0.13
H+OH+H$_2$O/Au$_{stripe}$/MgO/Ag	0.60	-0.68	0.23	0.17	-0.24
H$_{Au-edge}$+OH+H$_2$O/Au$_{stripe}$/MgO/Ag	-0.12	-0.66	0.43	0.23	0.20

water dissociation because the adsorption energy for two intact water molecules on Mg-top sites was -1.32eV.

$$H_{Au-edge}+OH/Au_{stripe}/MgO/Ag \qquad H_{Au-edge}+OH+H_2O/Au_{stripe}/MgO/Ag$$
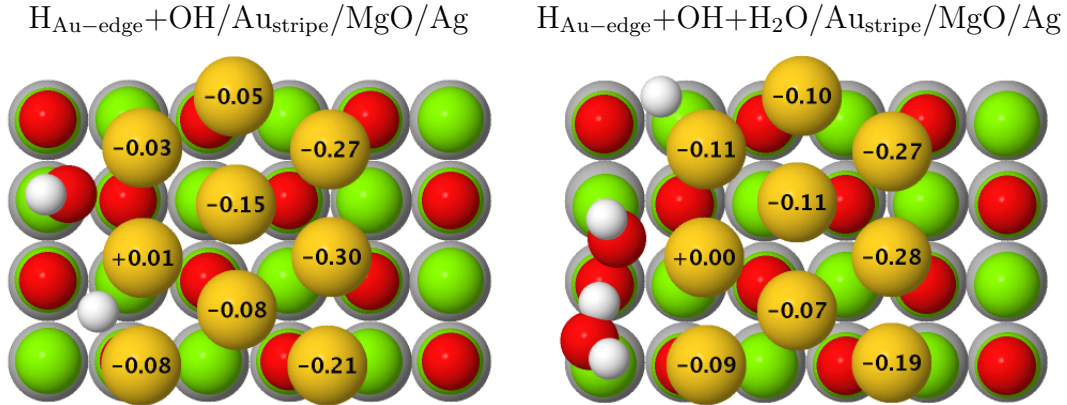
Figure 46: The left figure shows the Bader charges of the individual Au atoms with a dissociated water molecule adsorbed on the Au stripe edge. The right figure shows the same charges in the case of a higher water coverage. The atomic color codes are the same as in figure 27.

The Bader charges for considered adsorbate configurations were determined and the results are given in table 15. The H adsorption site has a similar effect on the charge of H as in the case of a single H atom on the Au/MgO/Ag surface. When H absorbs on an O-top site it is charged positively. When H adsorbs on an Au-edge site it remains almost neutral. The opposite charge transfer is observed for the support metal. The adsorbed OH is charged negatively in all cases. The Au stripe gains a larger positive charge when H is adsorbed on an Au-edge site compared to the H adsorbed on an O-top site. The intact water molecule has a small negative charge in both cases. The Bader charges for the individual Au atoms are given in figure 46. The increased water coverage has only a small effect on the charges of the individual Au atoms.

The density difference plots are given in figure 47 for a charge transfer visualization in the energetically most favorable case of dissociative adsorption. The top view shows a charge depletion from the Au stripe edge. The charge is accumulated at the adsorbed H atom. The side view shows a polarization of the O atoms adjacent to the OH adsorption site. The integrated density difference plot also shows some polarization of the MgO film. This is contrary to the case of dissociative water adsorption on a stepped MgO/Ag surface where the charge transfer was primarily between the adsorbed H and OH. The charge transfer to the adsorbed H and OH on the Au/MgO/Ag surface seems to occur similarly even when H and OH are in the same computational cell. The integrated density difference plot is given in figure 48.

The LDOS plot is given in figure 49. The LDOS for the adsorbed OH is evenly distributed. The peak close to -4.4eV observed for an OH adsorbed on the same site without H atom in the same computational cell has vanished. There are only minor differences in the d-band centers of Ag and Au and in the p-band center of O compared to a clean Au/MgO/Ag surface.

The average binding energies for Au atoms in the Au stripe calculated for the adsorbate configurations with the lowest final state energies are given in figure 50. The average Au binding energy is defined as in equation (4.2) and indicates how the different adsorbates affect the binding of the Au stripe to the surface. All considered adsorbates increased

$$H_{Au-edge}+OH/Au_{stripe}/MgO/Ag$$
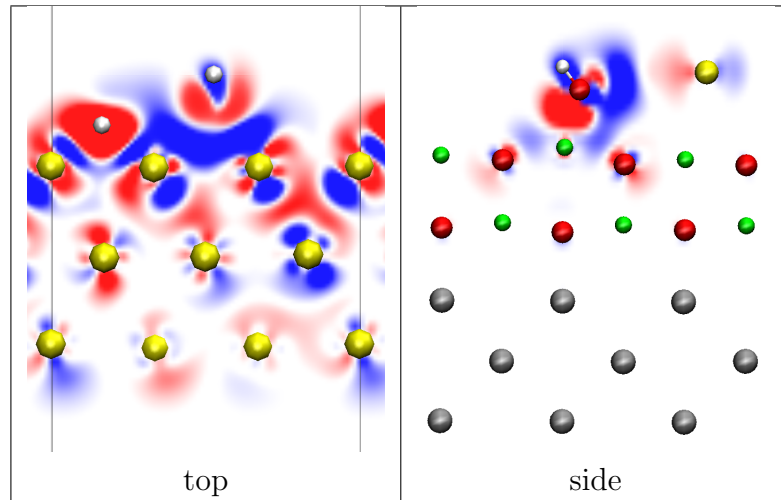
Figure 47: The density difference plots for the adsorption of H on an Au-edge site and OH on a Mg-top site on the Au/MgO/Ag. Red (blue) shows the accumulation (depletion) of charge. The atomic color codes are the same as in figure 27.

the average Au adsorption energy when they were adsorbed on the energetically favored sites. The adsorption of H on an Au-edge site increased the binding of Au atoms more than the adsorption of OH or H_2O on the Mg-top site. The lowest average Au adsorption energy was for system with H and OH adsorbed on their preferred sites.

$$H_{Au-edge}+OH_{Mg-top}/Au_{stripe}/MgO/Ag$$
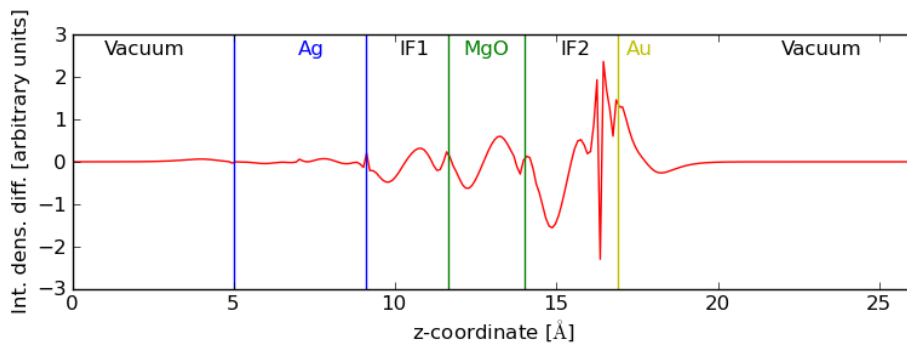
Figure 48: The integrated density difference plot for the adsorption of H on an Au-edge site and OH on a Mg-top site of the Au/MgO/Ag surface. The colored vertical lines are as in figure 30.

$H_{Au-edge}+OH_{Mg-top}/Au_{stripe}/MgO/Ag$
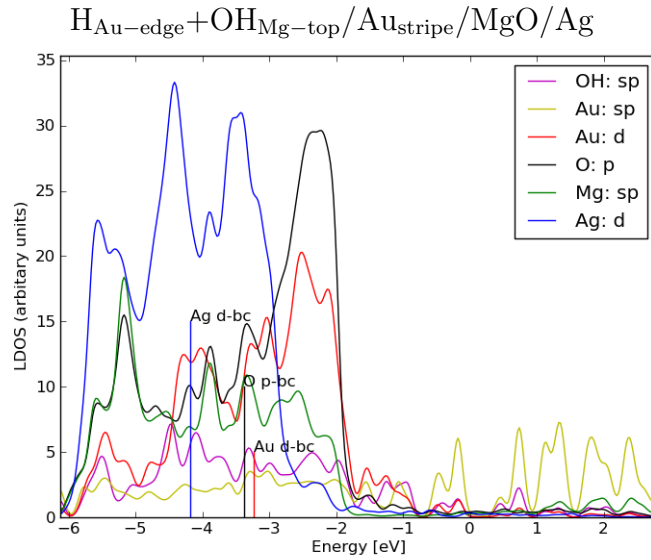
Figure 49: The local density of states for the Au/MgO/Ag with H adsorbed on an Au-edge site and OH adsorbed on a Mg-top site. The blue (red) vertical line indicates the d-band center for Ag (Au) and the black vertical line indicates the p-band center for O. The Fermi energy is set to zero.
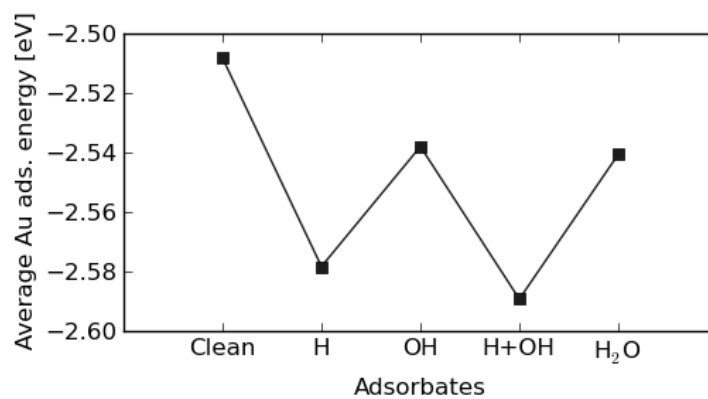
Figure 50: The average adsorption energy of the Au atoms in the Au stripe with different adsorbates on the Au/MgO/Ag surface. The adsorption site for H is an Au-edge site and for OH and H_2O a Mg-top site. When H and OH are adsorbed in the same unit cell H is on an Au-edge site and OH is on a Mg-top site. This adsorbate configuration is noted with H+OH.

8.5 Adsorption of OH on a defect site in the Au stripe

OH/Au$_{\text{stripe}}^{\text{defect}}$/MgO/Ag		2OH/Au$_{\text{stripe}}^{\text{defect}}$/MgO/Ag	
top	side	top	side
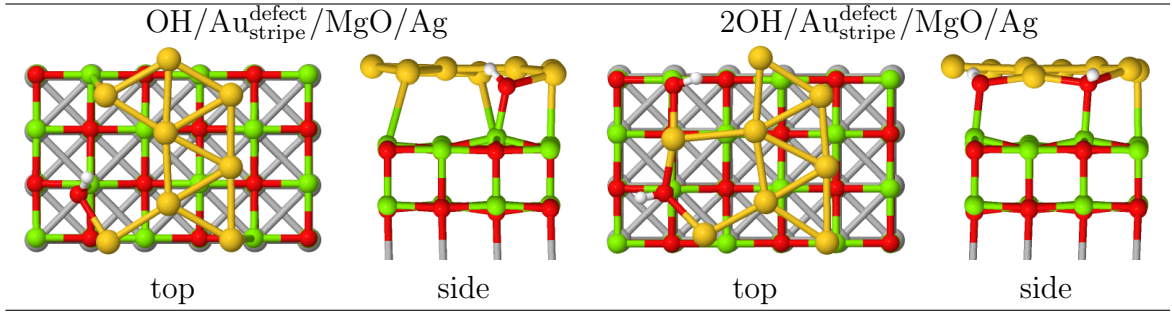
Figure 51: The relaxation geometries for one and two OH groups adsorbed on a MgO/Ag surface together with a defected Au stripe. Top and side views are denoted with top and side. The atomic color are the same as in figure 27.

The Au$_{14}$ cluster is known to interact strongly with O by forming one dimensional O-Au chains at the edge of the Au cluster [40]. The geometric properties of the Au stripe prevent the formation of such chains with the oxygen in the hydroxyl group. In order to model the possible formation of Au-OH chain at the edge of a large Au cluster, one of the edge atoms was removed and replaced by an OH group. Because the observed distance between O and Au at the edge of Au$_{14}$ is close to 2Å, two OH groups were also placed to the edge of the Au stripe in an attempt to model the possible formation of Au-OH chain. For the used unit cell this would lead to periodic distance between OH and Au of about 2Å for two OH groups at the edge of the Au stripe. Au vacancy could also be considered as a model to a corner site of an Au cluster. The corner sites have been suggested to be the active sites in WGS catalysis [41].

Table 16: The adsorption energies and atomic distances for the adsorption of OH on an Au defect site. The distances $d_{\text{Au,MgO}}$ and $d_{\text{MgO,Ag}}$ are as in table 10. The minimum distances between the O atom in the adsorbed OH group and the surface Au and Mg atoms are given as $d_{\text{O,Au}}$ and $d_{\text{O,Mg}}$. The Bader charges for adsorbates are also given in the table. The charge $q(\text{OH})_1$ is for the OH group with H facing towards the Au stripe. The Bader charges for Au, MgO and Ag are the total charges.

	E_{ads}	$d_{\text{O,Au}}$	$d_{\text{O,Mg}}$	$d_{\text{Au,MgO}}$	$d_{\text{MgO,Ag}}$
OH/Au$_{\text{stripe}}^{\text{defect}}$/MgO/Ag	0.91	2.20	2.03	2.86	2.55
2OH/Au$_{\text{stripe}}^{\text{defect}}$/MgO/Ag	0.58	2.07	2.08	2.79	2.55
	$q(\text{OH})_1$	$q(\text{OH})_2$	$q(\text{Au})$	$q(\text{MgO})$	$q(\text{Ag})$
OH/Au$_{\text{stripe}}^{\text{defect}}$/MgO/Ag		-0.64	-1.27	1.54	0.39
2OH/Au$_{\text{stripe}}^{\text{defect}}$/MgO/Ag	-0.55	-0.60	-0.82	1.57	0.41

No bonding was detected with the Au/MgO/Ag surface and OH despite the introduced defect in the Au stripe. The adsorption energies were endothermic in both studied cases. The reference system for the calculation of the adsorption energy of a single OH group $E_{\text{ads}}(\text{OH})$ was the defect free Au stripe with the average adsorption energy of one Au atom $E_{\text{ads}}^{\text{ave}}(\text{Au})$ subtracted

$$E_{\text{ads}}(\text{OH}) = E_{\text{OH/Au(defect)/MgO/Ag}} - (E_{\text{Au/MgO/Ag}} - E_{\text{ads}}^{\text{ave}}(\text{Au}) + E_{\text{H}_2\text{O}} - \text{1/2}E_{\text{H}_2}). \quad (8.1)$$
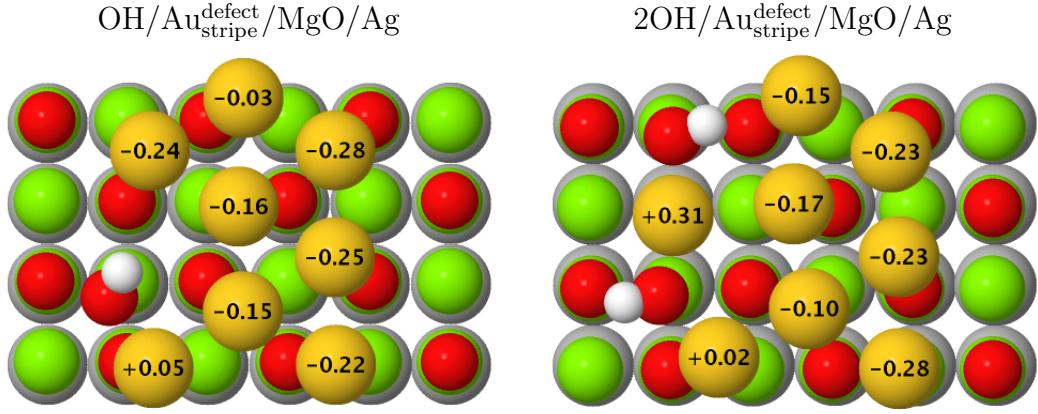
Figure 52: In the left figure the Bader charges of the individual Au atoms with OH adsorbed on the defect site of Au stripe edge are given. In the right figure the charges are given in the case of two adsorbed OH groups. The atomic color codes are the same as in figure 27.

The reference system for the calculation of the adsorption energy in the case of two OH groups was the system with defected Au stripe and one OH group

$$E_{ads}(OH) = E_{2\,OH/Au(defect)/MgO/Ag} - (E_{OH/Au(defect)/MgO/Ag} + E_{H_2O} - \frac{1}{2}E_{H_2}). \qquad (8.2)$$

The relaxation geometries for one and two OH groups adsorbed with defected Au stripe are shown in figure 51. The formation of an Au-OH chain at the edge of the defected Au stripe is seen in the adsorption of two OH groups. The Bader charge analysis shows a positive charge of 0.31 electrons for the Au atom between the OH groups. A similar charge was reported for an Au atom between two O atoms at the edge of a Au_{14} cluster [40]. The Bader charges for individual gold atoms are given in figure 52. The adsorption energies together with Bader charges and atomic distances are given in table 16.

9 Conclusions

9.1 Water dissociation on MgO step
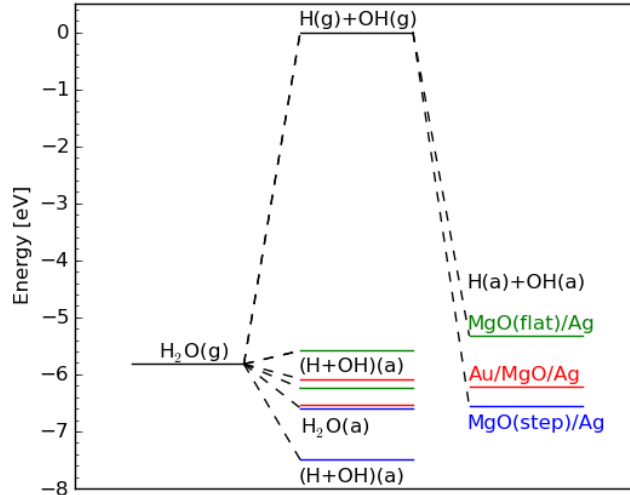
Figure 53: The enthalpy cycle for water dissociation on the Au/MgO/Ag system, a flat MgO/Ag surface and a stepped MgO/Ag surface. The gas phase species are denoted with (g) while the adsorbed species are denoted with (a). The lower green line corresponds to the energy of the adsorbed H_2O on a flat MgO/Ag surface.

Water dissociates spontaneously on a bulk MgO surface with a step type defect. Water also dissociates spontaneously on an Ag supported stepped MgO film, depending on the initial geometry of the water molecule. The molecular adsorption is exothermic on studied MgO and MgO/Ag surfaces but the dissociative adsorption is significantly more exothermic on the stepped surfaces. When water dissociation products H and OH adsorb individually to a stepped MgO or MgO/Ag surfaces their adsorption energies are much larger than in the co-adsorption. This indicates that the interaction between adsorbates on the step sites leads to a stronger binding of the adsorbates. This could result from the smaller change in the interlayer distance, a dipole-dipole interaction between the adsorbed OH and a surface OH, the shifted p-band center for the oxygen atoms and a direct Coulomb interaction between the positively charged H and a negatively charged OH. The energies for the different configurations of adsorbates on the studied Au/MgO/Ag system, a flat MgO/Ag and a MgO/Ag surface with a step defect are summarized in the enthalpy cycle shown in figure 53.

H adsorption on stepped MgO/Ag increases the interlayer distance between the step and top MgO layers. When OH is adsorbed on an adjacent site the distance between the step layer and top layer is the same as for the bare surface. H and OH co-adsorption on flat MgO/Ag surface increases the interlayer distance between the top and bottom MgO layers. The distance between top and bottom MgO layers does not change from the clean surface in the molecular water adsorption. A similar behavior was observed for the bulk MgO surfaces. The dissociative adsorption on the flat surfaces causes a larger change in the interlayer distance and thus increases the energy of the surface. The dissociative adsorption on stepped surfaces has almost no effect on the interlayer distance.

The adsorbed H forms a surface OH group where the H is facing towards the O atom in the adsorbed OH. Both hydroxyl groups are turned to a more diagonal alignment to the MgO lattice. The same geometry was observed on both bulk and thin film surfaces. On a flat surface the adsorbed H again forms a surface OH group. In this case the surface OH group is facing in a different direction compared to the adsorbed OH. This alignment was also similar on both bulk MgO and the Ag supported MgO thin film. The OH dipoles are aligned on stepped surfaces which decreases the energy of the final system.

The p-band centers of the edge and top O atoms are shifted towards the Fermi energy compared to the p-band center of the average surface O atom. The shift is stronger for the O atom at the step edge compared to the top O atom. A further increase in the shift is seen when OH is adsorbed on the surface. The increased p-band center was associated with the activation of the top and edge O atoms leading to a more exothermic H adsorption. This change in the electronic structure applies to both MgO and MgO/Ag surfaces. In the bulk MgO the relation between the O p-band center and H adsorption energy was seen as analogous to the d-band model. The activation of an O atom at the step edge did not result from an increased negative charge. The Bader charge analysis gave the same charge of -1.68 electrons as the average charge of the surface oxygens and the Bader charge of the individual O atom at the step edge. The top layer oxygen atom on a flat MgO/Ag surface was only slightly more negatively charged with a Bader charge of -1.70 electrons while the average charge of all surface oxygens was -1.68 electrons.
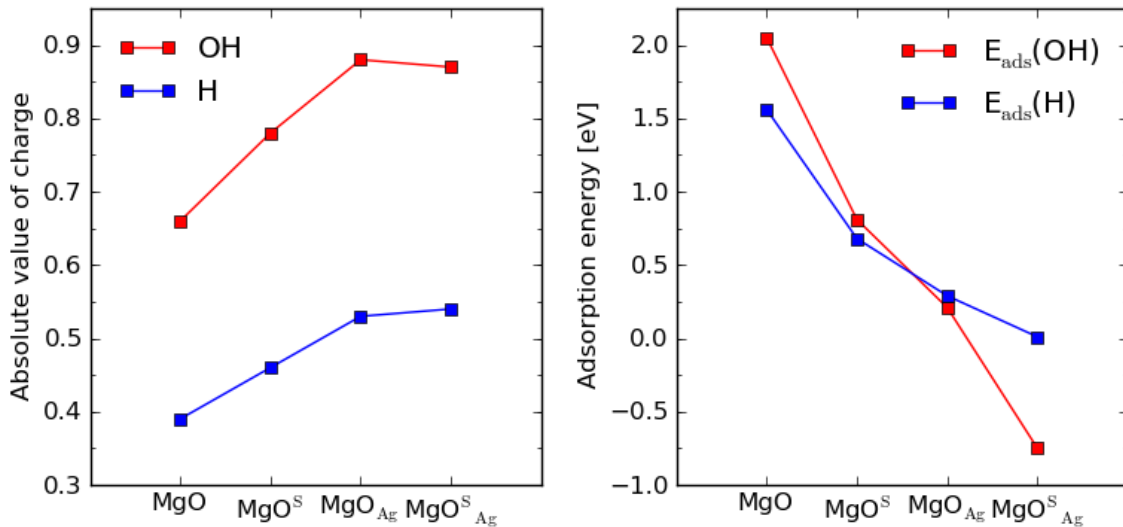
Figure 54: In the left plot is the absolute charge of H and OH adsorbed on different surfaces. The adsorbed H (OH) gains positive (negative) charge. In the right plot is the adsorption energy of H and OH on different surfaces. The stepped surfaces are noted with superscript S and the Ag supported thin film surfaces with subscript Ag.

Binding of H and OH on the different surfaces increased in order

$$MgO < MgO_{step} < MgO/Ag < MgO_{step}/Ag.$$

The decreased adsorption energies correlated with an increased charge transfer to the adsorbates as seen in figure 54. Only the introduction of a step defect on the MgO/Ag surface did not result in a clear increase to the charging of the adsorbates. When H and OH adsorbed to the same computational cell the charge transfer to adsorbates increased. The additional charge transfer was considered to be between the adsorbed H and OH. On

the stepped MgO/Ag surface the charge transfer occurred mainly between the adsorbed H and OH with very little polarization of the MgO film which could lead to an attractive Coulomb interaction between the adsorbed species.

9.2 Adsorption of H, OH and H$_2$O on Au/MgO/Ag

Different sites for water adsorption and the adsorption of its dissociation products H and OH were considered. The support oxide had a different periodicity than the Au stripe leading to a difference in the adsorption sites on the different sides of the Au stripe. Water molecule and OH group had the lowest adsorption energies at the left side of the Au stripe potentially due to the more accessible Mg-top site. The H adsorption was only considered at the left side of the Au stripe since the adsorbed hydrogen should be produced by water dissociation and water preferred to adsorb at the left side. The H adsorption on Au-edge site has the lowest adsorption energy and is preferred to the adsorption on an O-top site of the MgO film.

OH group adsorbed on a Mg-top site near the edge of the Au stripe with almost thermoneutral adsorption energy. Molecular water preferred the same site with an exothermic adsorption energy. The adsorption geometries in these cases differed in the alignment of the adsorbates. The H atom in the adsorbed OH faced away from the Au stripe and the hydrogen atoms in the adsorbed water molecule faced towards the Au stripe edge. A Bader charge analysis gave a negative charge for the Au stripe in agreement with the alignment of the water molecule. The positively charged H atoms in the water molecule faced the negatively charged Au stripe edge. In the OH adsorption this electrostatic effect no longer appeared in the relaxation geometry. Instead there was charge transfer between the adsorbed OH and the Au stripe. The Au stripe charged positively and the density difference plot shows a charge transfer from the edge of the Au stripe to the adsorbed OH group. The two adjacent Au atoms to the adsorbed OH were almost neutral. The Bader charges for different adsorption sites of H and OH are summarized in figure 55.
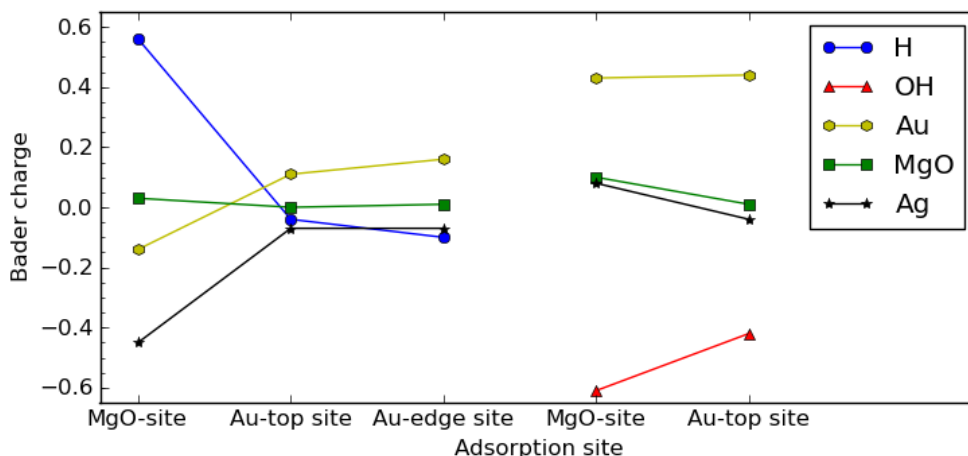
Figure 55: Bader charges for adsorbates H and OH in different adsorption sites. Bader charges of Au, MgO and Ag indicate the difference in the total Bader charge due to adsorbate in given site.

Increasing the coverage of water did not have a strong effect to the adsorption. Both adsorbed water molecules had a similar relaxation geometry with the H atoms facing the

Au stripe edge. The charge transfer was similar as in the case of a smaller coverage and the average adsorption energy was only slightly decreased from the adsorption energy for one water molecule. The adsorption energies for water and its dissociation products on different adsorption sites are summarized in figure 56.
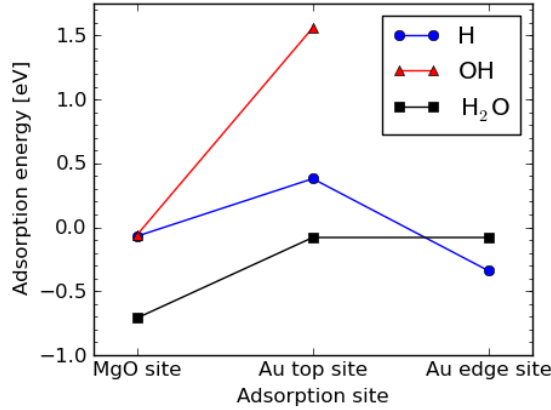
Figure 56: Adsorption energies for water and its dissociation products for different sites of the Au/MgO/Ag surface.

9.3   Water dissociation on the Au/MgO/Ag surface

Water dissociation on the Au/MgO/Ag was studied by comparing the adsorption energies between the molecular and dissociative adsorption. The lowest adsorption energy in the co-adsorption of H and OH was less exothermic than for the molecular adsorption. In the energetically favored dissociative adsorption H adsorbs on an Au-edge site and OH adsorbs on a Mg-top site. When H is adsorbed on an O-top site the combined adsorption energy was close to the previous preferred adsorbate configuration. There is a difference in the interaction between the adsorbates in these two cases. When H and OH were both adsorbed on the oxide, the combined adsorption energy is slightly decreased from the summed adsorption energy of H and OH in separate unit cells. When H was adsorbed on an Au-edge site, the combined adsorption energy was slightly increased from the summed adsorption energy of H and OH in separate unit cells. This correlates with H having a positive and almost neutral charges. The interaction between positively charged H and negatively charged OH could account for the decreasing co-adsorption energy.

For increased water coverage the difference between the two adsorption sites of H was much larger compared to the smaller water coverage. This could result from the positive interaction between the adsorbed OH and H_2O when H adsorbed on an Au-edge site. When H was adsorbed on an O-top site the OH group was facing towards the adsorbed H. When H adsorbed on the Au stripe edge the OH was facing towards the intact water molecule with the H atoms in the water molecule turned towards the negatively charged edge of the Au stripe and the O atom in the OH group. These electrostatic interactions of the intact water molecule could be preferred to the case of H adsorbed on the oxide. In that case the intact water molecule was next to the surface OH group and the electrostatic interaction between them is repulsive. Also the H adsorption was more exothermic on an Au-edge site than on an O-top site.

The H adsorption was more exothermic than the adsorption of OH. Thus the Au/MgO/Ag system did not appear to be able to bind OH strongly enough to dissociate water. The periodic boundary conditions used in the Au/MgO/Ag system did not allow the Au stripe edge to be as flexible as for a model with a full Au cluster included. To compensate for this and to try to answer whether a more flexible Au stripe edge could bind OH, a vacancy was introduced into the Au stripe. With the defect a OH-Au chain formed at the edge of the Au stripe. The adsorption energy for OH to this chain site was endothermic and Au/MgO/Ag system was concluded not to bind OH and thus not being able to dissociate water. This is in agreement with results in the literature. In the WGS reaction the support oxide has been concluded to dissociate water while the Au clusters oxidize the CO.

References

[1] R. Burch, *Gold catalysts for pure hydrogen production in the water-gas shift reaction: activity, structure and reaction mechanism*, Phys. Chem. Chem. Phys. **8**, 5483 (2006).

[2] C. Ratnasamy, and J. P. Wagner, *Water Gas Shift Catalysis*, Catal. Rev. **51**, 325 (2009).

[3] E. D. Park, D. Lee, and H. C. Lee, *Recent progress in selective CO removal in a H(2)-rich stream*, Catal. Today, **139**, 280 (2009).

[4] A. Haryanto, S. D. Fernando, S. D. F. To, P. H. Steele, L. Pordesimo, and S. Adhikari, *Hydrogen Production through the Water-Gas Shift Reaction: Thermodynamic Equilibrium versus Experimental Results over Supported Ni Catalysts*, Energy & Fuels **23**, 3097 (2009).

[5] G. J. Hutchings, *Catalysis by gold*, Catal. Today **100**, 55 (2005).

[6] J. A. Rodriguez, *Gold-based catalysts for the water-gas shift reaction: Active sites and reaction mechanism*, Catal. Today **160**, 3 (2011).

[7] Karoliina Honkala, Anders Hellman, and Henrik Grönbeck. *Water Dissociation on MgO/Ag(100): Support Induced Stabilization or Electron Pairing?* J. Phys. Chem. C **114** 7070 (2010).

[8] P. Hohenberg and W. Kohn. *Inhomogeneous electron gas.* Phys. Rev. Lett. **136**, 864 (1964).

[9] W. Kohn and L.J. Sham. *Self-consistent equations including exchange and correlation effects.* Phys. Rev. **140**, 1133 (1965).

[10] W. Kohn, *Nobel Lecture: Electronic structure of matter - wave functions and density functionals*, Rev. Mod. Phys., **71**, 1253 (1999).

[11] C. Klaus, *A bird's-eye view of density-functional theory*, Braz. J. Phys., **36**, 1318 (2006).

[12] P. Frondelius, *Electronic, Structural and chemical properties of gold clusters on ultra-thin oxide films.* Academic Dissertation for the Degree of Doctor of Philosophy, University of Jyväskylä (2009).

[13] R. M. Martin. *Electronic structure - basic theory and practical methods.* Cambridge university press, UK (2004).

[14] R. C. Albers, N. E. Christensen, and A. Svane *Hubbard-U band-structure methods* J. Phys.: Condens. Matter **21**, 343201 (2009).

[15] B. Hammer, L. B. Hansen and J. K. Nørskov, *Improved adsorption energetics within density-functional theory using revised Perdew-Burke-Ernzerhof functionals*, Phys. Rev. B **59**, 7413 (1999).

[16] J. P. Perdew, *Density-functional approximation for the correlation of the inhomogeneous electron gas.*, Phys. Rev. B **33**, 8822 (1986).

[17] K. Burke, J. P. Perdew, and Matthias Ernzerhof, *Why the Generalized Gradient Approximation Works and How to Go Beyond It*, Int. J. of Quantum Chem. **61**, 287 (1997).

[18] S. Kurth J. P. Perdew, P. Blaha, *Molecular and Solid-State Tests of Density Functional Approximations: LSD, GGAs, and Meta-GGAs*, Int. J. of Quantum Chem. **75**, 889 (1999).

[19] P. Zieschea, S. Kurth, and J. P. Perdew, *Density functionals from LDA to GGA*, Comp. Mater. Sci. **11**, 122 (1998).

[20] H.J. Monkhorst and J.D. Pack, *Special points for Brillonin-zone integrations*, Phys. Rev. B **13**, 5188 (1976).

[21] J. J. Mortensen, L. B. Hansen , and K. W. Jacobsen *Real-space grid implementation of the projector augmented wave method* Physical Review B, Vol.**71**, 035109 (2005).

[22] J. Enkovaara, C. Rostgaard, J. J. Mortensen et al. *Electronic structure calculations with GPAW: a real-space implementation of the projector augmented-wave method* J. Phys.: Condens. Matter **22**, 253202 (2010).

[23] S. R. Bahn and K. W. Jacobsen *An object-oriented scripting interface to a legacy electronic structure code* Comput. Sci. Eng., **4**, 56 (2002).

[24] W. Humphrey, A. Dalke, and K. Schulten, *VMD - Visual Molecular Dynamics*, J. Molec. Graphics, **14**, 33 (1996)

[25] Jmol: an open-source Java viewer for chemical structures in 3D. http://www.jmol.org/

[26] J. P. Perdew, K. Burke, M. Ernzerhof. *Generalized Gradient Approximation Made Simple.* Phys. Rev. Lett. **77**, 3865 (1996).

[27] Grönbeck, H. *First principles studies of metal-oxide surfaces*, Top. Catal. **28**, 59 (2004).

[28] G. S. Karlberg, and G. Wahnström, *Density-functional based modeling of the intermediate in the water production reaction on Pt(111).* Phys. Rev. Lett. **92**, 13610 (2004).

[29] W. Tang, E. Sanville, and G. Henkelman *A grid-based Bader analysis algorithm without lattice bias*, J. Phys.: Condens. Matter **21**, 084204 (2009).

[30] E. Sanville, S. D. Kenny, R. Smith, and G. Henkelman *An improved grid-based algorithm for Bader charge allocation*, J. Comp. Chem. **28**, 899 (2007).

[31] G. Henkelman, A. Arnaldsson, and H. Jónsson, *A fast and robust algorithm for Bader decomposition of charge density*, Comput. Mater. Sci. **36**, 254 (2006).

[32] R. Ren, C. Niu, S. Bu, Y. Zhou, Y. Lv, and G. Wang, *Why is metallic Pt the best catalyst for methoxy decomposition?*, J. Nat. Gas Chem., **20**, 90 (2011).

[33] G. Bond, *Mechanisms of the gold-catalysed water-gas shift*, Gold Bull. **42**, 337 (2009).

[34] J.A. Rodríguez, P. Liu, J. Hrbek, M. Pérez, J. Evans *Water-gas shift activity of Au and Cu nanoparticles supported on molybdenum oxides*, J. Mol. Catal. A **281**, 59 (2008).

[35] M. Mavrikakis, B. Hammer, and J.K. Nørskov *Effect of Strain on the Reactivity of Metal Surfaces*, Phys. Rev. Lett., **81**, 2819 (1998).

[36] B. Hammer, and J. K. Nørskov *Electronic factors determining the reactivity of metal surfaces*, Surf. Sci., **343**, 211 (1995).

[37] J. A. Rodriguez, S. Ma, P. Liu, J. Hrbek, J. Evans, M. Pérez *Activity of CeO_x and TiO_x Nanoparticles Grown on Au(111) in the Water-Gas Shift Reaction*, Science **318**, 1757 (2007).

[38] J. A. Rodriguez, J. Evans, J. Graciani, J.-B. Park, P. Liu, J. Hrbek, J. F. Sanz, *High Water-Gas Shift Activity in TiO_2(110) Supported Cu and Au Nanoparticles: Role of the Oxide and Metal Particle Size* J. Phys. Chem. C **113**, 7364 (2009).

[39] X. Lin, N. Nilius, H.-J. Freund, M. Walter, P. Frondelius, K. Honkala, and H. Häkkinen, *Quantum Well States in Two-Dimensional Gold Clusters on MgO Thin Films*, Phys. Rev. Lett., **102**, 206801 (2009)

[40] P. Frondelius, H. Häkkinen, and K. Honkala, *Formation of Gold(I) Edge Oxide at Flat Gold Nanoclusters on an Ultrathin MgO Film under Ambient Conditions*, Angew. Chem. Int. Ed., **49**, 7913 (2010).

[41] W. D. Williams, M. Shekhar, W.-S. Lee, V. Kispersky, W. N. Delgass, F. H. Ribeiro, S. M. Kim, E. A. Stach, J. T. Miller, and L. F. Allard, *Metallic Corner Atoms in Gold Clusters Supported on Rutile Are the Dominant Active Site during Water-Gas Shift Catalysis*, J. Am. Chem. Soc., **132**, 14018, (2010).

[42] R. van Leeuwen, *Condensed Matter Physics II*, Lecture notes, University of Jyväskylä (2009).

[43] M. L. Boas. *Mathematical Methods in the Physical Sciences*. John Wiley & Sons Inc., Third Edition, (2006).

A   The Hohenberg-Kohn theorems

Consider two Hamiltonians of the form

$$\hat{H}_i = \hat{T} + \hat{V}_i + \hat{W} \tag{A.1}$$

where $\hat{T}$ describes the kinetic energy of the particles, $\hat{W}$ describes the interaction between the particles, $\hat{V}_i$ is the potential energy due to an external potential V_i, where $i = 1, 2$. Suppose they both have the same ground state wave function Ψ. Then they both fulfill the Schrödinger equation of the form

$$\hat{H}_i|\Psi\rangle = E_i|\Psi\rangle \tag{A.2}$$

where E_i is the ground state energy for the Hamiltonian i. Subtracting equations with $i = 1$ and $i = 2$ gives

$$\hat{H}_1 - \hat{H}_2|\Psi\rangle = \hat{V}_1 - \hat{V}_2|\Psi\rangle = E_1 - E_2|\Psi\rangle. \tag{A.3}$$

By denoting $C = E_1 - E_2$ and substracting $C|\Psi\rangle$ from both sides the above equation can be rewritten as

$$(\hat{V}_1 - \hat{V}_2 - C)|\Psi\rangle = 0 \tag{A.4}$$

which leads to conclusion

$$\hat{V}_1 = \hat{V}_2 + C. \tag{A.5}$$

Thus if there is two external potentials with the same ground state wave function they can not differ more than a constant. Consider two Hamiltonians $\hat{H}_1$ and $\hat{H}_2$ of the same form but with two different non degenerate ground state wave functions Ψ_1 and Ψ_2. By writing the first Hamiltonian as $\hat{H}_1 = \hat{H}_2 + \hat{V}_2 - \hat{V}_1$ following inequality can be obtained

$$
\begin{aligned}
E_1 &= \langle\Psi_1|\hat{H}_1|\Psi_1\rangle \\
&= \langle\Psi_1|\hat{H}_2|\Psi_1\rangle + \langle\Psi_1|\hat{V}_1 - \hat{V}_2|\Psi_1\rangle \\
&> E_2 + \int \mathrm{d}\boldsymbol{r}\, n_1(\boldsymbol{r})(V_1(\boldsymbol{r}) - V_2(\boldsymbol{r}))
\end{aligned} \tag{A.6}
$$

where $n_1(\boldsymbol{r})$ is the ground state density for Hamiltonian $\hat{H}_1$. The inequality arises from the assumption that ground state wave function for the Hamiltonian $\hat{H}_2$ is non-degenerate and thus every other state has a higher energy than the ground state Ψ_2. Especially $\langle\Psi_1|\hat{H}_2|\Psi_1\rangle > E_2$. In the above inequality the indexes $i = 1$ and $i = 2$ can be interchanged to obtain

$$E_2 > E_1 + \int \mathrm{d}\boldsymbol{r}\, n_2(\boldsymbol{r})(V_2(\boldsymbol{r}) - V_1(\boldsymbol{r})). \tag{A.7}$$

Adding both inequalities together gives

$$E_1 + E_2 > E_1 + E_2 + \int \mathrm{d}\boldsymbol{r}\, n_1(\boldsymbol{r})(V_1(\boldsymbol{r}) - V_2(\boldsymbol{r})) + \int \mathrm{d}\boldsymbol{r}\, n_2(\boldsymbol{r})(V_2(\boldsymbol{r}) - V_1(\boldsymbol{r})). \tag{A.8}$$

This can be simplified to equation

$$\int d\boldsymbol{r}(V_2(\boldsymbol{r}) - V_1(\boldsymbol{r}))(n_1(\boldsymbol{r}) - n_2(\boldsymbol{r})) > 0 \tag{A.9}$$

which leads to conclusion

$$n_1(\boldsymbol{r}) \neq n_2(\boldsymbol{r}) \tag{A.10}$$

for set with non zero measure since functions $V_i(\boldsymbol{r})$ and $n_i(\boldsymbol{r})$ are continuous. Thus two different ground state wave functions produce different ground state densities. Combining the above results shows that there is one to one correspondence between external potential and ground state electron density. Thus the external potential can be expressed as a functional of the ground state density. Similarly the ground state wave function is a functional of the density. From this it follows that the expectation values O for the ground state observables $\hat{O}$ are also functionals of density

$$O[n] = \langle \Psi[n] | \hat{O} | \Psi[n] \rangle \tag{A.11}$$

especially the ground state energy E is a functional of the ground state density

$$E[n] = \langle \Psi[n] | \hat{H} | \Psi[n] \rangle. \tag{A.12}$$

B   Functional derivatives

Considering a general functional $F[\phi]$ [42]. Assuming that ϕ_0 minimizes the functional and define function $g(t)$ as

$$g(t) = F[\phi_0 + th] \tag{B.1}$$

where h is an arbitrary variation to the function ϕ_0. THe derivative of $g(t)$ for $t = 0$ is then zero

$$\frac{dg}{dt}(t) = \lim_{t \to 0} \frac{F[\phi_0 - th] - F[\phi_0]}{t} = 0. \tag{B.2}$$

For the functional $V[n]$ the above equation gives

$$\begin{aligned}
&\lim_{t \to 0} \frac{V[n + th] - V[n]}{t} \\
=\ &\lim_{t \to 0} \frac{1}{t} \left(\int d\boldsymbol{r} v(\boldsymbol{r})(n(\boldsymbol{r}) + th(\boldsymbol{r})) - \int d\boldsymbol{r} v(\boldsymbol{r}) n(\boldsymbol{r}) \right) \\
=\ &\int d\boldsymbol{r} v(\boldsymbol{r}) h(\boldsymbol{r}) \\
=\ &0
\end{aligned} \tag{B.3}$$

which is true for arbitrary variation h only if $v(\boldsymbol{r})$ is zero for all $\boldsymbol{r}$. Therefore $v(\boldsymbol{r})$ is the functional derivative of $V[n]$

$$\frac{\delta V[n]}{\delta n(\boldsymbol{r})} = v(\boldsymbol{r}). \tag{B.4}$$

Similarly the functional derivative of $V_H[n]$ can be calculated as follows

$$\lim_{t \to 0} \frac{V_H[n + th] - V_H[n]}{t} \tag{B.5}$$

$$= \lim_{t \to 0} \frac{1}{t} \left(\frac{1}{2} \int \int \mathrm{d}\boldsymbol{r}\mathrm{d}\boldsymbol{r}' \frac{(n(\boldsymbol{r}) + th(\boldsymbol{r}))(n(\boldsymbol{r}') + th(\boldsymbol{r}'))}{|\boldsymbol{r} - \boldsymbol{r}'|} \right)$$

$$= \lim_{t \to 0} \frac{1}{t} \left(\frac{1}{2} \int \int \mathrm{d}\boldsymbol{r}\mathrm{d}\boldsymbol{r}' \frac{n(\boldsymbol{r})th(\boldsymbol{r}')}{|\boldsymbol{r} - \boldsymbol{r}'|} + \frac{1}{2} \int \int \mathrm{d}\boldsymbol{r}\mathrm{d}\boldsymbol{r}' \frac{n(\boldsymbol{r}')th(\boldsymbol{r})}{|\boldsymbol{r} - \boldsymbol{r}'|} + \mathcal{O}(t^2) \right)$$

$$= \int \mathrm{d}\boldsymbol{r} \int \mathrm{d}\boldsymbol{r}' \frac{n(\boldsymbol{r}')}{|\boldsymbol{r} - \boldsymbol{r}'|} h(\boldsymbol{r})$$

$$= 0$$

where integration variables $\boldsymbol{r}$ and $\boldsymbol{r}'$ have been switched in the first term on the third line and the last term in the third line vanishes as the limit $t \to 0$ is taken. Similarly as above in the earlier case the functional derivative of $V_H[n]$ is

$$\frac{\delta V_H[n]}{\delta n(\boldsymbol{r})} = \int \mathrm{d}\boldsymbol{r}' \frac{n(\boldsymbol{r}')}{|\boldsymbol{r} - \boldsymbol{r}'|}. \tag{B.6}$$

Lastly the functional derivative for $T_s[n]$ can be calculated as follows. First by noting that single particle kinetic energy operator can be written as $\hat{T}_s = \hat{H}_s - \hat{V}_s$ the expectation value $T_s[n]$ can be expressed as

$$T_s[n] = \langle \Phi_s | \hat{H}_s | \Phi_s \rangle - \langle \Phi_s | \hat{V}_s | \Phi_s \rangle \tag{B.7}$$

$$= E_s - \int \mathrm{d}\boldsymbol{r} \Phi_s^*(\boldsymbol{r}) V_s(\boldsymbol{r}) \Phi_s(\boldsymbol{r})$$

$$= E_s - \int \mathrm{d}\boldsymbol{r} V_s(\boldsymbol{r}) n(\boldsymbol{r}).$$

Where expectation value for Hamiltonian is the energy E_s. Then equation (B.2) for functional $T_s[n]$ gives

$$\lim_{t \to 0} \frac{T_s[n + th] - T_s[n]}{t} \tag{B.8}$$

$$= \lim_{t \to 0} \frac{1}{t} \left(E_s - \int \mathrm{d}\boldsymbol{r} V_s(\boldsymbol{r})(n(\boldsymbol{r}) + th) - E_s + \int \mathrm{d}\boldsymbol{r} V_s(\boldsymbol{r}) n(\boldsymbol{r}) \right)$$

$$= - \int \mathrm{d}\boldsymbol{r} V_s(\boldsymbol{r}) h(\boldsymbol{r})$$

$$= 0$$

and thus the functional derivative is

$$\frac{\delta T_s[n]}{\delta n(\boldsymbol{r})} = -V_s(\boldsymbol{r}). \tag{B.9}$$

C   Energy as a sum of single particle energies

Energy of the Kohn-Sham system E_s can be calculated as the expectation value

$$E_s = \langle \Phi_s[n] | \hat{H}_s | \Phi_s[n] \rangle = \langle \Phi_s[n] | \hat{T}_s | \Phi_s[n] \rangle + \langle \Phi_s[n] | \hat{V}_s | \Phi_s[n] \rangle \tag{C.1}$$

In order to get to the single particle states ϕ_i the Slater determinant in the wave function $\Phi_s[n]$ can be written as

$$\Phi_s[n] = \frac{1}{\sqrt{N!}} \sum_P (-1)^{|P|} \phi_{P(1)}(\boldsymbol{r}_1) \ldots \phi_{P(N)}(\boldsymbol{r}_N), \tag{C.2}$$

where $|P|$ is the number of permutations, the sum is over all possible permutations and $P(j)$ is the index of the permuted wave function. Then the expectation value for the kinetic energy operator is

$$\langle \Phi_s[n] | \hat{T}_s | \Phi_s[n] \rangle = -\frac{1}{2N!} \sum_{i=1}^N \sum_{P,P'} (-1)^{|P|+|P'|} \int \mathrm{d}\boldsymbol{r} \prod_{j=1}^N \phi_{P'(j)}^*(\boldsymbol{r}_j) \nabla_i^2 \prod_{j=1}^N \phi_{P(j)}^*(\boldsymbol{r}_j). \tag{C.3}$$

This can be decomposed as a product of integrals

$$T_s[n] = -\frac{1}{2N!} \sum_{i=1}^N \sum_{P,P'} (-1)^{|P|+|P'|} \int \mathrm{d}\boldsymbol{r}_i \phi_{P'(i)}^*(\boldsymbol{r}_i) \nabla_i^2 \phi_{P(i)}(\boldsymbol{r}_i) \prod_{j \neq i} \int \mathrm{d}\boldsymbol{r}_j \phi_{P'(j)}^*(\boldsymbol{r}_j) \phi_{P(j)}(\boldsymbol{r}_j). \tag{C.4}$$

A further simplification gives

$$T_s[n] = -\frac{1}{2N!} \sum_{i=1}^N \sum_{P,P'} (-1)^{|P|+|P'|} \int \mathrm{d}\boldsymbol{r}_i \phi_{P'(i)}^*(\boldsymbol{r}_i) \nabla_i^2 \phi_{P(i)}(\boldsymbol{r}_i) \prod_{j \neq i} \delta_{P'(j),P(j)} \tag{C.5}$$

by using the orthonormality requirement of the single particle states

$$\int \mathrm{d}\boldsymbol{r}_j \phi_{P'(j)}^*(\boldsymbol{r}_j) \phi_{P(j)}(\boldsymbol{r}_j) = \delta_{P'(j),P(j)}. \tag{C.6}$$

Since this equation is zero for every $P'(i) \neq P(i)$ one obtains $(N-1)!$ permutations for every index $P'(i) = P(i) := k$ where the product differs from zero and $|P| = |P'|$

$$T_s[n] = -\frac{1}{2N} \sum_{i=1}^N \sum_{k=1}^N \int \mathrm{d}\boldsymbol{r}_i \phi_k^*(\boldsymbol{r}_i) \nabla_i^2 \phi_k(\boldsymbol{r}_i). \tag{C.7}$$

Further, the N integrals differing only with the integrating variable can be summed together

$$\langle \Phi_s[n] | \hat{T}_s | \Phi_s[n] \rangle = -\frac{1}{2} \sum_{i=1}^N \int \mathrm{d}\boldsymbol{r} \phi_i^*(\boldsymbol{r}) \nabla^2 \phi_i(\boldsymbol{r}). \tag{C.8}$$

With similar reasoning one can obtain

$$\langle \Phi_s[n] | V_s | \Phi_s[n] \rangle = \sum_{i=1}^N \int \mathrm{d}\boldsymbol{r} \phi_i^*(\boldsymbol{r}) V_s(\vec{r}) \phi_i(\boldsymbol{r}). \tag{C.9}$$

Using the divergence theorem [43, p. 318]

$$\int \mathrm{d}\boldsymbol{r} \nabla \cdot (\phi_i^*(\boldsymbol{r})\nabla\phi_i(\boldsymbol{r})) = \int \mathrm{d}\boldsymbol{A}\phi_i^*(\vec{r})\nabla\phi_i(\boldsymbol{r}) = 0 \tag{C.10}$$

and that surface integral vanishes due to vanishing of the wave functions and their derivatives the equation

$$\int \mathrm{d}\vec{r}\phi_i^*(\boldsymbol{r})\nabla^2\phi_i(\boldsymbol{r}) = -\int \mathrm{d}\boldsymbol{r}|\nabla\phi_i(\boldsymbol{r})|^2 \tag{C.11}$$

is obtained. This can be used to further simplify equation (C.8) into

$$T_s[n] = \frac{1}{2}\sum_{i=1}^{N} \int \mathrm{d}\boldsymbol{r}|\nabla\phi_i(\boldsymbol{r})|^2 \tag{C.12}$$

with the linearity of the integral and the vector identity

$$\nabla \cdot (\phi_i^*(\boldsymbol{r})\nabla\phi_i(\boldsymbol{r})) = |\nabla\phi_i(\boldsymbol{r})|^2 + \phi_i^*(\boldsymbol{r})\nabla^2\phi_i(\boldsymbol{r}). \tag{C.13}$$

The expectation value for the single particle energy ϵ_i is

$$\epsilon_i = \langle\phi_i| -\frac{1}{2}\nabla^2|\phi_i\rangle + \langle\phi_i|V_s|\phi_i\rangle = -\frac{1}{2}\int \mathrm{d}\vec{r}\phi_i^*(\boldsymbol{r})\nabla^2\phi_i(\boldsymbol{r}) + \int \mathrm{d}\boldsymbol{r}\phi_i^*(\boldsymbol{r})V_s(\boldsymbol{r})\phi_i(\boldsymbol{r}). \tag{C.14}$$

By combining equations (C.3), (C.8), (C.9) and (C.14) the result

$$E_s = -\frac{1}{2}\sum_{i=1}^{N} \int \mathrm{d}\boldsymbol{r}\phi_i^*(\vec{r})\nabla^2\phi_i(\vec{r}) + \sum_{i=1}^{N} \int \mathrm{d}\boldsymbol{r}\phi_i^*(\boldsymbol{r})V_s(\boldsymbol{r})\phi_i(\boldsymbol{r}) = \sum_{i=1}^{N} \epsilon_i \tag{C.15}$$

is obtained.